DYNAMIC STATE ESTIMATION ASSISTED POWER SYSTEM MONITORING AND PROTECTION

A Dissertation
Submitted to the Graduate Faculty
of the
North Dakota State University
of Agriculture and Applied Science

By

Yinan Cui

In Partial Fulfillment of the Requirements
for the Degree of
DOCTOR OF PHILOSOPHY

Major Department:
Electrical and Computer Engineering

November 2016

Fargo, North Dakota

NORTH DAKOTA STATE UNIVERSITY

Graduate School

Title

DYNAMIC STATE ESTIMATION ASSISTED POWER SYSTEM MONITORING AND PROTECTION

By

Yinan Cui

The supervisory committee certifies that this dissertation complies with North Dakota State University's regulations and meets the accepted standards for the degree of

DOCTOR OF PHILOSOPHY

SUPERVISORY COMMITTEE:

Dr. Rajesh Kavasseri
Chair

Dr. Ivan T. Lima, Jr.

Dr. Sumathy Krishnan

Dr. Nilanjan Ray Chaudhuri

Approved:

10 March 2017
Date

Dr. Scott C. Smith
Department Chair

ABSTRACT

The advent of phasor measurement units (PMUs) has unlocked several novel methods to monitor, control, and protect bulk electric power systems. This thesis introduces the concept of "Dynamic State Estimation" (DSE), aided by PMUs, for wide-area monitoring and protection of power systems. Unlike traditional State Estimation where algebraic variables are estimated from system measurements, DSE refers to a process to estimate the dynamic states associated with synchronous generators. This thesis first establishes the viability of using particle filtering as a technique to perform DSE in power systems. The utility of DSE for protection and wide-area monitoring are then shown as potential novel applications. The work is presented as a collection of several journal and conference papers.

In the first paper, we present a particle filtering approach to dynamically estimate the states of a synchronous generator in a multi-machine setting considering the excitation and prime mover control systems. The second paper proposes an improved out-of-step detection method for generators by means of angular difference. The generator's rotor angle is estimated with a particle filter-based dynamic state estimator and the angular separation is then calculated by combining the raw *local* phasor measurements with this estimate. The third paper introduces a particle filter-based dual estimation method for tracking the dynamic states of a synchronous generator. It considers the situation where the field voltage measurements are not readily available. The particle filter is modified to treat the field voltage as an unknown input which is sequentially estimated along with the other dynamic states. The fourth paper proposes a novel framework for event detection based on energy functions. The key idea is that any event in the system will leave a signature in WAMS data-sets. It is shown that signatures for four broad classes of disturbance events are buried in the components that constitute the energy function for the system. This establishes a direct correspondence (or mapping) between an event and certain component(s) of the energy function. The last paper considers the dynamic latency effect when the measurements and estimated dynamics are transmitted from remote ends to a centralized location through the networks.

ACKNOWLEDGEMENTS

I would like to thank the following people for contributing to the success in the endeavors:

Professors and fellow students at NDSU for creating a favorable academic environment and their kind support. I would like to thank my advisor, Dr. Rajesh Kavasseri, for his patience, knowledge and wisdom to guide me through the last four years. Special thanks to Dr. Sukumar M. Brahma and Dr. Nilanjan Ray Chaudhuri for their time and expertise in the research work. Finally, I want to thank the remaining members of the dissertation committee, Dr. Ivan T. Lima, Jr. and Dr. Sumathy Krishnan for their valuable comments and suggestions on improving this work.

My family for their contributions and supports all these years.

This work was supported by the National Science Foundation through grant CPS 1544621.

DEDICATION

This dissertation is dedicated to my parents, Xinwei and Lihong, and to my lovely wife, Jingyang.

TABLE OF CONTENTS

ABSTRACT iii

ACKNOWLEDGEMENTS iv

DEDICATION v

LIST OF TABLES x

LIST OF FIGURES xi

LIST OF APPENDIX TABLES xiv

1. INTRODUCTION 1

1.1. A Particle Filter for Dynamic State Estimation of Synchronous Generators 2

1.2. Dynamic State Estimation Assisted Out-of-Step Detection for Generators 2

1.3. Dynamic State Estimation Using Dual-filtering 3

1.4. Dynamic State Estimation Assisted Application in Wide Area Measurement System 3

1.5. Dissertation Organization 5

2. A PARTICLE FILTER FOR DYNAMIC STATE ESTIMATION IN MULTI-MACHINE SYSTEMS WITH DETAILED MODELS 6

2.1. Introduction 6

2.2. Particle Filtering Method 7

2.2.1. Initialization of The Filter 9

2.2.2. System Dynamics Propagation 9

2.2.3. Weights Generation 9

2.2.4. Particles Resampling 10

2.2.5. State Estimation 10

2.3. Dynamic Models 10

2.4. Particle Filter based Dynamic State Estimation 15

2.5. Results 16

2.5.1. Temporary (6 cycles) 3 Phase to Ground Fault on Line 18

2.5.2. Three-phase Ground Fault with Permanent Line Trip 21
2.5.3. Temporary Additional Load 21
2.6. Evaluation and Discussion 23
2.7. Conclusion 25
3. DYNAMIC STATE ESTIMATION ASSISTED OUT-OF-STEP DETECTION FOR GENERATORS USING ANGULAR DIFFERENCE 26
3.1. Introduction 26
3.2. Rationale and Assumptions Behind the Conventional OOS Protection Relay 28
3.3. DSE-assisted OOS Detection Based on Angular Difference Monitoring 30
3.3.1. Estimation with Particle Filter 32
3.3.2. Modal Analysis of Angular Difference 35
3.4. Simulation Results 35
3.4.1. Verifying the Security of the Proposed Method 37
3.4.2. Verification of Dependability of the Proposed Scheme and Advantages of the Predictive Feature 40
3.4.3. Supervision of Relay Behavior 42
3.5. Discussion 43
3.6. Conclusions 44
4. PARTICLE FILTER-BASED DUAL ESTIMATION FOR SYNCHRONOUS GENERATORS 46
4.1. Introduction 46
4.2. Dual-Estimator for State and Parameter Estimation 47
4.2.1. State Estimation Using Particle Filtering 48
4.2.2. Parameter Estimation Using Particle Filtering 49
4.3. Dual Estimation for Power Systems 51
4.3.1. Generator Dynamic States Tracking 51
4.3.2. Field Voltage Estimation 52
4.4. Simulation Results 54

4.4.1. Filter Performance with External Disturbance 54
4.4.2. Filter Performance with Exciter Model Mismatch 59
4.4.3. Loss of Excitation Events 61
4.5. Discussion 62
4.6. Conclusion 62
5. A NEW APPROACH FOR EVENT DETECTION BASED ON ENERGY FUNCTIONS 64
5.1. Introduction 64
5.2. Key Ideas 65
5.2.1. The Particle Filter 66
5.2.2. Construction of Energy Function Components with Particle Filter Estimates 67
5.2.3. Sensitivity of Energy Function Components 70
5.3. Results and Discussion 71
5.4. Conclusions 75
6. MODELING AND SIMULATION OF DYNAMIC COMMUNICATION LATENCY AND DATA AGGREGATION FOR WIDE-AREA APPLICATIONS 76
6.1. Introduction 76
6.2. Modeling Time-varying Delay 78
6.3. Data Aggregation at PDC 80
6.4. Results 82
6.4.1. Latency Variation During Transients 83
6.4.2. Estimation of Electromechanical Mode Using Ringdown Data 85
6.5. Conclusions 89
7. CONCLUSIONS AND RECOMMENDATIONS FOR FUTURE WORK 90
REFERENCES 94
APPENDIX 106
A.1. Network Algebraic Constraints and DSE using global measurements from WAMS . . 106
A.2. Implementation of physical limit constraints in PF 106

A.3. Definitions for constants in synchronous machine modeling 107

A.4. OOS relay settings 107

LIST OF TABLES

Table Page

2.1. RMSD of estimation results of G_5 and its controllers for different choices of N (number of particles) 24

3.1. Modal analysis results at different time 41

4.1. RMSD of estimation results of G_2 for different TVE levels by proposed dual-estimator and EKFUI 55

4.2. RMSD of estimation results of G_5 for different TVE levels by proposed dual-estimator and EKFUI 57

4.3. RMSD of estimation results of G_8 for different TVE levels by proposed dual-estimator and EKFUI 58

6.1. Summary of delay source and range 77

6.2. Delay variation in the channels 85

6.3. Latency variation in the channels 86

6.4. Modal analysis before time-alignment 88

6.5. Modal analysis after time-alignment 88

LIST OF FIGURES

Figure Page

2.1. A quasi-static phasor diagram for a synchronous generator with d-axis leading. 14

2.2. IEEE 14-bus system. 17

2.3. Measured quantities for G_2. 18

2.4. Estimation results for G_2 and its exciter by PF and UKF. 19

2.5. Estimation results of mechanical torque for G_2 (hosts a hydro-turbine) by PF and UKF in 10 trials, dashed line is the actual mechanical torque. 19

2.6. Estimation results for G_4 and its exciter by PF and UKF. 20

2.7. Estimation results of mechanical torque for G_4 (hosts a hydro-turbine) by PF and UKF in 10 trials, dashed line is the actual mechanical torque. 20

2.8. Estimation results for G_1 and its exciter by PF and UKF. 21

2.9. Estimation results for G_3 and its exciter by PF and UKF. 22

2.10. Estimation results of mechanical torque for G_3 by PF and UKF in 10 trials, dashed line is the actual mechanical torque. 22

2.11. RMSD of selected 9 states for $G1$ to G_4 by PF (upward-pointing triangle) and UKF (circle). Bars refer to standard deviations. The out-of-range results are due to the divergences of the filter in the trials 23

3.1. OOS protective relay (device 78) for a generator. 28

3.2. Typical operation logic of a OOS relay for a generator. 29

3.3. Block diagram of the OOS relaying scheme for a generator. 30

3.4. Processes in the swing analysis block. 31

3.5. New England 10-generator 39-bus system. 36

3.6. Angular difference curves for different clearing time. 37

3.7. Impedance locus for the worst stable swing and estimated angular difference for G_8. . . 38

3.8. Generator's estimated rotor angles and angular difference for G_6 and G_7. 38

3.9. Partial LOE case: impedance locus seen by LOE relay and estimated angular difference for G_4. 39

3.10. Complete LOE case: impedance locus seen by LOE relay and estimated angular difference for G_4. 40

3.11. Impedance locus for the unstable swing and estimated angular difference for G_8. 41

3.12. Impedance locus and relay characteristics at G_2 for the OOS condition. 42

3.13. Angular difference between G_2 and voltage angle of bus #6 along with the reproduced curve. 42

3.14. Impedance locus for the unstable swing and estimated angular difference for G_2. 43

4.1. A diagram of a sequential method for dual estimation. 48

4.2. Block diagram of detecting LOE incident using the proposed method. 53

4.3. State tracking results (with 3% measurement noise) by the proposed dual-estimator for G_2 for three-phase to ground fault 55

4.4. State tracking results (with 3% measurement noise) by the proposed dual-estimator for G_2 for a load rejection event at bus 20. 56

4.5. State tracking results by proposed dual-estimator for G_8 with a 3-phase-to-ground fault. 58

4.6. Discrepancy in estimation with approximate parameters for a standard PF with a line outage incident. 59

4.7. Tracking performance for a malfunctioning voltage regulator (pLOE), the generator loses its synchronism at $t = 17s$. 60

4.8. Field voltage tracking results by proposed dual-estimator with partial and complete LOE incidents. 61

5.1. Four-machine, two-area system. 71

5.2. Dynamic states $(\delta, \bar{\omega}, E'_q, E'_d, E_{fd})$ estimated from the particle filter for Generator 1 in Event-1. The dashed/red lines denote estimated values. The solid/blue lines denote actual values from a numerical dynamic simulation. 72

5.3. Energy function components constructed with particle filtering estimated states for Event 1 72

5.4. Energy function components constructed with particle filtering estimated states for Event 2 73

5.5. Energy function components constructed with particle filtering estimated states for Event 3 73

5.6. Energy function components constructed with particle filtering estimated states for Event 4 74

6.1. Representation of data transmission with time-delay 78
6.2. A typical structure for synchrophasor data collection 80
6.3. Latency of data aggregation in PDC 81
6.4. New England 10-generator 39-bus system 82
6.5. Distorted signal with time-varying latency received a PDC 83
6.6. Latency change effect on PDC receiving-end 84
6.7. Comparison of P_e information at different locations due to delay variation 84
6.8. Comparison of P_e on tie-lines at different locations due to delay variation 87

LIST OF APPENDIX TABLES

Table Page

A.1. Definitions for constants in synchronous machine modeling 107

A.2. Generator Relay settings 107

1. INTRODUCTION

Unlike traditional State Estimation where algebraic variables (voltage magnitudes and phase angles) are estimated from system measurements, DSE refers to a process to estimate the dynamic states associated with synchronous generators. Since State Estimation (SE) is based on the idea that the system is in steady or quasi-steady state, it is extensively used for energy management applications in modern control centers [1] in the steady-state operational context. When the system is subject to a disturbance, the ensuing variations in states associated with all the dynamic components cannot be extracted or retrieved through SE. In contrast with SE, DSE refers to the problem of estimating and dynamically tracking the states of a synchronous generator and associated control units given a model of the system dynamics and measurements of physical variables. In principle, DSE can be applied to any component whose dynamics are described through Ordinary Differential Equations (ODEs). Synchronous generators constitute the heart of a power system and not surprisingly, it is the most valuable asset in all system operation. A synchronous generator and its primary control units – excitation system and turbine-governor are therefore natural choices for the task of DSE.

Assuming that DSE can be performed, this thesis examines several fundamental questions – How can the estimated dynamic states be put to use? Can they be computed in near real-time to allow control and protection functions – traditionally done using readily measurable algebraic variables - because of strict timing requirements? If so, can the functions be validated against traditional methods in terms of their dependability and security?

This thesis shows that not only can DSE be robustly performed with the particle filter, a purely nonlinear probability-based filter, but that the estimated states can be used to serve protection and monitoring functions that are traditionally done using SE-type algebraic variables. These advancements require the presence of Phasor Measurement Unit (PMU) for the angular reference and the availability of computational resources which are increasingly becoming cheaper.

The following sections describe a road map for the development of the principal ideas and results in this thesis.

1.1. A Particle Filter for Dynamic State Estimation of Synchronous Generators

DSE problem of a synchronous generator, which is at the heart of the power system dynamics, will involve solving sets of nonlinear algebraic and differential equations. Customarily, DSE is done using Kalman-based methods, using a model for the system dynamics and a model for the system measurements.The extended Kalman filter (EKF) provides a natural starting point using Bayesian nonlinear filtering techniques [2, 3]. Because the EKF relies on linearization, both the accuracy of estimates and the tuning of the EKF strongly depend on the accuracy of linearization. The unscented Kalman filter (UKF) improves the linearization accuracy of the EKF and provides significant improvements over EKF estimates [4, 5]. An alternative to Kalman filtering based approaches is the particle filter (PF)—a purely probability based estimator. Unlike the EKF and UKF, PF is immune to nonlinearities and the presumption of Gaussian noise [6]. Therefore it yields superior results at the expense of increased computational requirements. The scope for particle filter-based estimator can be considerably expanded given the increasing availability of performance computing resources and high fidelity measurements from PMUs with good sampling rates.

1.2. Dynamic State Estimation Assisted Out-of-Step Detection for Generators

The results of DSE can be used to develop an application for synchronous generators, specifically, Out of Step (OOS) protection. The state-of-the-art methods for OOS still use algebraic variables – voltage and/or current. In contrast, we show that OOS can be performed using DSE. While the approach requires the use of a PMU, it enables direct estimation/observation of the angular variables during power swings unlike traditional methods where this variable is directly unobservable. An out-of-step (OOS) event occurs when a generator (or a coherent group) exhibits unstable power swings triggered by system disturbances which may potentially lead to loss of synchronism between the unit(s) and the rest of the system. The prevalent methods for OOS relay tuning are based on monitoring the rate of change and the trajectory of the positive impedance. Since the problem of detecting the angle separation is projected into another space, it will require substantial amount of system stability studies under different scenarios to determine the optimal relay parameters. In this dissertation, a DSE-based method is proposed that calls for the most direct form of stability assessment: by monitoring the angular difference between machine's rotor angle

and the phase angle of the voltage at the high-voltage (HV) side of the step-up transformer. This provides a direct indication of the OOS conditions without making any simplifying assumptions, and using local measurements.

1.3. Dynamic State Estimation Using Dual-filtering

Additionally, this dissertation develops a technique that allows DSE even under imperfect or partially unknown models for the excitation subsystem. It is shown that the method can be used to detect loss of excitation (LOE), an event that can severely undermine system stability. The particle filter is modified to treat the field voltage as an unknown input which is sequentially estimated along with the other dynamic states. The proposed method is able to provide reasonable tracking results for the dynamic states and the field voltage simultaneously and rapidly tracks minor excitation loss due to exciter internal failure while maintaining selectivity.

1.4. Dynamic State Estimation Assisted Application in Wide Area Measurement System

Wide Area Measurement Systems (WAMS) utilize measurements of several system variables from geographically dispersed locations and most commonly used for system monitoring and control. It enables the monitoring of the transmission system over a large area. Wide area monitoring, protection, and control system refers to using WAMS information and applying control actions from a control center to remote sites. Such systems are targeted to utilize aggregated local data to prevent the propagation of a disturbance and widespread outages. This dissertation applies the syncrophasor measurements and estimated generator dynamics to one of the EMS application-event detection. Power blackouts over the world have shown that power systems, although carefully planned and protected, suffer from unforeseen events triggering instability. Such events often include misoperations of protective relays that result in unintended line trips, load shedding and generation trip, which severely challenges the integrity of the system. Sometimes, these misoperations go unchecked because global knowledge about actual system conditions is lacking. In order to make the control actions more reliable, a new set of detection tools and analytical schemes are developed based on wide area monitoring, protection and control system. Disturbance data from PMUs have been used for identifying different disturbance events. One of the disadvantages of this method is that it is purely data-driven. There is no physical basis to understand or correlate which feature is most affected by which disturbance event. In contrast, a different method based

on energy functions is proposed in this dissertation. Any event or a disturbance in the system will leave a signature (like a fingerprint) in WAMS datasets. Such a signature is actually buried in the components that constitute the energy function for the system. The trick is in determining which (among the numerous) components of the energy function is sensitive, or reflective of the corresponding disturbance. The components of an energy function depend on bus voltages that can be measured directly and network parameters, as well as several internal state variables of generators. The proposed PF-based estimator enables us to continuously track the internal state variables and hence the construct the energy function components. The new approach is completed by monitor the sensitivity of specific energy function components to detect and classify events.

The increases in the volume of the data has to be accommodated by communication networks while honoring the timing requirements for wide area monitoring, control and protection applications. This requires careful analysis of two factors: the latencies introduced by the communication network and the Phasor Data Concentrator (PDC) - the entity responsible for time alignment of PMU data to ensure the measurements are synchronized. It has been shown that variable latencies up to tens of milliseconds can be tolerated for several wide area applications. However, there are certain scenarios where the latencies can build up to hundreds of milliseconds [7] (e.g. communication system error correction and data re-transmission). A PDC commonly is in charge of aggregate data from multiple channels, when the transmitted data is lost in one channel (or more than one channel) and retrieval is requested and performed, the time consumption of arrival at PDC side can be significantly prolonged. As long as the waiting time threshold is not exceeded, PDC will not forward any new data. Generally, the end-to-end latency is affected by the network, transport, data link and the physical layer. Variability of the latency is subject to several non-deterministic factors. Given the diversity in communication channels, routing protocols, and the competition for increased data throughput subject to finite link capacities, it is suggested in this dissertation that the latencies that actually occur in these systems can be dynamic. A transport delay model is used to account for continuously varying latencies in communication systems, a PDC model is proposed for time synchronization subject to time varying latencies. A power oscillation monitoring application with standard modal analysis tools is utilized to study the impact of dynamic latency.

1.5. Dissertation Organization

This dissertation is organized as follows: the background for the dynamic state estimation problem and application based on the estimated dynamics are introduced in the first chapter; the second chapter develops the particle filter-based method to solve the DSE problem considering detailed models for synchronous generators in a multi-machine setting; the third chapter discusses a new out-of-step detection approach based on the estimated rotor angle by a particle filter-based estimator. The fourth chapter develops the DSE method under partially unknown models; the fifth chapter introduces a novel method for event detection in a wide area sense, by utilizing the synchrophasor information from PMUs as well as the estimated dynamics; the sixth chapter examines the effect of dynamic latency for WAMS applications, and the last chapter concludes this dissertation.

2. A PARTICLE FILTER FOR DYNAMIC STATE ESTIMATION IN MULTI-MACHINE SYSTEMS WITH DETAILED MODELS

This chapter is based on the work "A particle filter for dynamic state estimation in multi-machine systems with detailed models," *IEEE Transactions on Power Systems*, vol. 30, no. 6, pp. 3377-3385, Nov 2015 (doi: 10.1109/TPWRS.2014.2387792). The authors of the paper are Yinan Cui[1] and Rajesh G. Kavasseri.

2.1. Introduction

Dynamic State Estimation (DSE) in the context of a synchronous machine refers to the problem of estimating and dynamically tracking the states of a synchronous generator and associated control units given a model of the system dynamics and measurements of physical variables [8]. PMU-assisted DSE is the key enabler for emerging paradigms such as the so called "setting-less" protection [9] where potential applications for DSE are discussed. The extended Kalman filter (EKF) [6] provides a natural starting point since the DSE is a nonlinear filtering problem. The feasibility of EKF for DSE was reported in [10]. Because the EKF relies on linearization, both the accuracy of estimates and the tuning of the EKF strongly depend on the accuracy of linearization. The unscented Kalman filter (UKF) improves the first order accuracy of the EKF and provides significant improvements over EKF estimates. The work in [11] shows that the UKF improves the estimation accuracy compared to the EKF. A decentralized DSE scheme has been proposed in [5] and tests have been implemented thoroughly on a multi-machine system. In a single machine infinite bus (SMIB) setting, the EKF and UKF have also been proposed in [12] and [13] respectively. In [13], input mechanical power (from the prime mover) and field voltage are assumed to be accessible to PMUs while paper [12] estimates the field voltage as well as the the generator states.

An alternative to Kalman filtering based approaches is the particle filter - a purely probability based estimator. Unlike the EKF and UKF, the particle filter is immune to nonlinearities and yields superior results at the expense of increased computational requirements, [6]. However,

[1] Yinan Cui was the first author and responsible for writing the manuscript and applying simulation tests. Dr. Rajesh G. Kavasseri served as the proofreader and gave recommendations and guidance on drafting the paper.

the scope for particle filter-based estimation can be considerably expanded given the increasing availability of performance computing resources and high fidelity measurements from PMUs with good sampling rates. A particle filter (PF) considering the classical generator model is reported in [14] and extended in [15] to cover a generator model with transient dynamics, again in a SMIB setting. In [15], the mechanical power (assumed noise-free) is estimated using a lower-pass filter and the field voltage is estimated with pseudo-dynamic model which eliminates the fast dynamics from the exciter. The results also demonstrate that the particle filter would diverge when the sampling rate of the measurement is lower than the frequency of implementation of iteration.

In this paper, we show that the particle filter is suitable for DSE in a much more general case and can provide superior results (compared to UKF) at the expense of increased computational resources. Specifically, we include: (a) detailed models for synchronous generators - where the transient and subtransient dynamics are represented, (b) dynamic models for the excitation (IEEE DC1A, DC2A, AC5A) and prime mover components (steam and hydro) and (c) consider a multi-machine setting (the IEEE-14 bus system).The estimation accuracy of the proposed particle filter is compared with the UKF for several case studies. The rest of this paper is organized as follows. Sec. 2.2 presents the relevant background on particle filters. Sec. 2.3 describes the dynamic models and Sec. 2.4 describes how DSE is achieved with particle filters. The main results are presented in Sec. 2.5 along with evaluation/discussion in Sec. 2.6. The conclusions are noted in Sec. 2.7.

2.2. Particle Filtering Method

A discrete time state representation of the system dynamics is assumed of the form:

$$x_k = f_k(x_{k-1}, u_{k-1}, n_{k-1}) \tag{2.1}$$

where the system state at step k x_k is a function (possibly nonlinear, represented by f) of the previous state x_{k-1}, system input u_{k-1} and n_{k-1}, which is an $i.i.d$ (independent and identically distributed) system process noise. The objective of the filter is to estimate the state x_k recursively based on the system representation along with the measurements function, given by:

$$z_k = h_k(x_k, u_k, m_k) \tag{2.2}$$

where measurement z_k is a function (possibly nonlinear, represented by h) of the state x_k, input u_k and m_k, which is an $i.i.d$ measurement process noise sequence.

From a Bayesian perspective, the state x_k can be recursively calculated if measurements up to step k are accessible. The PF is a filtering technique which implements Bayesian tracking using Sequential Monte Carlo method, in which case the posterior density function is approximated by a set of weighted randomly generated samples. As the number of samples increases, the posterior density function provides a closer approximation to the true representation (optimal Bayesian solution). The density function is represented by:

$$p(x_{0:k}|z_{0:k}) \approx \sum_{j=1}^{N} w_k^j \Delta(x_{0:k} - x_{0:k}^j) \tag{2.3}$$

where $x_{0:k}$ is the set of all states up to step k, $z_{0:k}$ the set of measurements up to step k, Δ the delta function, $x_{0:k}^j (j = 1, \ldots, N)$ a set of particles, N the number of particles and w_k^j a set of weights for particles chosen by Importance Sampling (IS) normalized such that $\sum_j w_k = 1$ [16]. A common problem with IS is degeneracy.

A suitable measurement of the degeneracy is the effective sample size (ESS) (small value would indicate severe degeneracy), which is introduced in [17]:

$$ESS = \frac{N}{1 + Var(\hat{w}_k^j)} \approx \frac{1}{\Sigma_{j=1}^{N}(w_k^j)^2} = \widehat{ESS} \tag{2.4}$$

where $Var(\hat{w}_k^i)$ is the variance of the true weights, which is practically impossible to obtain. The approximation $\widehat{ESS}$ is often used.

It is shown in [18] that the variance of the importance weights can only increase (stochastically) over time. Therefore, most of the particles would have negligible corresponding weights, which means only a few particles will actually contribute to the estimation. One of the methods to overcome this undesirable problem is resampling.

The fundamental objective of resampling is to substitute those particles with negligible weights by drawing new samples from an approximated posterior density function such that the new sample would have equal weights. Among all the resampling methods, systematic resampling is often preferred because of its computational simplicity, good empirical performance [19] and

efficiency [17]. We implement systematic resampling method for particle filtering in this paper. The general particle filtering algorithm is summarized as follows:

2.2.1. Initialization of The Filter

The system states are initialized with steady-state value at step $k = 0$, N particles are randomly generated based on the initial value for each system state:

$$\begin{cases} \mathbf{x}_0 = \mathbf{x}_0^* \\ x_p^j = x_{p0} + \varepsilon^j \quad p = 1, \ldots, l \end{cases} \tag{2.5}$$

where $\mathbf{x}_0$ is the system initial state vector, $\mathbf{x}^*$ the steady-state values (or the expected value) of the states, x_p^j is a support particle, x_{p0} is a state in $\mathbf{x}_0$, l is the number of system states and ε^j is a scalar randomly drawn from the known pdf of ε.

2.2.2. System Dynamics Propagation

At step $k = 1, \ldots, L$, *a priori* (denoted by "$-$") estimate of particles is calculated using (2.1) with knowledge of last step system input and *a posterior* estimate of particles (denoted by "$+$"):

$$x_k^{j-} = f_k(x_{k-1}^{j+}, u_{k-1}, n_{k-1}^j) \quad j = 1, \ldots, N \tag{2.6}$$

where process noise n_{k-1}^j is randomly generated based on the known pdf of n_{k-1}.

2.2.3. Weights Generation

If the measurement function with respect to system states (particles) and inputs and pdf of the measurement noise are known, then the conditional probability of the particle x_k^{j-} can be evaluated after the the measurement is received at step k. The associated weight w_k^j of particle x_k^{j-} is equal to the probability of measurement vector $\mathbf{z}_k$, which equals to the corresponding vector measured values $\mathbf{z}_k^*$, given that the state x_k is assumed to be equal to the particle x_k^{j-}, denoted by $P[\mathbf{z}_k = \mathbf{z}_k^* | x_k = x_k^{j-}]$. Generally, the measurement noise vector $\mathbf{m}_k$ is normal distributed ($\mathbf{m}_k \sim N(0, R)$, R is measurement covariance matrix). Therefore, as introduced in [6], the weights can be obtained by:

$$w_k^j = P[\mathbf{z}_k = \mathbf{z}^* | x_k = x_k^{j-}] = P[\mathbf{m}_k = \mathbf{z}_k^* - \mathbf{h}(x_k^{j-})]$$

$$\propto \frac{1}{\sqrt{R(2\pi)^d}} exp(\frac{-[\mathbf{z}_k^* - \mathbf{h}(x_k^{j-})]^t R^{-1} [\mathbf{z}_k^* - \mathbf{h}(x_k^{j-})]}{2}) \tag{2.7}$$

where d is the dimension of measurement vector $\mathbf{z}_k$ and $\mathbf{h}$ represents a measurement function vector. If the above function is implemented to all the particles, then both sides of the representation are equal to each other.

After getting all the associated weights, a normalization is applied to make sure the summation of conditional probability equals to one:

$$\mathbf{w}_k = \frac{\mathbf{w}_k}{\Sigma_{j=1}^N w_k^j} \tag{2.8}$$

where $\mathbf{w}_k$ is the weight vector at step k.

2.2.4. Particles Resampling

Based on systematic resampling method, if $\widehat{ESS}$ in (2.4) is less than a certain threshold value $\widehat{ESS}_{Th}$, new particles for step k will be sampled based on the normalized weights. The following steps would be implemented for each particle $x_k^{j-}(j = 1, \ldots, N)$:

- Generate a random number u, where $u \sim U(0, 1)$
- Find an integer r such that $\Sigma_{i=1}^{r-1} w_k^i < \frac{j-1+r}{N} \leq \Sigma_{i=1}^{r} w_k^i$
- Assign the corresponding values to *a posterior* particle: $x_k^{j+} = x_k^{r-}$
- Set all the weights equal: $w_k^j = \frac{1}{N}$

2.2.5. State Estimation

Since *a posterior* particles $x_k^{j+}(j = 1, \ldots, N)$ at step k are distributed based on the pdf $p(x_k|z_k)$, the state x_k could be estimated simply by calculating the algebraic mean of the particles:

$$x_k \approx \sum_{j=1}^{N} x_k^{j+} w_k^j = \frac{1}{N} \sum_{j=1}^{N} x_k^{j+} \tag{2.9}$$

2.3. Dynamic Models

While detailed models for synchronous machines can extend up to the fourteen-th order model [20], several transients related to the system network/machine stator usually decay very

rapidly and the influence caused by those transients could be neglected [21]. Here, we represent dynamics up to the subtransient level and consider the following synchronous machine model (for notations, please see [22]):

$$\begin{aligned}
\dot{\delta}_i &= 2\pi f_0(\omega_i - \omega_0) \\
\dot{\omega}_i &= \frac{1}{H_i}(T_{m_i} - T_{e_i} - D_i\omega_i) \\
\dot{E}'_{d_i} &= \frac{1}{T'_{qo_i}}(-E'_{d_i} - (X_{q_i} - X'_{q_i})i_{q_i}) \\
\dot{E}'_{q_i} &= \frac{1}{T'_{do_i}}(E_{fd_i} - E'_{q_i} + (X_{d_i} - X'_{d_i})i_{d_i}) \\
\dot{E}''_{d_i} &= \frac{1}{T''_{qo_i}}(E'_{d_i} - E''_{d_i} - (X'_{q_i} - X''_{q_i})i_{q_i}) \\
\dot{E}''_{q_i} &= \frac{1}{T''_{do_i}}(E'_{q_i} - E''_{q_i} + (X'_{d_i} - X''_{d_i})i_{d_i})
\end{aligned} \tag{2.10}$$

where i is the synchronous generator index ($i = 1, 2, \ldots, m$), δ the rotor angle, f_0 the nominal frequency, ω_0 the nominal synchronous speed, ω the rotor speed, H the inertia constant, T_m the mechanical torque, T_e the electrical torque across the air gap (approximately equal to the real power, $T_e \approx P_e$) and E_{fd} the output voltage of the exciter. E'_d and E'_q are dq components of internal voltage behind a transient reactance ($E' = V_s + jX'_dI_s$); E''_d and E''_q are dq components of internal voltage behind a subtransient reactance ($E'' = V_s + jX''_dI_s$) [23]; V_s is the terminal voltage and I_s is the stator current.

As mentioned in the last section, our work does not require (or assume) that the quantities T_m and E_{fd} are accessible through the PMUs. Therefore, these two states are treated as system states and tracked by the estimator. To setup a more general study, IEEE DC1A, DC2A and AC5A excitation systems [24] are considered for different generators. If the transient gain reduction unit is not required (since Power System Stabilizer (PSS) is applied to the excitation system and assumed to be measurable), the voltage regulator and exciter for synchronous machines could be expressed as follows:

$$\begin{aligned}
\dot{V}_{R_i} &= \frac{1}{T_{A_i}}(K_{A_i}(V_{PSS_i} + V_{ref_i} - |V_{s_i}| - V_{f_i}) - V_{R_i}) \\
\dot{E}_{fd_i} &= \frac{1}{T_{E_i}}(V_{R_i} - K_{E_i}E_{fd_i})
\end{aligned} \tag{2.11}$$

where V_R is the voltage output of a voltage regulator, V_{PSS} the measured PSS signal, V_{ref} the reference terminal voltage magnitude, V_{f_i} the output of the excitation system stabilizer and $|V_{s_i}|$ the stator voltage magnitude (also treated as terminal voltage magnitude). Other notations are defined in the Appendix.

We simplify ESS for different excitation systems as:

$$\dot{V}_{f_i} = \frac{1}{T_{f_i}}(K_{f_i}\dot{E}_{fd_i} - V_{f_i}) \tag{2.12}$$

or

$$\dot{V}_{f_i} = \frac{1}{T_{f_i}}(K_{f_i}\dot{V}_{R_i} - V_{f_i}) \tag{2.13}$$

Equation (2.12) is applied to DC1A and DC2A systems while equation (2.13) is to the AC5A system.

A general steam turbine with no reheater and governor models [25] (a faster response to a perturbation) is considered for the prime-mover control system. The speed governor is in boiler leading mode of control, which leads to a unit boiler pressure approximately [26]. Automatic generation control is applied with integral control (load frequency control(LFC)). Neglecting the speed relay process, the prime-mover dynamics is represented by:

$$\begin{aligned}
\dot{P}_{s_i} &= -(\frac{1}{R_{p_i}}\dot{\omega}_i + K_{L_i}(\omega_i - \omega_0)) \\
\dot{P}_{go_i} &= \frac{1}{T_{sm_i}}(P_{s_i} + P_{ref_i} - P_{go_i}) \\
\dot{T}_{m_i} &= \frac{1}{T_{CH_i}}(P_{go_i} - T_{m_i})
\end{aligned} \tag{2.14}$$

where P_s is the power change after the droop and LFC unit, R_p the permanent droop, P_{go} the gate opening signal and P_{ref} the mechanical power reference.

We also include hydraulic turbine and governor equivalent models for stability studies [25,27] in prime-mover control system. The speed governor is modeled as a PI controller, we neglect the transient droop compensation, power error goes through the permanent droop. We apply the approximate linear model for hydro-turbine for the sake of generality. The model is represented

by:

$$\begin{aligned}
\dot{P}_{s_i} &= K_{p_i}\dot{\omega_{err}} + K_{i_i}\omega_{err} \\
\dot{P}_{go_i} &= \frac{1}{T_{sm_i}} K_{sm_i}(P_{s_i} - P_{go_i}) \\
\dot{T}_{m_i} &= \frac{2}{T_{w_i}}(P_{go_i} - T_{w_i}\dot{P_{go_i}} - T_{m_i})
\end{aligned} \tag{2.15}$$

Where

$$\omega_{err} = (\omega_0 - \omega_i) - R_{p_i}(Te_i - P_{ref_i})$$

P_s is the output of PI controller in speed governor, R_p the permanent droop, P_{ref} the mechanical power reference, P_{go} the gate opening signal and T_w the water time constant.

Physical limits on the excitation and prime-mover variables in (2.11), (2.14) (2.15) are accounted by:

$$\begin{aligned}
V_{R_i,min} \leq V_{R_i} \leq V_{R_i,max} \\
0 \leq P_{go_i} \leq P_{go_i,max}
\end{aligned} \tag{2.16}$$

Since stator transients are neglected, the stator voltage equation neglecting resistance is given by:

$$\begin{aligned}
V_{d_i} &= E''_{d_i} - X''_{q_i} I_q \\
V_{q_i} &= E''_{q_i} + X''_{d_i} I_d
\end{aligned} \tag{2.17}$$

We assume that the states in each estimation step are in quasi-steady state for dynamic estimation, and therefore, it is appropriate to use algebraic equations to model the interconnecting of transmission network. Therefore, the multi-machine system model can be represented by (2.10) - (2.15), which subject to (2.16), (2.17) and network algebraic constraints (A.1) (see Appendix for details).

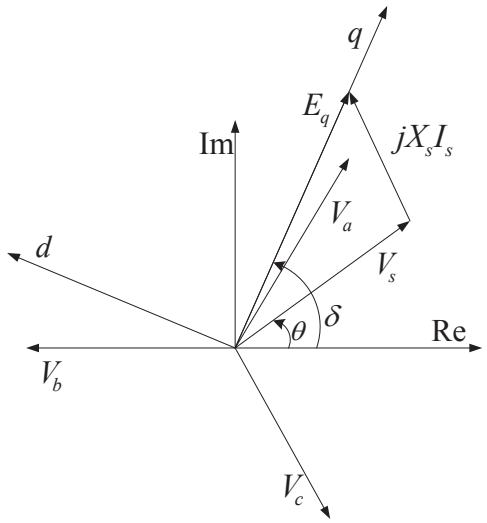

Figure 2.1. A quasi-static phasor diagram for a synchronous generator with d-axis leading.

According to the phasor diagram shown in Fig. 2.1, rotor angle δ is defined as the phase angle of q-axis component of generator internal voltage behind a reactance ($E_q = V_s + jX_qI_s$). Assuming the terminal voltage is measurable from a PMU denoted by $V_s = |V_s|\angle\theta$, stator voltage components in dq reference of frame can be obtained as:

$$\begin{aligned} V_{d_i} &= |V_{s_i}|sin(\theta_i - \delta_i) \\ V_{q_i} &= |V_{s_i}|cos(\theta_i - \delta_i) \end{aligned} \tag{2.18}$$

Substituting corresponding terms in (2.17), stator current components are given by:

$$\begin{aligned} I_{d_i} &= \frac{|V_{s_i}|cos(\theta_i - \delta_i) - E''_{q_i}}{X''_{d_i}} \\ I_{q_i} &= \frac{E''_{d_i} - |V_{s_i}|sin(\theta_i - \delta_i)}{X''_{q_i}} \end{aligned} \tag{2.19}$$

Hence, the real power and reactive power from machine i can be calculated by:

$$\begin{aligned} P_{g_i} &= V_{d_i}I_{d_i} + V_{q_i}I_{q_i} \\ Q_{g_i} &= V_{d_i}I_{q_i} - V_{q_i}I_{d_i} \end{aligned} \tag{2.20}$$

2.4. Particle Filter based Dynamic State Estimation

From the models developed in Sec. 2.3, the overall system model can be represented by:

$$\begin{aligned} \dot{\tilde{\mathbf{x}}}_\mathbf{i} &= \mathbf{f_i}(\tilde{\mathbf{x}}_\mathbf{i}, \tilde{\mathbf{u}}_\mathbf{i}, \tilde{\mathbf{n}}_\mathbf{i}) \\ \tilde{\mathbf{z}}_\mathbf{i} &= \mathbf{h_i}(\tilde{\mathbf{x}}_\mathbf{i}, \tilde{\mathbf{u}}_\mathbf{i}, \tilde{\mathbf{m}}_\mathbf{i}) \end{aligned} \tag{2.21}$$

subject to inequality and equality constraints:

$$\begin{aligned} \mathbf{g_{i,min}} \leq \mathbf{g_{1,i}}(\tilde{\mathbf{x}}_\mathbf{i}) \leq \mathbf{g_{i,max}} \\ \mathbf{0} = \mathbf{g_{2,i}}(\tilde{\mathbf{x}}_\mathbf{i}, \tilde{\mathbf{u}}_\mathbf{i}) \end{aligned} \tag{2.22}$$

The state vector $\tilde{\mathbf{x}}_\mathbf{i}$ is defined as:

$$\begin{aligned} \tilde{\mathbf{x}}_\mathbf{i} &= [x_{1_i}\ x_{2_i}\ x_{3_i}\ x_{4_i}\ x_{5_i}\ x_{6_i}\ x_{7_i}\ x_{8_i}\ x_{9_i}\ x_{10_i}\ x_{11_i}\ x_{12_i}]^T \\ &= [\delta_i\ \omega_i\ E'_{d_i}\ E'_{q_i}\ E''_{d_i}\ E''_{q_i}\ V_{R_i}\ E_{fd_i}\ V_{f_i}\ P_{s_i}\ P_{go_i}\ T_{m_i}]^T \end{aligned}$$

The input vector $\tilde{\mathbf{u}}_\mathbf{i}$ is defined as:

$$\tilde{\mathbf{u}}_\mathbf{i} = [u_{1_i}\ u_{2_i}\ u_{3_i}\ u_{4_i}\ u_{5_i}]^T = [|V_{s_i}|\ \theta_i\ |I_{s_i}|\ \phi_i\ V_{PSS_i}]^T$$

The output vector $\tilde{\mathbf{z}}_\mathbf{i}$ is defined as:

$$\mathbf{z_i} = [z_{1_i}\ z_{2_i}] = [P_{g_i}, Q_{g_i}]^T$$

where i is the i-th generator in the system, $\mathbf{f_i}$ describes the system dynamics referring to (2.10) - (2.15), $\tilde{\mathbf{n}}_\mathbf{i}$ the process error, $\mathbf{h_i}$ the measurement representation referring to (2.18) - (2.20), $\tilde{\mathbf{m}}_\mathbf{i}$ the measurement error, $\mathbf{g_{1,i}}$ the controller limits referring to (2.16), $\mathbf{g_{i,min}}$ and $\mathbf{g_{i,max}}$ the lower and higher bounds of voltage regulator output and gate opening signal, $\mathbf{g_{2,i}}$ the system network equation algebraic constraints (A.1). We assume that each generator bus in the system is equipped with a PMU which provides measurements of terminal voltage and current, namely, $|V_s|\angle\theta = V_s$ and $|I_s|\angle\phi = I_s$. The power injections from generators are accessible through the PMUs, we neglect the

equality constraints in (2.22) in this study. All the phasor measurements are from positive sequence calculation using raw three-phase phasors produced by discrete Fourier transform [28]. We assume that real and reactive power outputs of the generators are also available from the PMUs since they be computed from the measurable phasors.

We notice that differential equations (2.11) - (2.13) of x_{7_i}, x_{8_i} and x_{9_i} (V_{R_i} and E_{fd_i} and V_{f_i}) do not involve any other system states except for themselves, and hence variables in measurement equations (2.18) - (2.20) do not include these states. Direct propagation under these circumstance may degrade the estimates. In order to relate these measurements to corresponding states and apply importance sampling to generate the weights, we replace $|V_{s_i}|$ in (2.11) with a function of current phasor measurement and the states. Similar to the transformation performed in (2.18) for voltage term, the *dq* current components are given by:

$$\begin{aligned} I_{d_i} &= |I_{s_i}| sin(\phi_i - \delta_i) \\ I_{q_i} &= |I_{s_i}| cos(\phi_i - \delta_i) \end{aligned} \tag{2.23}$$

The magnitude of the terminal voltage is then represented by:

$$\begin{aligned} |V_{s_i}| = ([x_{5_i} - X''_{q_i} u_{3_i} cos(u_{4_i} - x_{1_i})]^2 \\ + [x_{6_i} + X''_{d_i} u_{3_i} sin(u_{4_i} - x_{1_i})]^2)^{\frac{1}{2}} \end{aligned} \tag{2.24}$$

To simplify the procedure of recursive dynamic tracking of the system states, Euler's method is applied on (2.21) to obtain the state sequence representations. In general, the difference equation is formulated approximately by:

$$x_k^{j-} = x_{k-1}^{j+} + [f(x_{k-1}^{j+}, u_{k-1}) + n_{k-1}]\Delta t \tag{2.25}$$

where Δt is the estimation sampling time interval, k the estimation step and j the particle number.

2.5. Results

The performance of the proposed PF and UKF are tested and evaluated on IEEE 14-bus system [29], shown in Fig. 2.2. Each generator contributes 12 state variables which yields a total of

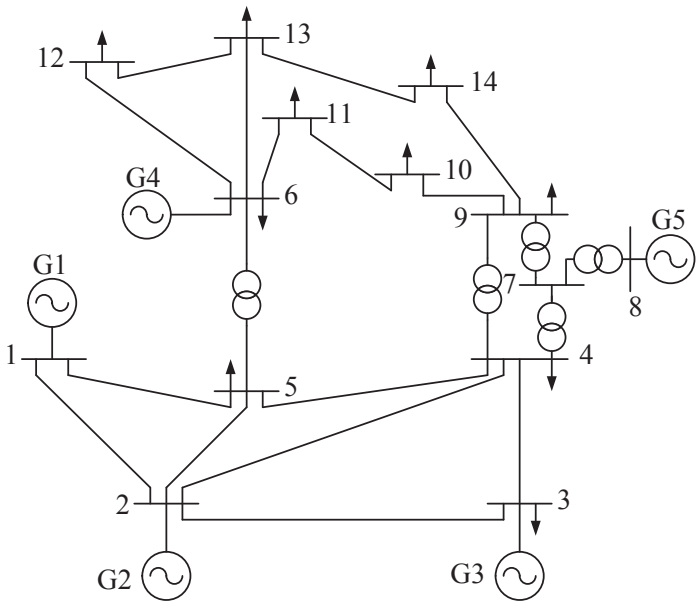

Figure 2.2. IEEE 14-bus system.

60 state variables for the entire system. According to a NERC report [30], most PMUs are capable of sampling 30 measurements per second. In this study, the measurement sampling rate for all test cases is 30 measurements/s. In our DSE algorithm, we assume that the system output remains unchanged for each estimation step between every two PMUs' measurement sampling instants. We simulate the system in MATLAB/Simulink, and synthesize the corrupted measurements from the noise-free simulation results. We assume the simulation results are true values of system states. The sampling rate of DSE is 200 steps per second. In accordance with the IEEE standard for synchrophasors [31], the maximum allowable total vector error (TVE) is 1%. Therefore, measured values (voltage, current, real and reactive power) in (2.21) would have 1% Gaussian white noise; 1% Gaussian white noise would be added to each equations in (2.21) as process noise. The PF and UKF are both initialized with steady state values (obtained from pre-disturbance system condition). Two universally constant values are defined as: $f_0 = 60\ (Hz)$, $\omega_0 = 1.0\ (pu)$

In the following subsections, tracking results are presented for three cases listed below:

- Temporary (6 cycles) 3 phase to ground fault on line;
- 3 phase to ground fault on line section: followed by permanent loss of line
- Sudden addition of load at bus

The simulations were carried out on a desktop PC with 3.4 GHz, core i7 processor and 8G memory. In all simulations that present estimation results, the true states are represented by dashed lines, while solid lines represent UKF estimations and dotted lines are PF estimations. Note that in many cases, the PF and UKF, both very closely track the true states and hence the lines overlap. However, there are exceptions when the hydro-turbine models are considered. These are noted separately and discussed. In what follows, we first present the dynamic tracking results for three cases.

2.5.1. Temporary (6 cycles) 3 Phase to Ground Fault on Line

a three-phase ground fault is applied on line connecting bus #2 and bus #3 near bus #2, at $t = 6.0$ (s). 6 cycles later, at $t = 6.1$ (s), the fault is cleared without opening the circuit breakers, the network configuration is unchanged and the post-disturbance system is stable. Generator #2 (denoted by G_2) hosts a hydro-turbine and a DC1A exciter. The measurements for G_2 are displayed in Fig. 2.3 (the measurements for G_4 and other generators in the following cases are similar). Estimation results by PF and UKF for G_2 and its excitation controller are illustrated in Fig. 2.4. Number of particles for PF for each state variable in this study case is 50. Estimation results from 10 randomly selected trials out of 100 for the mechanical torque for $G2$ are shown in Fig. 2.5. Generator #4 (denoted by G_4) is equipped with a steam-turbine and an AC5A exciter. Estimation results by PF and UKF for G_4 and its excitation controller are illustrated in Fig. 2.6. 10 (randomly selected) trials of mechanical torque estimation are shown in Fig. 2.7.

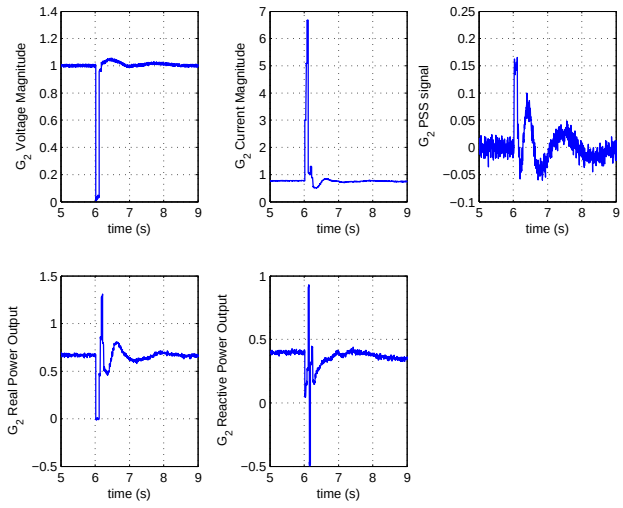

Figure 2.3. Measured quantities for G_2.

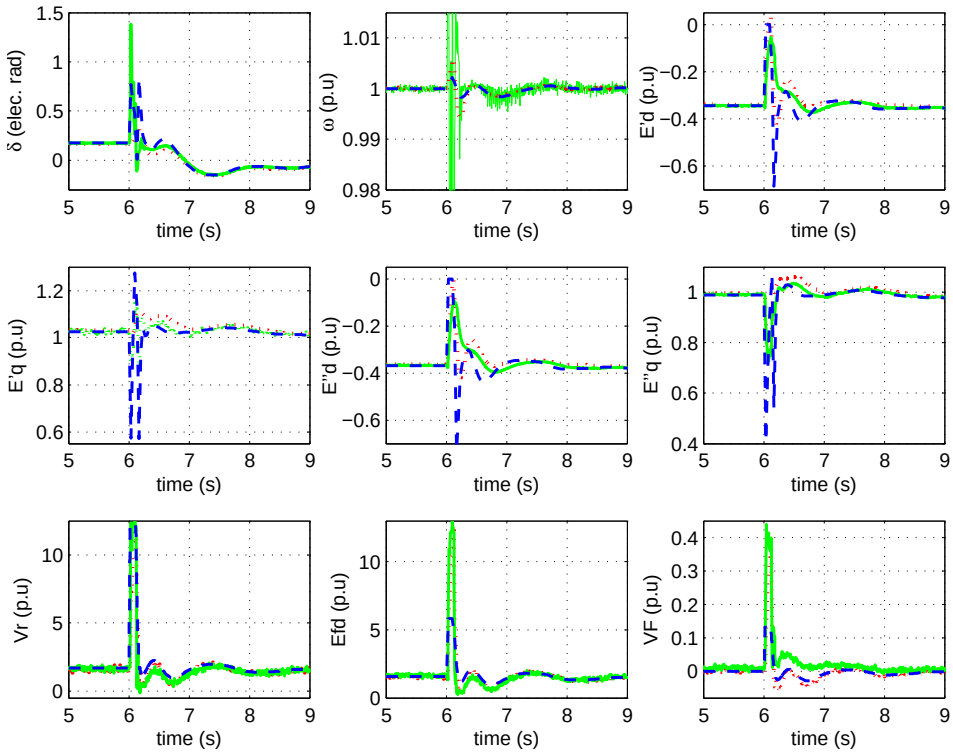

Figure 2.4. Estimation results for G_2 and its exciter by PF and UKF.

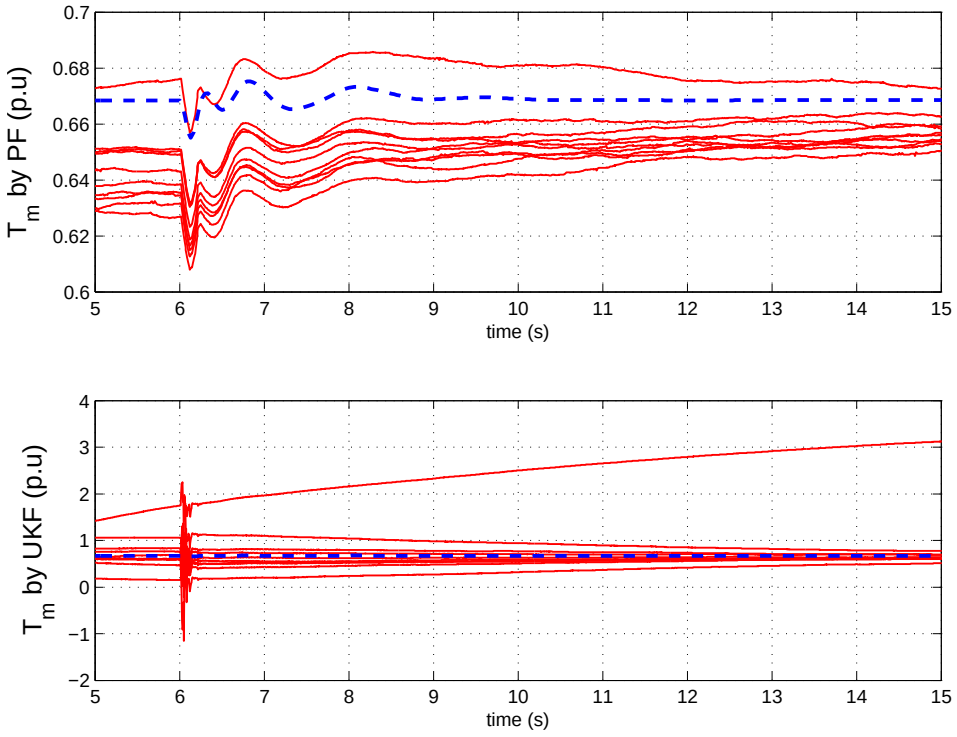

Figure 2.5. Estimation results of mechanical torque for G_2 (hosts a hydro-turbine) by PF and UKF in 10 trials, dashed line is the actual mechanical torque.

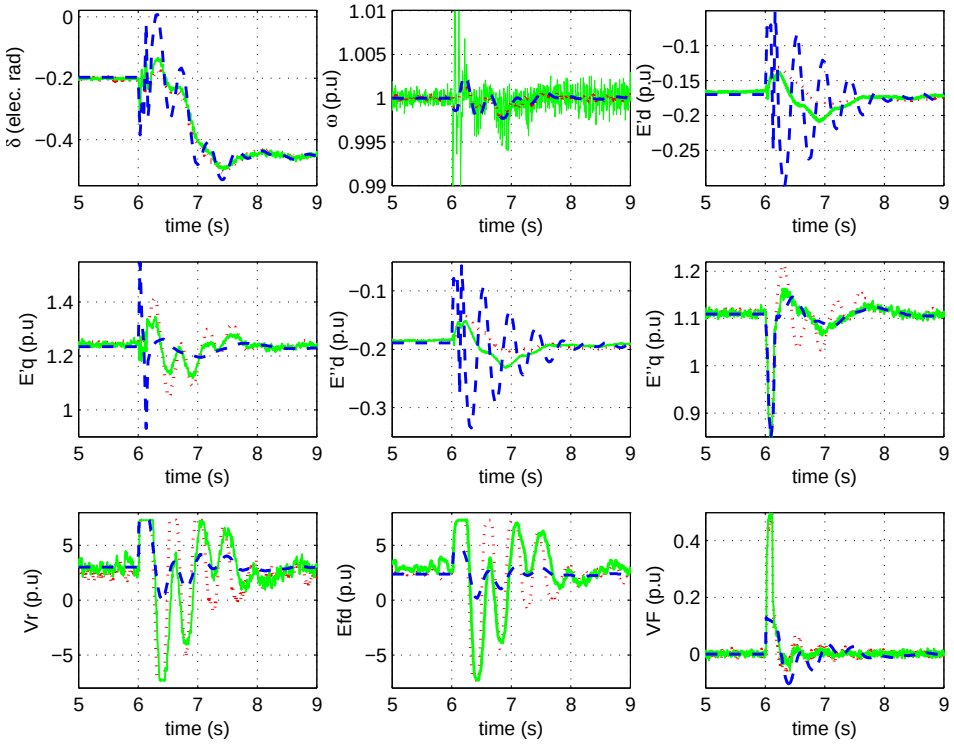

Figure 2.6. Estimation results for G_4 and its exciter by PF and UKF.

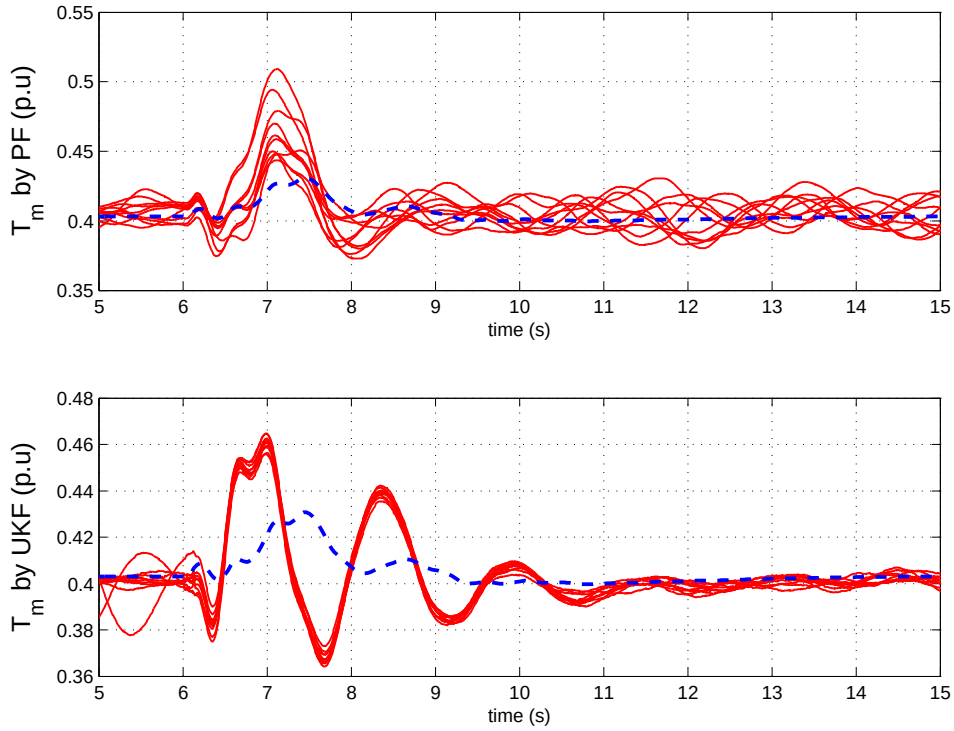

Figure 2.7. Estimation results of mechanical torque for G_4 (hosts a hydro-turbine) by PF and UKF in 10 trials, dashed line is the actual mechanical torque.

2.5.2. Three-phase Ground Fault with Permanent Line Trip

A three-phase ground fault is applied on line connecting bus #2 and bus #3 near bus #2, at $t = 6.0$ (s). 9 cycles later, at $t = 6.15$ (s), the fault is cleared by opening the circuit breakers equipped at both end of the line, the network configuration is changed and the post-disturbance system is stable. Generator #1 (denoted by G_1) is equipped with a steam-turbine and an AC5A exciter. Estimation results by PF and UKF for G_1 and its excitation controller are illustrated in Fig. 2.8. The true states values from simulation results are given by dashed lines while solid lines represent UKF estimations and dotted lines are PF estimations. Number of particles for PF for each state variable in this study case is 50.

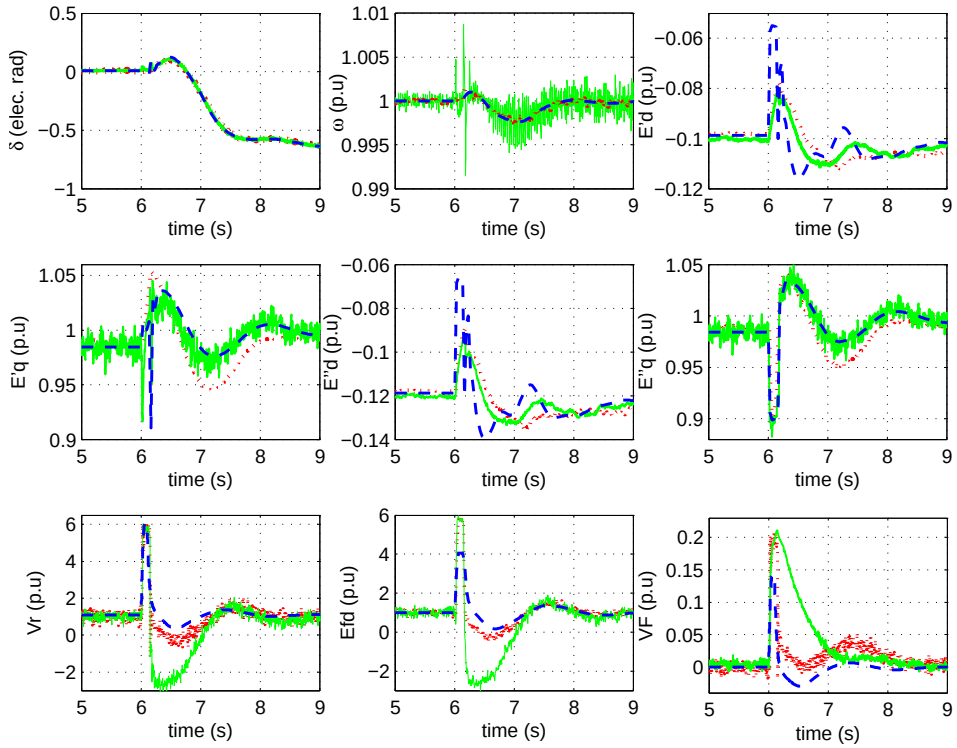

Figure 2.8. Estimation results for G_1 and its exciter by PF and UKF.

2.5.3. Temporary Additional Load

A temporary load addition at bus #12 is considered. The load (constant impedance voltage dependent) is applied at bus #12 at $t = 6.0$ (s), and the load is dropped at $t = 11.0$ (s).The network configuration is unchanged and the post disturbance system is stable. Generator #3 (denoted by G_3)is equipped with a hydro-turbine and a DC2A exciter. Estimation results using PF and UKF

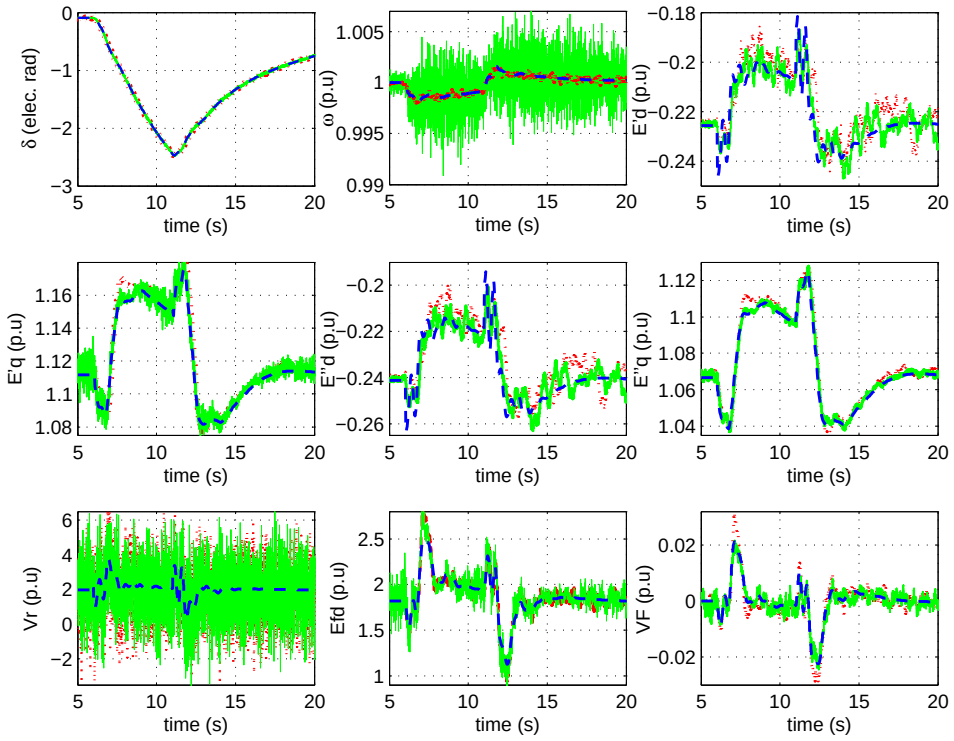

Figure 2.9. Estimation results for G_3 and its exciter by PF and UKF.

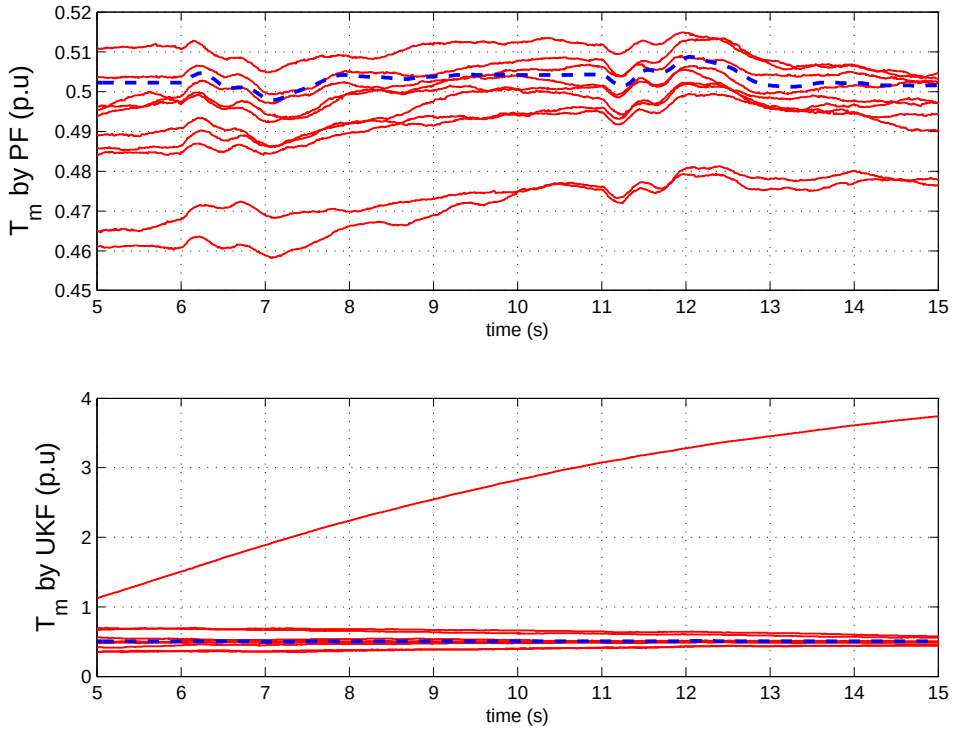

Figure 2.10. Estimation results of mechanical torque for G_3 by PF and UKF in 10 trials, dashed line is the actual mechanical torque.

and its controllers are illustrated in Fig. 2.9. The true states values from simulation results are given by dashed lines while solid lines represent UKF estimations and dotted lines are PF estimations. Number of particles for each state variable is 50 in this case. Estimation results (10 trials out of 100) of mechanical torque for G_3 are shown in Fig. 2.10.

Mean values and corresponding standard deviations of RMSD in 100 trials are evaluated, comparison of performance between PF and UKF in Case 2.5.1, 2.5.2 and 2.5.3 are summarized in Fig. 2.11.

2.6. Evaluation and Discussion

In general, we note (from Figs. 2.4, 2.6, 2.8 and 2.9) that PF and UKF are all able to track the states with comparable performance for different classes of disturbances. To evaluate their performance further and explore the stochastic features more carefully, we implement 100 tracking trials. The tracking performance of PF and UKF are presented in Fig. 2.11 which depicts the standard deviation and mean for both filters, for all the state variables.

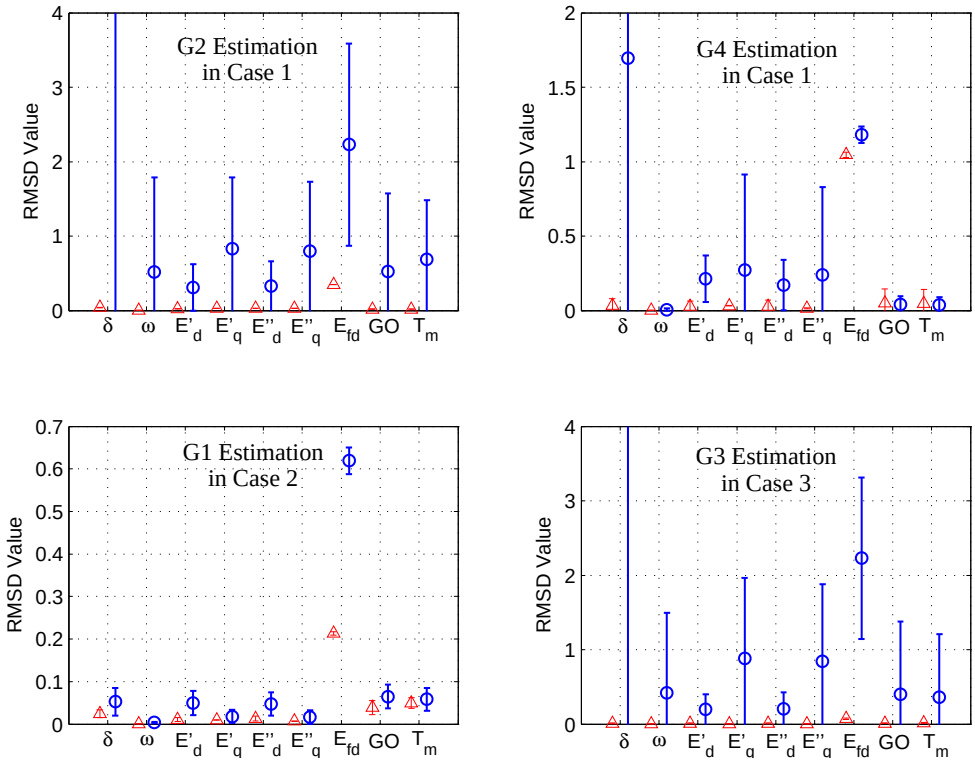

Figure 2.11. RMSD of selected 9 states for $G1$ to G_4 by PF (upward-pointing triangle) and UKF (circle). Bars refer to standard deviations. The out-of-range results are due to the divergences of the filter in the trials

Table 2.1. RMSD of estimation results of G_5 and its controllers for different choices of N (number of particles)

	Number of Particle			
State Variable (UKF rmsd)	50	80	120	150
δ_5 (0.0319)	0.0336	0.0259	0.0238	0.0233
ω_5 (0.0028)	0.0005	0.0003	0.0003	0.0002
E'_{d_5} (0.0276)	0.0263	0.0215	0.0204	0.0200
E'_{q_5} (0.0097)	0.0145	0.0142	0.0126	0.0133
E''_{d_5} (0.0295)	0.0295	0.0240	0.0226	0.0222
E''_{q_5} (0.0097)	0.0122	0.0109	0.0099	0.0103
V_{R_5} (0.5910)	0.5668	0.5672	0.5679	0.5658
E_{fd_5} (0.1919)	0.1145	0.1162	0.1210	0.1204
V_{f_5} (0.0135)	0.0128	0.0129	0.0128	0.0128
P_{s_5} (0.4235)	0.4380	0.4244	0.4223	0.4222
P_{go_5} (0.0118)	0.0536	0.0301	0.0177	0.0121
T_{m_5} (0.0098)	0.0482	0.0255	0.0144	0.0097

Fig. 2.11 shows that while the performance of both filters are comparable for Case 2, the PF significantly outperforms the UKF for the Cases 1 and 3. We also note from Figs.2.5, 2.10 and 2.11 that for cases involving an approximate linear model for the hydroturbine, the PF again, provides better tracking performance over the UKF. For the cases that involve a steam-turbine, both filters provide comparable performance as seen from Fig. 2.7.

Next, we consider the "best-case" result for the UKF (i.e. when the UKF's performance is better than the PF) and study the effect of increasing the number of particles. The higher the number of particles N, the better the accuracy and higher the computational burden. The results are summarized in Table. 2.1 (It should be noted that the run-time times are hardware dependent). This set considers Generator #5 (denoted by G_5), which hosts a steam-turbine, an AC5A type exciter under Case 2.5.3. From Table 2.1, we find that by increasing the number of particles N , the tracking performance of the PF can attain parity or outperform the UKF. For both filters, we also note that the RMSD is relatively higher for V_R and E_{fd} compared to the other state variables. This may be attributed to the high gain in the excitation control loop. However, one should also note that: (a) PF may not generate more accurate estimation in some cases for

some state variables(e.g. E'_{q_5} in Table. 2.1), (b) the PF may also diverge in certain circumstances and (c) the computational burden for PF increases with the number of particles. For computation time comparison of EKF, UKF and PF with different number of particles, please note [32], though the results there consider a lower dimension nonlinear system. It should be pointed out that the PF inherits limitations typical to nonlinear filters such as: (a) sensitivity to initial conditions: poor choices may cause divergence, (b) convergence speed: the higher the number of particles, the faster the convergence and vice-versa: lower number of particles leads to a sluggish convergence and (c) model parameter errors will influence the filter performance.

2.7. Conclusion

A particle filter is developed to dynamically estimate the states for a detailed synchronous generator model in a multi-machine setting. The filter allows the inclusion of dynamic subcomponents - mainly the exciter and the prime mover control system. While the three IEEE standard exciters, a general steam turbine and a hydro-turbine model are considered here, the proposed model can be readily extended to include other dynamic models for these components. The filter factors available measurements from the generator (real/reactive power outputs) and exploits phasor information (both stator voltage and current) from PMUs assumed available at the generator bus. The performance of the proposed filter is compared with the unscented Kalman filter and assessed by determining the RMSD of the estimation. Dynamic simulations indicate that the proposed filter tracks the states with reasonable accuracy and reliability for three classes of disturbances, for several trials on the IEEE 14-bus system. The proposed filter: (i) does not require the field voltage and mechanical power from PMUs and (ii) allows the inclusion of dynamic blocks such as the exciter and prime mover and (iii) is illustrated on a multi-machine setting. With advances in computational resources, the work suggests the potential of using particle filters for (near) real-time security and control applications.

3. DYNAMIC STATE ESTIMATION ASSISTED OUT-OF-STEP DETECTION FOR GENERATORS USING ANGULAR DIFFERENCE

This chapter is based on the work "Dynamic State Estimation Assisted Out-of-Step Detection for Generators Using Angular Difference," *IEEE Transactions on Power Delivery* (doi: 10.1109/TPWRD.2016.2615594). The authors of the paper are Yinan Cui[1], Rajesh G. Kavasseri and Sukumar M. Brahma.

3.1. Introduction

An out-of-step (OOS) event occurs when a generator (or a coherent group) exhibits unstable power swings triggered by system disturbances which may potentially lead to loss of synchronism between the unit(s) and the rest of the system. Such events are traditionally detected by dedicated OOS relays. The prevalent methods for OOS relay tuning are based on monitoring the rate of change and the trajectory of the positive sequence impedance, and require substantial amount of system stability studies under different scenarios to determine the optimal relay parameters [33]. The most secure scheme for determining OOS condition is Trip-On-Way-Out in single and double blinder schemes [33]. However, the security comes at the cost of extended time for pole slipping, subjecting the generator to pulsating torque, high rotor iron currents, and stator currents potentially higher than short-circuit rating [34, 35]. This is considered as one of the gaps in secure detection of OOS conditions [36].

The other drawback of currently used OOS schemes is that the angular separation between breaker contacts is high when it is opened after detection of OOS condition, bringing extensive stress to the breaker. Unless the breaker is dedicated for an OOS duty, the tripping will be intentionally postponed until the angle separation goes beyond a certain value (e.g. 270°). This is tentatively achieved by the Trip-On-Way-Out in single and double blinder schemes [33], but at the cost of extended period of pole-slipping, and associated stresses on generator.

[1]Yinan Cui was the first author and responsible for writing the manuscript and applying simulation tests. Dr. Rajesh G. Kavasseri and Dr. Sukumar M. Brahma served as the proofreader and gave recommendations on drafting the paper.

It would therefore be useful if the detection of unstable swings can be made earlier without losing security. Considerable research work has been done to predict the swing stability beforehand such that trip could be initiated at a small angular value, so operation of both breaker and generator can be made safer. The equal-area criterion in time domain using only local power output information is studied in [37]. A state-plane method is applied to detect loss of synchronism in [38]. OOS protection for distributed generation unit using equal-area criterion is examined in [39]. While the equal-area criterion is a widely used basis to devise settings for the OOS relay, some of the underlying assumptions behind it include: (a) the single-machine-infinite bus (SMIB) treatment for the generator under consideration with the rest of the system abstracted as an infinite bus, (b) neglecting flux decay, effects of high-gain automatic voltage regulators (AVR), supplementary controllers such as power system stabilizers, and frequency control loops. When such effects are modeled in a general multi-machine scenario, unstable swings could occur beyond the first swing (time frame of interest can extend to 10 seconds and above) [40] and include multiple dynamic modes. Since these traditional assumptions are restrictive, alternate methods have been proposed to improve OOS schemes. Neural network and fuzzy logic based methods are reported in [41] and [42] respectively to predict the stability of the swings in real-time using synchrophasor information to enhance OOS detection. A standing limitation of such soft-computing based methods is the requirement for large training sets which involves extensive case studies. A Lyapunov-based direct method is applied to on-line monitoring of rotor angle stability [43] using the maximum Lyapunov exponent to predict an OOS condition. A real-time loss-of-synchronism detection algorithm using energy function analysis is proposed in [44]. While these methods show satisfactory performance, they do require wide-area information to make centralized decisions which elevates the complexity for *local* OOS protection.

Dynamic state estimation (DSE) is an emerging paradigm exploiting the computation power and availability of synchrophasor measurements to estimate the internal variables of generators. The dynamic nature and off-nominal-frequency behaviors of the power systems necessitates the need for DSE in both normal and emergency situations [45]. Initial work for wide-area and decentralized system control applications based on DSE has been reported in [46] and [47]. Since DSE provides firsthand information of the internal states (e.g rotor angles and flux-linkages) of the generators, it is intuitive to investigate the possibility of DSE-assisted protection applications for generators.

In this paper, we use DSE to propose an approach that calls for the most direct form of stability assessment: by monitoring the angular difference between machine's rotor angle and the phase angle of the voltage at the high-voltage (HV) side of the step-up transformer. This provides a direct indication of the OOS conditions without making any simplifying assumptions, and using *local* measurements. The other advantage of the proposed scheme is early prediction of marginally unstable swings by performing stability analysis on the angular difference if the the generator survives the first swing. We show that both DSE and instability prediction are possible in real time using available computing resources. We compare the proposed scheme with the Trip-On-Way-Out single-blinder approach and show that the scheme matches the security of this approach, while allowing early detection for OOS phenomena.

3.2. Rationale and Assumptions Behind the Conventional OOS Protection Relay

The OOS relay for a generator (device 78) is usually located at the terminal of the generator [35] as shown in Fig. 3.1, where $V_s\angle\phi$ and Z_{system} represent the system Thévenin equivalent (the other symbols are defined in the following section). The most widely-used OOS protection scheme attached to large generators [48] uses blinders (single or double) with a mho element, with sample characteristics as shown in Fig. 3.2. For the single-blinder scheme (left one in Fig. 3.2), the impedance has to enter the mho element from outside and then traverse both blinders ($B1$ and $B2$) to trigger a trip signal. The trip can be delayed until the impedance leaves the mho element [35]. For the double-blinder scheme, the OOS condition is detected when the impedance stays between the outer and inner blinders longer than a pre-set threshold. Determining the settings for these relays is based on careful stability studies to prevent operation during stable swings while tripping at an opportune moment when an unstable swing is interpreted. Single blinder scheme is easier to set and very secure in detecting OOS; however, it takes more time in detection.The double-blinder scheme

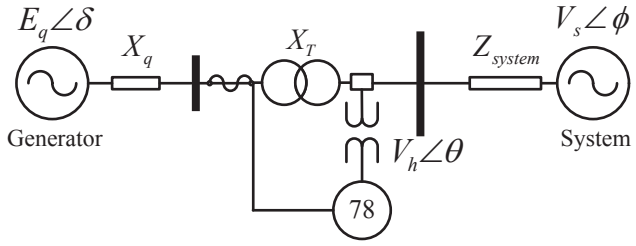

Figure 3.1. OOS protective relay (device 78) for a generator.

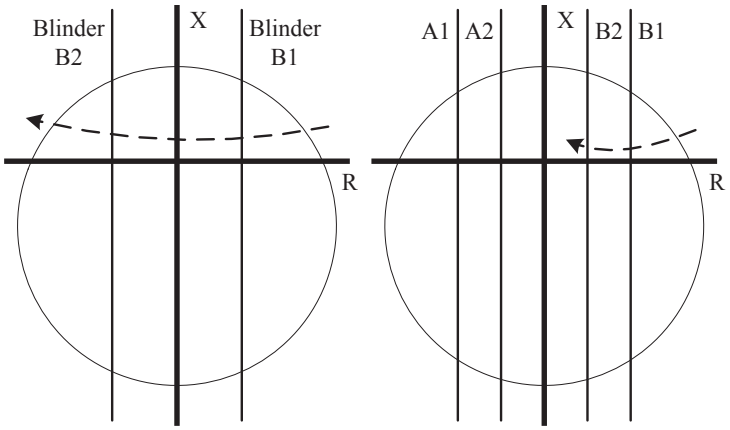

Figure 3.2. Typical operation logic of a OOS relay for a generator.

allows prompt operation, but determining the inner blinder ($B2$ in Fig. 3.2) settings requires very careful analysis; with poor choices leading to misoperation during stable swings. Since (falsely) tripping large generator units under stable swings can severely undermine system stability, the single-blinder scheme is generally preferred over the double-blinder scheme for OOS protection. The trip logic usually requires the impedance loci to traverse both blinders and then trip on either exiting the second blinder or the mho element.

The impedance seen by the distance relays during power swings has been well studied in [49]. Although the actual impedance loci can be more complex if AVR and governor effects are included, the theory approximately describes the behaviors during power swings and sets the foundation of convention OOS relay. It has been proved in [50] that decreasing apparent impedance magnitude implies increasing angular difference at the electrical center of a two-source model with equal voltage magnitude, [50]:

$$|\dot{Z}_m| = -\frac{X/4}{sin^2(\tilde{\delta}/2)}\dot{\tilde{\delta}} \tag{3.1}$$

where Z_m is the apparent impedance seen by the OOS relay, X, the total reactance between the two sources and $\tilde{\delta}$, the angular difference between the two sources.

Equation (3.1) indicates that diminishing values of the apparent impedance magnitude seen by the OOS relay is equivalent to an advancing angular difference $\tilde{\delta}$ before the electrical center is crossed. Since the angular difference is not available, relay 78 depends on the impedance mapping. However, since such mapping is made with simplifying assumption, extensive simulations of actual system-conditions are required for setting the relay. Therefore, accurate estimation of $\tilde{\delta}$ can provide a more generalized and dependable OOS protection. Such a scheme is described in the next section.

3.3. DSE-assisted OOS Detection Based on Angular Difference Monitoring

Due to the lack of phase angle information in the past, angle separations between the power system and generator was indirectly assessed using impedance measurements, as described in Section 3.2. Conventional OOS relays utilize the measured apparent impedance and pre-determined settings to detect a power swing, and initiate tripping when it is unstable. The availability of PMU measurements partially simplifies this task because the phase angle of the voltage phasor can be measured directly. Additionally, *internal* rotor angle (or power angle) of the machine could be derived or calibrated [51] based on the measurements, which has been adopted for generator modeling in voltage stability analysis [52]. However, the rotor angle of the generator is still not generally amenable to direct measurement and hence needs to be estimated. This is one of the key steps in the proposed approach outlined in this section. The overall scheme of the proposed approach is illustrated in Fig. 3.3. Components of the figure are explained now.

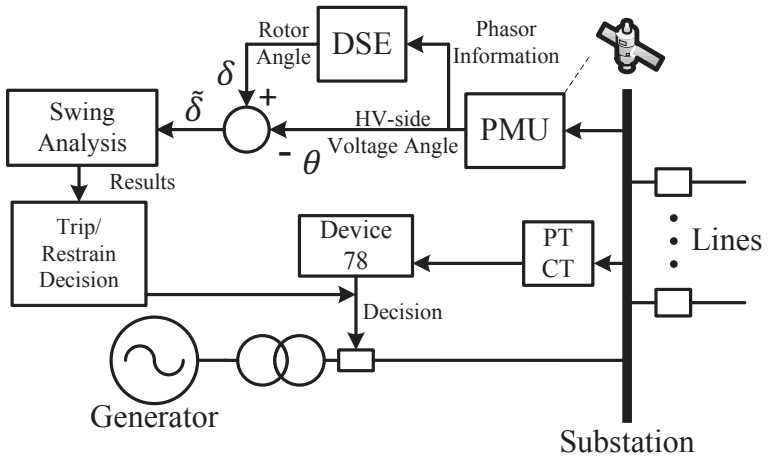

Figure 3.3. Block diagram of the OOS relaying scheme for a generator.

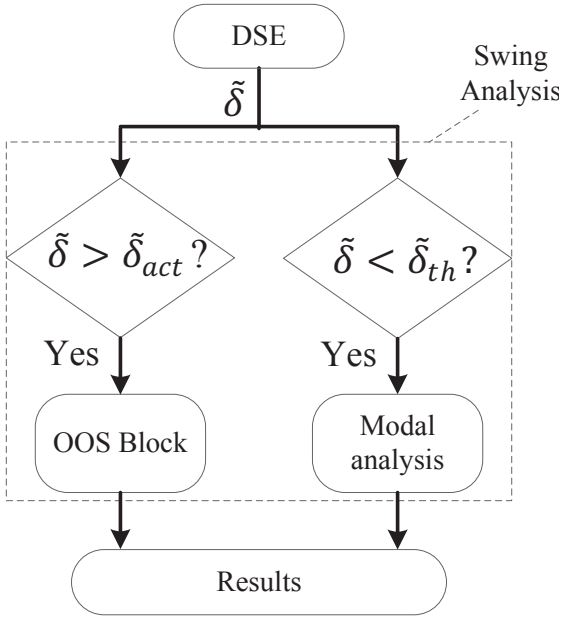

Figure 3.4. Processes in the swing analysis block.

1. Utilizing PMU measurements assumed available at the substation, we construct a particle filter (PF)-based dynamic state estimator (block *DSE* in Fig. 3.3). Based on the generator model and phasor information from the PMU, the filter generates estimates of the generator's internal dynamic states. For OOS protection, since we are interested in the swing dynamics, we focus on estimates of rotor angle δ. Formulation of PF-based estimator and reasons for its choice are described in section 3.3.1.

2. Swing analysis is performed based on the angular difference $\tilde{\delta}$ between rotor angle (δ) and voltage angle of HV-side of the transformer (θ) (block *Swing Analysis* in Fig. 3.3). This block is further explained in Fig. 3.4. $\tilde{\delta}_{act}$ (chosen to be 60°) serves as a threshold to flag the presence of a swing, and activate the OOS module. The purpose of this module is to trace the trajectory of a monotonically unstable swing. Once the swing is flagged, the observed $\tilde{\delta}$ is compared against a threshold to declare OOS. The threshold is set to $\tilde{\delta}_{th} = 120°$ - which is consistent with conventional relay settings [33,34]. Thus, in case of a monotonically unstable swing, this module will detect OOS using $\tilde{\delta}$, without needing to use the imperfectly converted impedance plane.

3. If the swing is marginally unstable, the generator may survive the first swing and $\tilde{\delta}$ may not cross $\tilde{\delta}_{act}$, and the OOS module may not be triggered. At this point, it would be useful to be able to determine quickly if this swing is stable or not. This is accomplished by the Modal Analysis block which provides the damping ratios associated with the swing mode. The angular difference $\tilde{\delta}$ is fed to the modal analysis tool (Matrix Pencils, in our case) to determine the damping factors of the swing dynamics. This helps early determination if the swing will be unstable or not. Matrix Pencils is briefly described in Section 3.3.2.

Results generated by either block are converted to trip/restrain decision and the breaker is commanded accordingly. It is to be noted that the breaker can also be actuated by the conventional OOS relay (78) as shown in Fig. 3.3, instead of recommending its replacement, we are proposing and evaluating an alternate method.

3.3.1. Estimation with Particle Filter

The use of a particle filter for DSE in the context of multi-machine systems is described in detail in [53]. A brief overview is presented here. The filter considers a discrete time representation of a nonlinear system given by:

$$x_k = f_k(x_{k-1}, u_{k-1}, n_{k-1}) \tag{3.2}$$

where the system state x_k at step k is a function of the previous state x_{k-1}, system input u_{k-1} and system process noise n_{k-1}. The filter is designed such that the state x_k can be estimated recursively based on the system model as well as the measurement model:

$$z_k = h_k(x_k, m_k) \tag{3.3}$$

where measurement z_k is a function of the state x_k and measurement model process noise m_k.

To solve the dynamic state estimation problem using a particle filter (PF), the posterior density at step k is approximated by:

$$p(x_k|z_{1:k}) \approx \sum_{j=1}^{N} w_k^j \Delta((x_k) - (x_k^j)) \tag{3.4}$$

where $z_{1:k}$ is a set of measurements available up to step k, Δ the delta function, $x_k^j (j = 1, \ldots, N)$ a set of particles, N the number of particles, w_k^j a set of weights. If we draw the particles x_k^j from a density $q(x_k|z_{1:k})$ (or *importance density*), which is easier to accomplish than drawing it from $p(x_k|z_{1:k})$, the importance sampling weight is given by:

$$w_k \propto \frac{p(x_k|z_{1:k})}{q(x_k|z_{1:k})} \tag{3.5}$$

This representation is further simplified as [6]:

$$w_k \propto P(m_k = z_k^* - h_k(x_k)) \tag{3.6}$$

where z_k^* is the obtained measurement at step k.

The steps of implementing PF for state estimation is summarized as follows:

- Initialize the particles $\{x_0^j, w_0^j\}_{j=1:N}$,
- Propagate the particles based on (3.2) at step k,
- Assign the corresponding weight to each particle based on (3.6),
- Normalize the weights using: $\mathbf{w}_k / \Sigma_{j=1}^N w_k^j$
- Resample a new set of particles from $\{x_k^j, w_k^j\}_{j=1:N}$ based on the likelihood of w_k^j (Resampling step)
- Obtain the estimated state by taking the mean of the particles.

Compared with other widely used DSE algorithms (extended Kalman filter (EKF) and unscented Kalman filter (UKF)), the PF is not restricted by model assumption (e.g probability distribution of measurement noise is Gaussian) and yields superior results on nonlinear/non-Gaussian systems at the expense of increased computational effort [6].

We use the same *6th-order model* [54] (or model 2.2) to represent the generator dynamics, the mathematical model in *per unit* is given by:

$$\begin{aligned}
\dot{\delta}_i &= 2\pi f_0 \Delta\omega_i, \\
\Delta\dot{\omega}_i &= \frac{1}{H_i}(P_{m_i} - P_{e_i} - D_i\Delta\omega_i), \\
\dot{E}'_{d_i} &= \frac{1}{T'_{qo_i}}(-E'_{d_i} - (X_{q_i} - X'_{q_i})i_{q_i}), \\
\dot{E}'_{q_i} &= \frac{1}{T'_{do_i}}(E_{fd_i} - E'_{q_i} + (X_{d_i} - X'_{d_i})i_{d_i}), \\
\dot{E}''_{d_i} &= \frac{1}{T''_{qo_i}}(E'_{d_i} - E''_{d_i} - (X'_{q_i} - X''_{q_i})i_{q_i}), \\
\dot{E}''_{q_i} &= \frac{1}{T''_{do_i}}(E'_{q_i} - E''_{q_i} + (X'_{d_i} - X''_{d_i})i_{d_i}).
\end{aligned} \tag{3.7}$$

where i is the generator index in a multi-machine system, $f_0 = 60Hz$ the nominal frequency, $\Delta\omega$ the speed deviation, E'_d and E'_q are dq components of internal voltage behind a transient reactance (X'_d) and E''_d and E''_q are dq components of internal voltage behind a subtransient reactance (X''_d). Definition of other constants in (3.7) can be found in [54].

In Fig. 3.3, a PMU is assumed available at the HV side of the step-up transformer providing us phasor measurements of voltage $|V_h|\angle\theta$ and current $|I_h|\angle\varphi$. Rotor angle δ is defined as the phase angle of the internal voltage ($E_q = \vec{V}_h + j(X_q + X_T)\vec{I}_h$) behind synchronous reactance X_q and step-up transformer reactance X_T. In addition, the measurements of the generator's field voltage (E_{fd}), mechanical power input (P_m) and power outputs (P_e and Q_e) are used. The state vector $\vec{\mathbf{x}}$, input vector $\vec{\mathbf{u}}$ and output vector $\vec{\mathbf{z}}$ in this paper are defined as:

$$\begin{aligned}
\vec{\mathbf{x}} &= [\delta,\ \omega,\ E'_d,\ E'_q,\ E''_d,\ E''_q] \\
\vec{\mathbf{u}} &= [|V_{hv}|,\ \theta,\ E_{fd},\ P_m] \\
\vec{\mathbf{z}} &= [P_e,\ Q_e]
\end{aligned} \tag{3.8}$$

3.3.2. Modal Analysis of Angular Difference

Since the oscillatory response involving inertial dynamics of generators includes several low frequency characteristic modes, typically in the range: $(0.2 \sim 0.7Hz)$ - corresponding to inter-area modes, or the local rotor modes in the range of $0.7 \sim 2Hz$ [21], the simplistic equal-area criterion may be inadequate, since stability could be lost even if the system survives the first swing after the disturbance. Modal analysis is a standard technique to identify the characteristic modes and their dampings from the dynamic response, thus serving as a tool to monitor stability. The basic principle is to represent an evenly sampled data set in terms of a weighted sum of exponentials from which the damping ratio can be extracted. While Prony analysis [55] has been customarily used in the past for online modal content analysis, we use Matrix Pencils [56] as an alternative, noting its robustness to noise. Some of the extracted modes with low or negative damping factor may result in false decisions of the stability. The procedure for modal analysis upon the angular difference in our study is as follows:

- We perform a modal analysis of the angular difference (estimated via Particle Filtering) using Matrix Pencils.
- From the modal analysis results, we determine the stability of rotor oscillations based on the damping factors of the local mode $(0.7 \sim 2Hz)$.

Simulation results are presented next to illustrate the proposed method and track its performance alongside the single blinder method.

3.4. Simulation Results

The proposed scheme is tested on the New England 10-generator system [57], which is shown in Fig. 3.5. For all test cases the measurement reporting rate of the PMU is set at a conservative value of 30 frames per second [51]. This was found suitable to complete all calculations required between two consecutive samples, based on the execution time of our code. All the phasor information (in complex form) is measured at the HV-side of the transformer and assumed to have 3% additive Gaussian white noise as measurement error. The phasor information is plugged into the PF-based estimator and all equations modeling the synchronous generator are assumed to have 1% additive Gaussian white noise as process error. We also assume that the system outputs stay unchanged for each PF estimation step between two consecutive PMUs' measurement sampling

instants. Note that PF operates with 80 (N) particles. Generally, the lager the number of particles, the higher the accuracy. The accuracy versus number of particles trade-off is discussed in detail in [53]. The generators are modeled accounting for subtransient dynamics [21]. The prime mover dynamics (steam-turbine governor) and the excitation system (IEEE DC1A) models are considered for each generator except for generator #10, which has constant excitation input. The impedance seen by the relays shown for all the cases are noise-free results. In the relay settings, the blinder distance for both sides are equal and based on a conservative value 120°, and the OOS relays are not responsible for cases where electrical centers reside on the system side. The size of the mho element is based on the recommendations from [48] and the settings are noted in Appendix. The results are shown for monotonically unstable and marginally unstable oscillatory swings. For numerous well defined stable swings, the proposed method is consistent with classical OOS operation with similar results. The simulation results show the estimated angular differences using PF/PMU and the impedance loci used by relay 78. It is to be noted that the breaker opening times considered in the simulation cases are unusually large and are chosen in order to generate the desired swing characteristics.

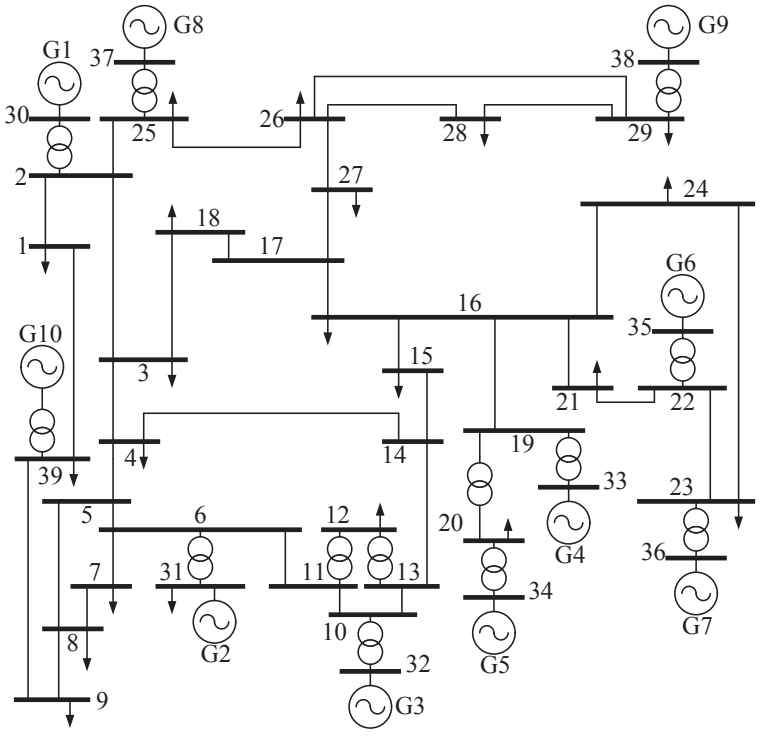

Figure 3.5. New England 10-generator 39-bus system.

3.4.1. Verifying the Security of the Proposed Method

3.4.1.1. Worst Stable Swing

A three-phase to ground fault occurs on line *25-26* at $t = 6s$. The faulted line is tripped and permanently removed by opening the circuit breaker at both ends of the line. The curves of angular difference ($\tilde{\delta}$) between rotor angle of generator #8 (denoted by G_8) and voltage angle of bus #25 for different clearing times are shown in Fig. 3.6. The worst stable swing is created by clearing the fault 1 cycle earlier than the unstable case, i.e., after 13 cycles.

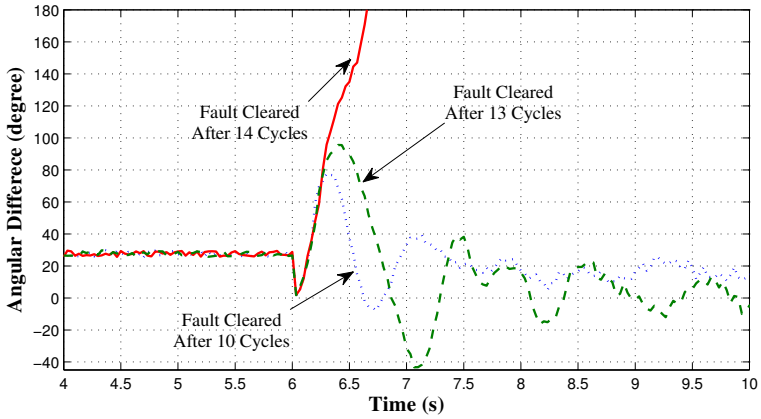

Figure 3.6. Angular difference curves for different clearing time.

The fault is cleared at $t = 6.217s$ (13 cycles after the fault), the stability is maintained after the first swing. Impedance seen by the OOS relay at the terminal of G_8, and the angular difference are illustrated in Fig. 3.7. The post fault impedance locus exits the mho element from the same quadrant it enters; the stable swing does not trigger any false trip. When $\tilde{\delta}$ crosses 60°, the OOS module is triggered, but since the value does not cross the 120° threshold, the module does not declare an OOS condition, consistent with the relay decision. Since the method is shown to work well for the worst stable swing, it also covers milder (stable) swings (which are not reported here)

.

3.4.1.2. Coordination with OOS Relay on the Transmission Line

A temporary three-phase to ground fault happens on line *22-23* close to bus #23 at $t = 6s$. The fault is self-cleared at $t = 6.25s$ (15 cycles later) without tripping the line. Generator #6 (denoted by G_6) and generator #7 (denoted by G_7) lose the synchronism with rest of the system

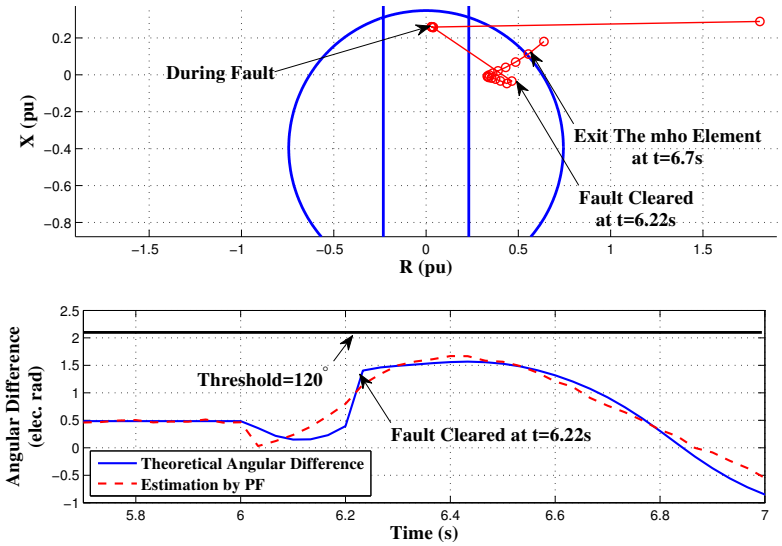

Figure 3.7. Impedance locus for the worst stable swing and estimated angular difference for G_8.

and together form a coherent group. Rotor angle estimations for generator 1 through 9 and angular differences for G_6 and G_7 are displayed in Fig. 3.8. In this case, the swing centers reside on the transmission lines, the proposed method is not supposed to respond to the disturbance. It was observed that though the OOS module was triggered for *G-6*, the proposed method did not generate a trip decision as $\tilde{\delta}$ did not cross the threshold. Thus, the decision made by the proposed method complies with the conventional relay as it does not interfere with the OOS protective relays on line *21-22* and line *23-24*.

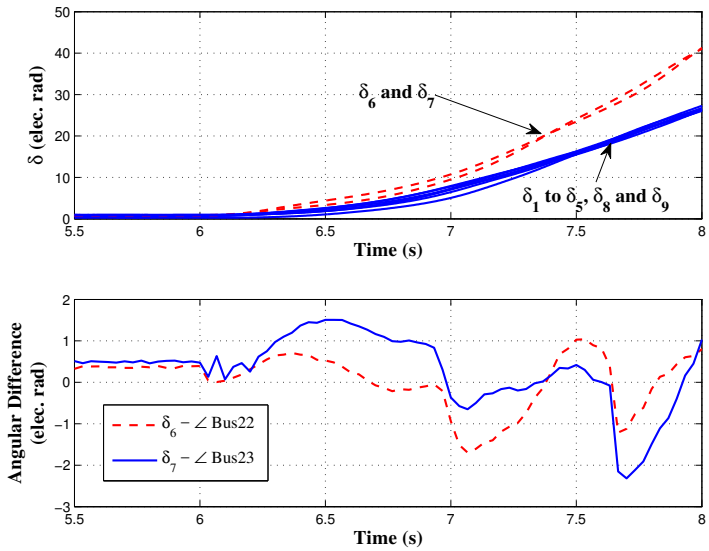

Figure 3.8. Generator's estimated rotor angles and angular difference for G_6 and G_7.

3.4.1.3. Performance During the Loss of Excitation Event

The occurrence a loss of excitation (LOE) event will force the generator to drain massive reactive power from the system. The decay of the field current will weaken the coupling between the rotor and the stator and eventually lead to an OOS condition [35]. An acceptable LOE protective relay for synchronous generators is an offset mho distance relay in single phase [58]. Considering the impact from stable swings and voltage regulator performance, we implement a two-zone scheme as proposed in [59]. The partial and complete LOE incidents are created by setting the field voltage for Generator #4 (denoted by G_4) 1.1 $p.u$ and 0 $p.u$ respectively (pre-fault value is 2.25 $p.u$). Impedance seen by the LOE relay for G_4 and the estimated angular difference for both cases are shown in Fig. 3.9 and 3.10. The results indicate the proposed approach correctly identifies the OOS condition for both partial and complete LOE cases and the operation is also consistent with the LOE relay which operates according to its corresponding zone time delay settings.

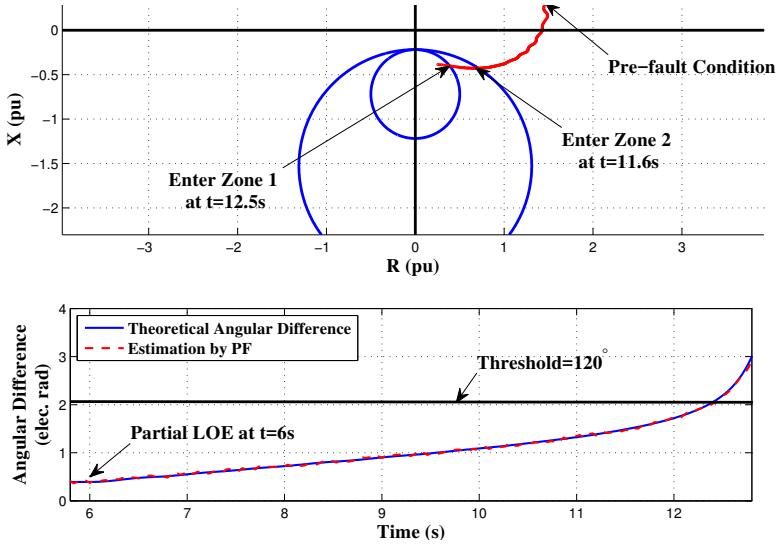

Figure 3.9. Partial LOE case: impedance locus seen by LOE relay and estimated angular difference for G_4.

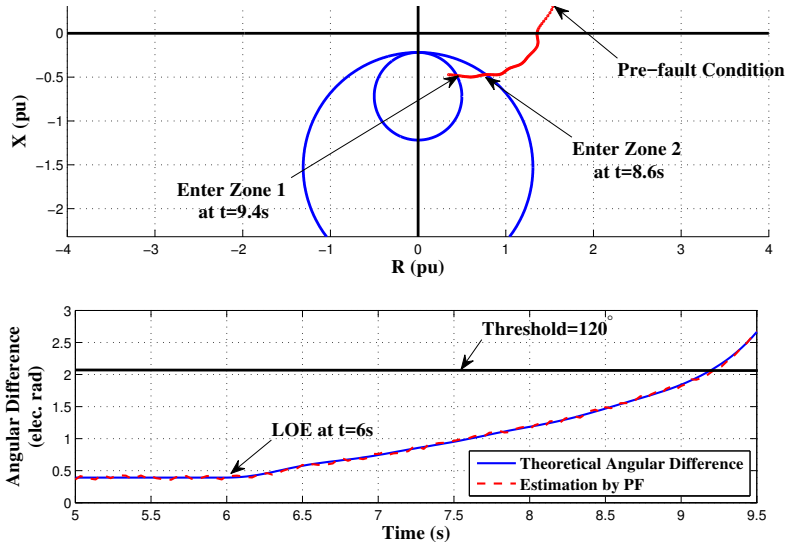

Figure 3.10. Complete LOE case: impedance locus seen by LOE relay and estimated angular difference for G_4.

3.4.2. Verification of Dependability of the Proposed Scheme and Advantages of the Predictive Feature

3.4.2.1. Detection of Monotonically Unstable Power Swings

Considering the same fault condition described in the "worst stable swing" case in Sec. 3.4.1.1, the fault is cleared $t = 6.233s$ instead (14 cycles after the fault) and stability is lost during the first swing as seen in Fig. 3.6. Generator #9 (denoted by G_9) and G_8 lose the synchronism with rest of the system and form two coherent groups individually. Angular difference between rotor angle of G_8 and voltage angle of bus #25 and impedance seen by the OOS relay at the terminal of G_8 are illustrated in Fig. 3.11. Considering the threshold of 120°, the suggestive tripping decision (at $6.467s$) by the proposed method abides by the actual relay decision (at $6.8s$). However, the breaker can be tripped at an early instant and also at a safe interruption angle (approximately 132° assuming 2-cycle breaker opening time). Clearly, for slower (unstable) swings, the proposed method will issue earlier alerts for potential threats compared to the conventional relay.

3.4.2.2. Detection of Marginally Unstable Power Swings

A temporary three-phase to ground fault is created on line *2-11* close to bus #2 at $t = 6s$. The fault is self-cleared at $t = 6.25s$ (15 cycles later) without tripping the line. Generator #2 (denoted by G_2) loses its synchronism due to the disturbance. The impedance seen by the OOS relay at G_2 are shown in Fig. 3.12. The swing trajectory exits the mho characteristics in the

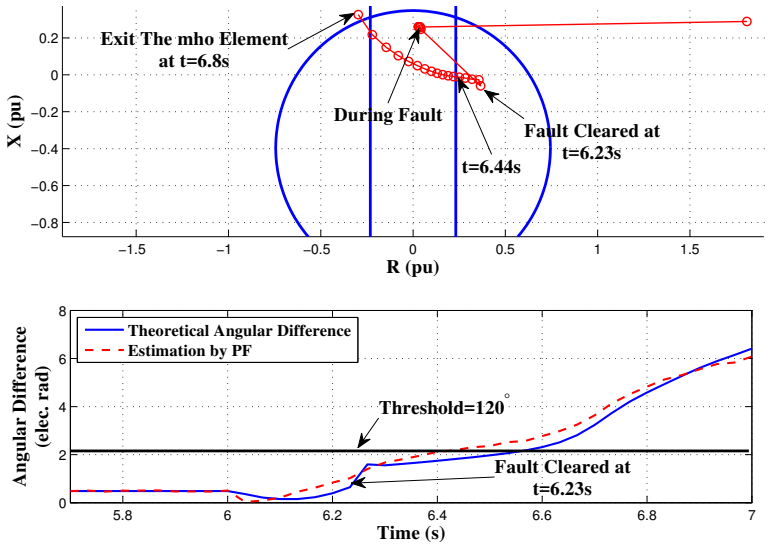

Figure 3.11. Impedance locus for the unstable swing and estimated angular difference for G_8.

vicinity of its intersection with the left-side blinder. The interruption angle at $t = 10.31s$ for the beakers is around 282° (assuming 2-cycle breaker opening time). Fig. 3.13 illustrates the angular difference between G_2 and voltage angle of bus #6 before loss-of-synchronism. We can notice that the peak values are below the pre-determined threshold $\pi/3$ ($elec.rad$), hence the OOS module is not enabled. The modal analysis tool which is active during the swing reports the damping ratios as shown in Table. 3.1. The tool continuously acquires the angular difference estimates and computes the damping ratio. The local mode (associated with the generator rotor dynamics) within $1 \sim 1.2Hz$ has a negative damping ratio throughout the analysis. As the minimum damping factor of any mode must be non-negative [60], the potential unstable swing can be identified as early as $t = 7.463s$. The conventional relay will trip at 10.28 s. The proposed method is able to detect this unstable swing much earlier compared to conventional method.

Table 3.1. Modal analysis results at different time

Report Time	**Frequency (Hz)**	**Damping Ratio (%)**
t=7.463s	1.096	-36
t=7.823s	1.192	-5.97
t=8.243s	1.202	-6.41
t=8.743s	1.259	-10.11

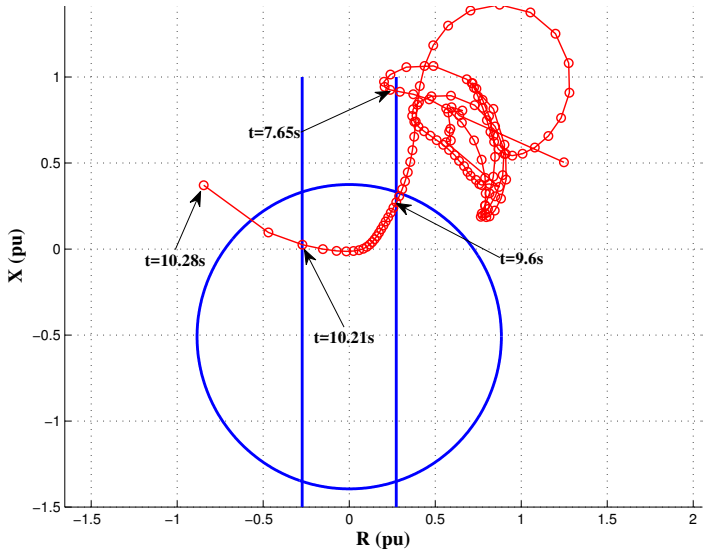

Figure 3.12. Impedance locus and relay characteristics at G_2 for the OOS condition.

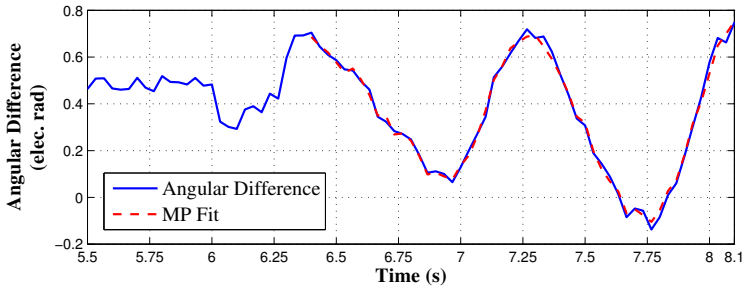

Figure 3.13. Angular difference between G_2 and voltage angle of bus #6 along with the reproduced curve.

3.4.3. Supervision of Relay Behavior

There is no reliable backup to OOS relay that will operate quickly if the swing locus goes through transformer or the generator impedance. Loss of field relay may pickup for OOS, but due to time delays it may not operate fast enough. As far as the distance backup relay on the generator is concerned it also may have a time delay and may not see the impedance going through the generator during OOS. Thus, the conventional OOS scheme can benefit from supervision.

We show that the proposed method is potentially useful in case the settings of a OOS relay are set incorrectly. For illustration, we assume there is a corrupted setting for the blinders, where they are placed with sub-optimal reach (indicated by dashed vertical lines) in Fig. 3.14. A three-phase to ground fault happens on line *6-11* at $t = 6s$. The faulted line is tripped and permanently

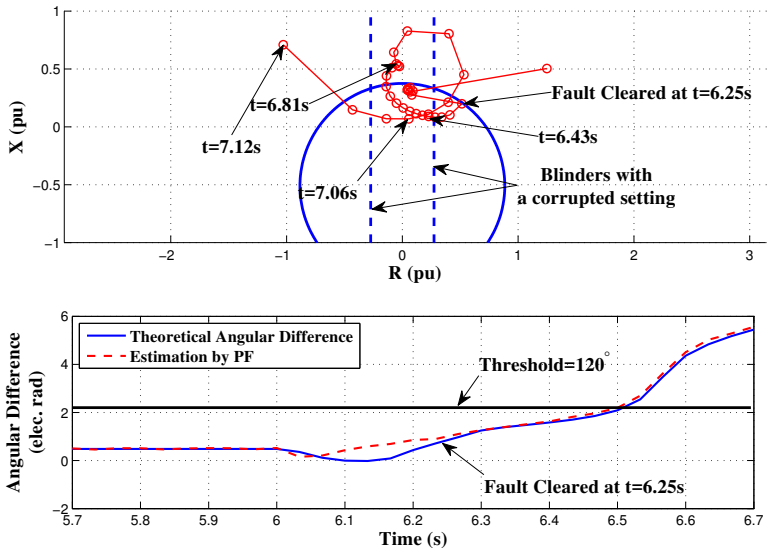

Figure 3.14. Impedance locus for the unstable swing and estimated angular difference for G_2.

removed at $t = 6.25s$. G_2 loses its synchronism due to the disturbance. Fig. 3.14 illustrates angular difference between rotor angle of G_2 and voltage angle of bus #6 and impedance seen by the OOS relay. Different from the test case in Sec. 3.4.2.1, we can see that conventional relay with corrupt settings detects the unstable swing after two pole slippings while the proposed approach is able to detect the unstable swing before the first pole slipping (around $t = 6.57s$). Such supervision can be advantageous in cases when the settings or the relay are compromised.

3.5. Discussion

The proposed method is tested on a multi-machine system and hence eliminates the need for establishing a two-source equivalent model (necessary for conventional relay setup), or simplifying assumptions of generator control. No wide-area information is needed. Hence the proposed method is completely independent of the system configuration, controls, or wide-area communications.

The proposed method brings more computational burden as the estimation of the rotor angle ought to be provided in real time. This means the whole procedure must be implemented between two consecutive PMU measurements. For 30 fps reporting rate, this time is $1/30 = 33ms$. The simulations demonstrated above are carried out on a desktop PC with *core i7* $3.4GHz$ processor and $8G$ memory. We use a *6th-order* model to describe the generator dynamics in PF. Time taken for different processes on this computer is: $7.1ms$ for PF to generate an estimate, and $6ms$ for MP to perform modal analysis. Since implementation on dedicated hardware will only make these processes faster, it is clear that the proposed method is compatible for real time implementation.

Note that the suggested detection timestamps are all postponed due to the inevitable time delays in sensing and processing time in PMU. Since the PMU is assumed to be at the generator bus, we assume the phasor measurements are directly fed to the DSE block, and not transmitted to and from a PDC, so the communication delays are ignored. According to IEEE C37.118.2-2011 [7], "delay in measurement is largely dependent on the processing window and filtering, which vary with the data reporting rate and the PMU class of service. Processing delays for calculating the measurement are generally very small compared with other delays." We assume that the time-stamp is associated with the center of the window, which means the delay due to windowing would be half the size of the window. We assume a P-Type PMU that typically has a 2-cycle window, meaning a delay of about $17ms$ for a $60Hz$ system. Adding filtering, PMU processing and transducer delays based on the table C.2 in IEEE C37.118.2-2011, the total delay in creating a PMU measurement would be about $25ms$. We adjust our time-stamps using a conservative value of 30 ms, plus the delays in PF (taken as $7.1ms$) and MP ($6ms$), when applicable.

The measurement noise level for PMU is selected to be 3%, which is a more stringent assumption compared to the suggested 1% in [51]. Note that noise level does not adversely affect the tracking performance (i.e. accuracy) of the PF.

3.6. Conclusions

We introduce an OOS detection method based on direct estimation of angular difference to serve as a supervisory unit of conventional impedance type relays. The concept rests on two modules: (1) the availability of PMU measurements at the generator bus and (2) a PF-based dynamic state estimator. The first two modules provide an estimate of the angular separation between the generator's rotor angle (treated as a dynamic state) and the external system. The

separation is analyzed using a modal analysis tool (matrix pencils in this case) to determine (in advance) the damping of the modal content(s) and hence, the likelihood of potentially unstable swings. Simulation results on the 10-generator, 39-bus system show that the proposed approach does not require any simplification of system topology. The proposed approach is compared against the most secure OOS scheme - single blinder scheme. It is shown that the approach matches the security of this scheme, while providing early detection of OOS for both monotonically unstable and marginally unstable swings, resulting in reduced stresses on generator and circuit breaker.

4. PARTICLE FILTER-BASED DUAL ESTIMATION FOR SYNCHRONOUS GENERATORS

This chapter is based on the work "Particle Filter-based Dual Estimation for Synchronous Generators," *IET Gener. Transmiss. Distrib* (doi: 10.1049/iet-gtd.2016.1294). The authors of the paper are Yinan Cui[1] and Rajesh G. Kavasseri.

4.1. Introduction

Given a dynamic model and a set of measurements, the process of Dynamic State Estimation (DSE) seeks to estimate and track the internal state variables in the model which may not be amenable to direct measurement. For synchronous generators, Phasor measurement unit (PMU)-based DSE can be achieved with Bayesian non-linear filtering techniques [5, 11, 12, 15, 53, 61]. The appeal of DSE lies in that it can be used to enable wide-area control schemes to improve the system's dynamic performance [46]. A preliminary study using DSE for event detection based on energy functions is reported in [62] and the use of estimated rotor angle for generator out-of-step protection is studied in [63]. Here, we focus on synchronous generators where two special challenges arise.

Most modern generators use brushless AC excitation systems where it is difficult to obtain measurements from shaft-mounted rotating components [54]. In this context, direct measurements of the field voltage may not be readily available. There are generally two ways to solve this problem for DSE: 1) model the entire excitation system and include the field voltage as a state variable, or 2) treat the field voltage E_{fd} as an unknown parameter and solve a *dual estimation* problem, which refers to estimating the system states and unknown system model parameters simultaneously. Commonly, the parameters to be estimated are treated as part of the system state vector. The first approach [5, 11, 53] is predicated upon the availability and complete knowledge of all accompanying models and herein lies the drawback, especially for excitation systems. If there is a failure in one or more portions of the excitation system, or if some of the parameters of the model are not known accurately, the underlying model itself is invalidated and hence the estimation results can

[1] Yinan Cui was the first author and responsible for writing the manuscript and applying simulation tests. Dr. Rajesh G. Kavasseri served as the proofreader and gave recommendations and guidance on drafting the paper.

be severely affected. This is different from the model validation and calibration problem considered in [64–67] where constant model parameters are estimated. The second approach is to treat the field voltage as an unknown parameter and jointly estimate it along with other dynamic states as reported in [12] and [46] with an extended Kalman filter (EKF). While the simulations show promising results for tracking the unknown field voltage, their performance/accuracy degrades with measurement noise.

In this paper, we introduce a dual-estimation strategy with a particle filter which is: (i) robust to measurement noise and (ii) accurate under modest model discrepancies in the excitation system. The field voltage is treated as an unknown parameter and estimated along with other generator dynamic states through a dual-estimator based on the particle filtering method. We also show the filter can provide reasonable results during partial or complete loss of excitation event - a condition cause by excitation system internal failure that can severely threaten system stability. Simulation results are presented on the New England 10-machine, 39-bus system to illustrate the capabilities of the proposed filter in various routine system disturbances. Since the scheme is based on the particle filter, higher accuracies and immunity to noise are gained at the expense of higher computational burdens compared with Kalman filter-based methods.

The rest of the paper is organized as follows. A brief overview of the particle filter-based dual estimation technique is outlined in Sec. 4.2 and its application to the system model is described in Sec. 4.3. Simulation results are presented in Sec. 4.4 along with a brief discussion in Sec. 4.5, and conclusions are noted in Sec. 4.6.

4.2. Dual-Estimator for State and Parameter Estimation

We consider the discrete time representation for a nonlinear system given by:

$$x_k = f_k(x_{k-1}, u_{k-1}, p, n_{k-1}) \tag{4.1}$$

where the system state x_k at step k is a function (represented by f) of the previous state x_{k-1}, system input u_{k-1}, unknown parameter p and system process noise n_{k-1}. The state x_k and unknown parameter p are estimated simultaneously and recursively based on the above system model and the measurement model:

$$z_k = h_k(x_k, p, m_k) \tag{4.2}$$

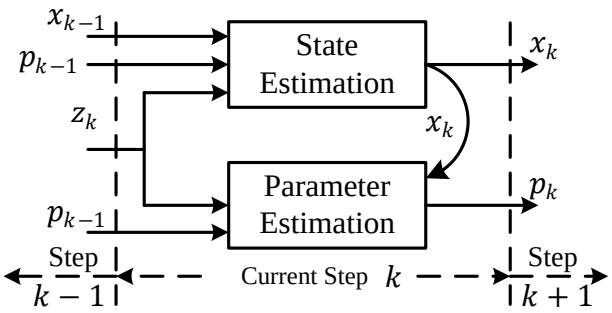

Figure 4.1. A diagram of a sequential method for dual estimation.

where measurement z_k is a function (represented by h) of the state x_k, unknown parameter p and measurement noise m_k.

The block diagram in Fig.4.1 describes the concept of the dual-estimator approach where the estimation problem is divided into two parts: state estimation and parameter estimation. At step k, the system and measurement models are assumed known as well as the parameter p, which is estimated at previous step $k-1$. Then the estimated states x_k are treated as known inputs to determine the parameter p, which will be used at the next step $k+1$. An expectation-maximization algorithm [68] is utilized to tackle the varying states with unknown parameters. In contrast with joint state and parameter estimation where the unknown parameter is simply augmented to the state, in the proposed dual-estimator, the states and unknown parameter are estimated *sequentially*. This "sequential" strategy has been credited with better tracking performance during scenarios where there is an abrupt change in the parameters [69]. The state and parameter estimation blocks shown in Fig. 4.1 are described next.

4.2.1. State Estimation Using Particle Filtering

Similar to solving a nonlinear dynamic state estimation problem using a particle filter (PF), the posterior density at step k is approximated by:

$$r(x_k|z_{1:k}) \approx \sum_{j=1}^{N} w_k^j \Delta((x_k, p_{k-1}) - (x_k^j, p_{k-1})) \tag{4.3}$$

where $z_{1:k}$ is a set of measurements available up to step k, Δ the delta function, $x_k^j (j = 1, \ldots, N)$ a set of particles, N the number of particles, w_k^j a set of weights and p_{k-1} the unknown parameter updated at step $k-1$. If we assume the proposal density $q(x_k, p_{k-1}|z_k)$ (or *importance density*),

where drawing the particles x_k^j only depends on the corresponding particle x_{k-1}^j from the previous step and the measurement z_k at the current step [16], the importance sampling weight w_k^j can be calculated recursively as:

$$w_k^j \propto w_{k-1}^j \frac{r(x_k^j, p_{k-1}|x_{k-1}^j) r(z_k|x_k^j, p_{k-1})}{q(x_k^j, p_{k-1}|x_{k-1}^j, z_k)} \tag{4.4}$$

The representation could be then simplified in terms of Eqn. (4.2) as [6]:

$$w_k \propto P(e_k = z_k^* - h_k(x_k, p_{k-1})) \tag{4.5}$$

where e_k is the measurement error and z_k^* the actual measurement at step k. Note that x_k here represents *a priori* estimate based on Eqn. (4.1).

The steps of implementing PF for state estimation is summarized as follows:

- Initialize the particles $\{x_0^j, w_0^j\}_{j=1:N}$ with unknown parameter initial guess p_0
- Update the system model with estimated unknown parameter p_{k-1} from step $k-1$ for $\forall k > 0$ using parameter estimation PF
- Propagate the particles based on Eqn. (4.1) at step k
- Assign the corresponding weight to each particle based on Eqn. (4.5)
- Normalize the weights using: $\mathbf{w}_k / \Sigma_{j=1}^N w_k^j$
- Resample a new set of particles from $\{x_k^j, w_k^j\}_{j=1:N}$ based on the likelihood of w_k^j (Resampling [6])
- Obtain the estimates by taking the mean of the particles.

4.2.2. Parameter Estimation Using Particle Filtering

An "artificial evolution" method is introduced to deal with the time-varying parameter estimation by adding small random noise to the parameter updating model:

$$p_k = p_{k-1} + \zeta_k \tag{4.6}$$

Where $\zeta_k \sim N(0, V_k)$ and p_{k-1} and ζ_k are conditionally independent. The over-dispersed approximation flaw caused by Eqn. (4.6) is corrected using a kernel location shrinkage [70] to approximate the parameter evolution with the Gaussian distribution. The unknown parameter is then estimated based on the recursive prediction error (RPE) [71] algorithm, where the objective function (expectation of the squared error) with respect to p_{k-1} is minimized:

$$J(p_{k-1}^j) = E(\epsilon(p_{k-1}^j)\epsilon^T(p_{k-1}^j)) \tag{4.7}$$

Where E is the expectation notation and $\epsilon^j = z_k^* - h_k(x_k, p_{k-1})$ the prediction error. Note that x_k represents *a posterior* estimate from Sec. 4.2.1. The algorithm includes the contribution of p_{k-1} from the previous step based on a shrinkage factor a, which will push the updated parameter back to p_{k-1} before artificial noise is added. The estimation model for p_k is given by [72]:

$$\begin{aligned} m_k^j &= p_{k-1}^j + \gamma_k R_k^j \psi_k^j \epsilon^j \\ p_k^j &= a m_k^j + (1-a)\bar{m}_{k-1} + \zeta_k^j \end{aligned} \tag{4.8}$$

Where $R_k^j = E(\epsilon^j(\epsilon^j)^T)$ is the variance of the prediction error, $\psi_k^j = \partial(h_k(x_k, p_{k-1}^j))/\partial(p_{k-1}^j)$ the partial derivative of the measurement function h_k with respect to p_{k-1}, h_k is defined as a function of parameter p_{k-1}, γ_k the step size and can be a sequentially decreasing value [73] or set to a fixed value, and $\bar{m}_{k-1}$ the mean value of $\{p_{k-1}^j\}$ (or estimate of p from the last step).

The implementation of PF for parameter estimation is similar to the one for state estimation, the estimated state x_k are now treated as a known input.

4.3. Dual Estimation for Power Systems

We consider a *fourth order* model for a synchronous generator dynamics -including one damper winding in the q-axis while neglecting subtransient dynamics as given by [54]:

$$\begin{aligned}
\dot{\delta}_i &= 2\pi f_0 \Delta\omega_i \\
\dot{\Delta\omega}_i &= \frac{1}{2H_i}(P_{m_i} - P_{e_i} - D_i\Delta\omega_i) \\
\dot{E}'_{d_i} &= \frac{1}{T'_{qo_i}}(-E'_{d_i} - (X_{q_i} - X'_{q_i})i_{q_i}) \\
\dot{E}'_{q_i} &= \frac{1}{T'_{do_i}}(E_{fd_i} - E'_{q_i} + (X_{d_i} - X'_{d_i})i_{d_i})
\end{aligned} \tag{4.9}$$

where i is the synchronous generator index in a multi-machine system, δ the rotor angle, f_0 the synchronous frequency, $\Delta\omega$ the rotor speed deviation, H the machine inertia constant, P_m the mechanical power input, P_e the real power output at the terminal of the generator, and E_{fd} the field voltage or the output voltage of the excitation system. X_d and X_q are d-axis and q-axis synchronous reactances. X'_d and X'_q are d-axis and q-axis transient reactances. T'_{do} and T'_{qo} are open-circuit d-axis and q-axis transient time constants. E'_d and E'_q are d, q components of transient internal voltage ($E' = V_s + jX'_dI_s$) behind X'_d. The rotor angle δ is defined as the phase angle of the internal voltage ($E_q = V_s + jX_qI_s$) behind X_q, V_s is the generator terminal voltage and I_s is the stator current.

4.3.1. Generator Dynamic States Tracking

The measurement model is derived from the following considerations. The power output (P_e and Q_e) and the terminal voltage phasor ($|V_s|\angle\theta = V_s$) are assumed accessible from a PMU located at the dedicated substation. The measurements P_e can be related to the states through the following relations:

$$P_e = V_dI_d + V_qI_q \tag{4.10}$$

where the d, q components can be represented by the phasor components and other dynamic variables:

$$V_d = |V_s|sin(\theta - \delta), \quad V_q = |V_s|cos(\theta - \delta)$$

$$I_d = (V_q - E'_q)/X'_d, \quad I_q = (E'_d - V_d)/X'_q \tag{4.11}$$

The state vector $\vec{\mathbf{x}}$, input vector $\vec{\mathbf{u}}$ and output vector $\vec{\mathbf{z}}$ are defined as:

$$\vec{\mathbf{x}} = [\delta \ \Delta\omega \ E'_d \ E'_q], \quad \vec{\mathbf{u}} = [|V_s| \ \theta_i \ P_m], \quad \vec{\mathbf{z}} = [P_e \ Q_e] \tag{4.12}$$

In this work, the mechanical power P_m is considered as a known input since the focus is on the field voltage. If not, the prime mover dynamics can be modeled and its associated state variables estimated routinely as reported in [53]. The state estimation procedure is summarized in Sec. 4.2.1. At each step k, E_{fd} in Eqn. (4.9) is assigned to a value obtained by the parameter estimator at step $k-1$.

4.3.2. Field Voltage Estimation

The field voltage E_{fd} is estimated based on the tracking results from the above estimator. Since the dynamics of E_{fd} is unknown, the artificial evolution method is applied to estimate the field voltage E_{fd}:

$$E_{fd,k} = E_{fd,k-1} + \zeta_k \tag{4.13}$$

In practice, field voltage E_{fd} is generally not a fixed quantity. One can anticipate variations during both regular and abnormal circumstances. Note that to determine an appropriate variance for ζ_k is not an easy task [73], a trade-off between tracking capability during abrupt change and performance in stead state should be considered. In this study, the variance is a compromise between tracking performance in steady-state and following capability during transients. The selected value is determined after different simulation trials.

Since the field voltage or direct measurements from the rotating components in the excitation system are assumed unavailable, there is no direct correlation between E_{fd} and any available system output variables in Eqn. (4.12). Therefore, the fourth differential equation regarding E'_q in Eqn. (4.9) is utilized to establish the measurement model in Eqn. (4.2):

$$I_{d,k} = \frac{\dot{E}'_{q,k} T'_{do} + E'_{q,k-1} - E_{fd,k}}{X_d - X'_d} \tag{4.14}$$

where $I_{d,k} = |I_{s,k}| sin(\phi_k - \delta_k)$, derivative $\dot{E}'_{q,k} \approx (E'_{q,k} - E'_{q,k-1})/\Delta t$ is approximated by Euler's

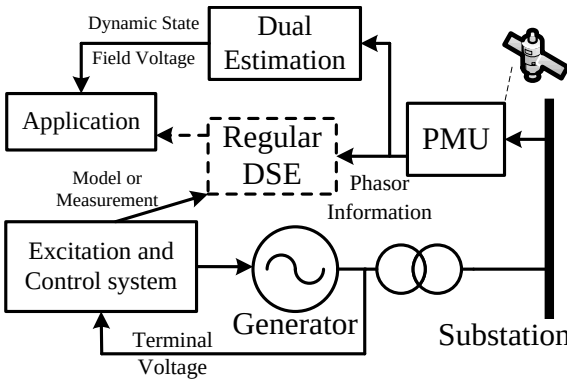

Figure 4.2. Block diagram of detecting LOE incident using the proposed method.

method and Δt is the sampling rate of estimation, which is usually same as the state tracking process. The derivative term $\dot{E}'$ can also be computed from the second order backward difference, but there is no appreciable difference in the estimation results between the two approximations. The states $[\delta_k \ E'_{q,k}]$ are available from the state estimator, the history data $E'_{q,k-1}$ is assumed accessible for current step k. The current phasor $|I_{s,k}|\angle\phi_k = I_{s,k}$ is assumed available from the PMU.

Treating E_{fd} as an unknown input is advantageous for excitation system internal failure events, which may lead to loss of excitation (LOE) for synchronous generators. An LOE event can occur due to an open or short circuit in the field circuit. Since an open field is less likely the origin of an LOE incident [35, 59], we focus our attention for conditions involving a short circuit in the field circuit. It must also be noted that for an open circuit case, the assumption of machine model parameters such as X'_d and T'_{do} being constant does not hold due to the open path and hence the estimation model itself is invalid. On the contrary, the machine model remains valid as long as there is a closed path for the field current, even if the fault occurs within the excitation system. Subsequently, the model defined in Eqn. (4.9) would be effective throughout the time frame of interest.

An overall diagram is shown in Fig. 4.2. Unlike conventional DSE, the dual estimation process can estimated the machine dynamics as well as the excitation subsystem output without the need to model the field circuit or direct measurements of field quantities.

4.4. Simulation Results

The performance of the proposed dual-estimator is tested and evaluated on the New England 10-machine system [57]. The one line diagram of the system can be found in [63].The simulations are implemented on *Matlab–Simulink* and the synthesized measurements are then calculated based on the simulation results. The measurement and system process errors are set to 3% and 1% respectively and both of them are modeled as additive white Gaussian noise. The PMU which provides all the available measurements is assumed to have a reporting rate at 30 frames per second [51]. The sampling rate of proposed PF-based dual-estimator is $5ms$. Between two measurement observations, the pseudo measurements are assumed to be unchanged for the estimator. The dual-estimator as well as *EKF with unknown inputs* (EKFUI) method proposed in [12] are all initialized with true states from the simulation and the number of particles is set to 80 for all test cases. The standard deviation of dynamic noise in field voltage estimation model is chosen to be 0.012, the step size and shrinkage factor in Eqn. (4.8) are selected to be 10^{-4} and 0.5 respectively. In all simulations, the solid lines denote the true values and estimated values are represented by the dashed lines or dotted lines. The results are organized in three subsections: (i) filter performance with external disturbance, (ii) filter performance with exciter model mismatch and (iii) performance during loss of excitation incidents due to field short circuit.

4.4.1. Filter Performance with External Disturbance

In this scenario, we assume that the excitation subsystem is intact and functioning normally. The performance of the proposed filter is compared with EKFUI method for three types of external disturbances where the post-fault system is stable: (i) a three-phase to ground fault and (ii) load rejection, and case (iii) where the post-fault system is unstable. These disturbances are chosen because they strongly influence the dynamics of the excitation system and hence the accuracy of the filter in tracking the field voltage excursions under such conditions can be assessed. For each simulation case, 100 independent trials are conducted to test the reliability of the proposed method and the time traces of all state variables show the mean and standard deviations ($\pm 3\sigma$) of the trials.

Case (i): A three-phase to ground fault is placed on line *6-11* near bus #6 at $t = 6s$ and the fault is cleared by permanently tripping the line at $t = 6.17s$ (10 cycles later) and the post-fault system is stable.

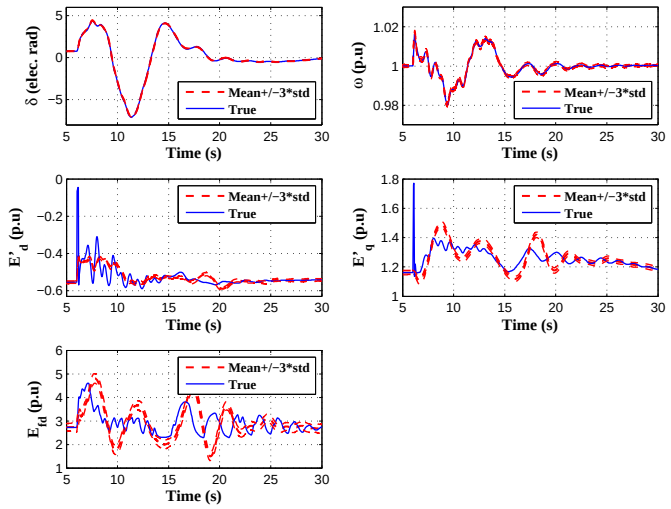

Figure 4.3. State tracking results (with 3% measurement noise) by the proposed dual-estimator for G_2 for three-phase to ground fault

Table 4.1. RMSD of estimation results of G_2 for different TVE levels by proposed dual-estimator and EKFUI

State Variable	**Method**	**RMSD with Different TVE Levels**		
		1%	3%	5%
δ_2	Dual-filter	0.0435±0.00085	0.0488±0.0034	0.0562±0.0018
	EKFUI	0.0381±0.0013	0.0411±0.0012	0.0531±0.0012
ω_2	Dual-filter	0.0004±0.000055	0.0005±0.00016	0.0006±0.000097
	EKFUI	0.0029±0.000089	0.0035±0.000083	0.0046±0.000088
E'_{d_2}	Dual-filter	0.0397±0.00017	0.0420±0.00081	0.0436±0.000304
	EKFUI	0.0442±0.00065	0.0424±0.00047	0.0431±0.00075
E'_{q_2}	Dual-filter	0.0405±0.0012	0.0614±0.0045	0.0677±0.0014
	EKFUI	0.0357±0.0014	0.0326±0.0018	0.0339±0.0017
E_{fd_2}	Dual-filter	0.4718±0.027	0.6272±0.045	0.5495±0.0099
	EKFUI	1.4592±0.028	3.0993±0.051	3.8173±0.047

The estimation results are shown for generator #2 (denoted by G_2), the generator closest to the fault. The time tracking traces by the proposed filter are displayed in Fig. 4.3. For comparison, the estimation error in terms of root mean square deviation (RMSD) is tabulated in Table 4.1 for all state variables for 1, 3 and 5 % total vector error (TVE) [51] levels, where the results generated by EKFUI method [12] are also presented. Note that the proposed approach and EKFUI method are initialized with the same state vector $\vec{\mathbf{x_0}} = [\delta_0\ \Delta\omega_0\ E'_{d_0}\ E'_{q_0}\ E_{fd_0}] = [0.76\ 0.00\ -0.55\ 1.16\ 2.73]$.

It can be observed that the proposed filter is relatively robust to a noise level up to 5% as compared to the EKFUI method where the field voltage (E_{fd}) estimates are significantly affected.

Case (ii): The load at bus #20 is permanently disconnected at $t = 6s$. The post-disturbance system is stable. The tracking results for generator #5 (denoted by G_5) are illustrated in Fig. 4.4. In the state-tracking results, the change in rotor angle for G_5 as referenced to bus 20 is shown to correlate the variables with respect to the load rejection scenario. The loss of load triggers the exciter dynamics at 6 s and calls for a reduction in field voltage which settles to a new reduced value shortly after 15 s. The estimation errors are tabulated in Table 4.2 for all state variables for 1, 3 and 5 % TVE levels. Again, from Table 4.2, it can be observed that the proposed filter is relatively robust to a noise level up to 5% as compared to the EKFUI method where the field voltage (E_{fd}) estimates are substantially affected.

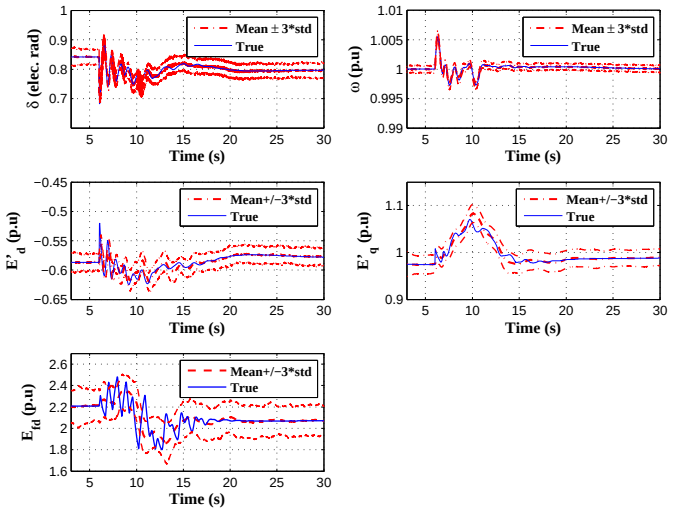

Figure 4.4. State tracking results (with 3% measurement noise) by the proposed dual-estimator for G_2 for a load rejection event at bus 20.

Table 4.2. RMSD of estimation results of G_5 for different TVE levels by proposed dual-estimator and EKFUI

State Variable	**Method**	**RMSD with Different TVE Levels**		
		1%	3%	5%
δ_5	Dual-filter	0.0081±0.0018	0.0118±0.0013	0.0186±0.0022
	EKFUI	0.0129±0.00039	0.0335±0.00105	0.0548±0.0017
ω_5	Dual-filter	0.0002±0.000055	0.0003±0.000036	0.0004±0.000047
	EKFUI	0.0010±0.000019	0.0026±0.000056	0.0040±0.000080
E'_{d_5}	Dual-filter	0.0058±0.00067	0.0082±0.00054	0.0119±0.0011
	EKFUI	0.0081±0.00034	0.0170±0.00095	0.0272±0.0015
E'_{q_5}	Dual-filter	0.0069±0.00097	0.0096±0.0013	0.0167±0.0024
	EKFUI	0.0082±0.00022	0.0223±0.00065	0.0376±0.0013
E_{fd_5}	Dual-filter	0.1705±0.016	0.1002±0.0079	0.1035±0.0091
	EKFUI	1.4520±0.027	4.3172±0.087	7.0538±0.17

Case (iii) Here, we consider a scenario which leads to loss of synchronism: a three-phase to ground fault occurs on line *25-26* near bus #25 at $t = 6s$ and the fault is cleared by permanently tripping the line at $t = 6.23s$ (14 cycles later). The clearing time is deliberately chosen long enough so that the post-fault dynamics is unstable, we can notice that the pole slipping starts at approximately $t = 7s$. The estimated states for generator #8 (denoted by G_8) with 3% TVE level are shown in Fig. 4.5. The estimation error (up to 7s) with 3 different TVE levels by proposed dual-estimator and EKFUI method are summarized in Table. 4.3.

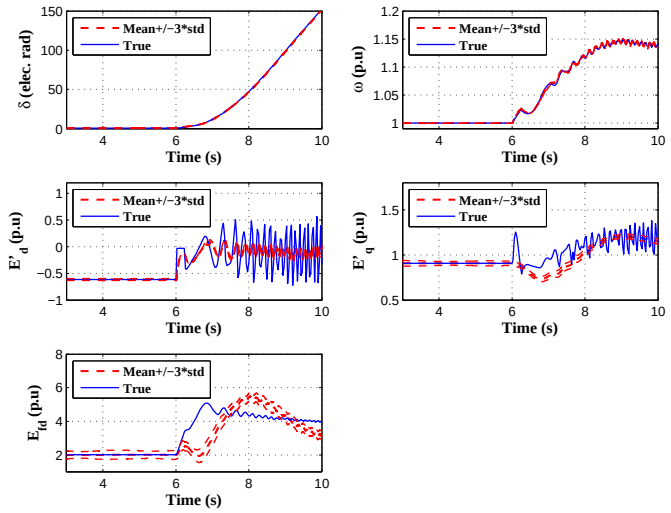

Figure 4.5. State tracking results by proposed dual-estimator for G_8 with a 3-phase-to-ground fault.

Table 4.3. RMSD of estimation results of G_8 for different TVE levels by proposed dual-estimator and EKFUI

State Variable	**Method**	**RMSD with Different TVE Levels**		
		1%	3%	5%
δ_8	Dual-filter	0.1042±0.0018	0.0967±0.0030	0.0943±0.0055
	EKFUI	0.0667±0.0010	0.0721±0.0023	0.0836±0.0036
ω_8	Dual-filter	0.0010±0.000055	0.0011±0.00013	0.0012±0.00021
	EKFUI	0.0039±0.000021	0.0042±0.000046	0.0048±0.000059
E'_{d_8}	Dual-filter	0.0626±0.00067	0.0620±0.00066	0.0622±0.0018
	EKFUI	0.0702±0.00043	0.0731±0.00013	0.0757±0.0021
E'_{q_8}	Dual-filter	0.0631±0.00097	0.0594±0.0023	0.0598±0.0025
	EKFUI	0.0348±0.0013	0.0347±0.00020	0.0417±0.0029
E_{fd_8}	Dual-filter	0.7749±0.016	0.7271±0.038	0.7309±0.030
	EKFUI	1.9459±0.063	3.5352±0.101	4.2268±0.098

Remark: The performance of the proposed filter is comparable to the EKFUI for all state variables for all cases and can be clearly observed from Tables 4.1, 4.2, and 4.3 with a notable exception for the field voltage under all noise levels. For this state, the proposed filter clearly outperforms the EKFUI method.

In the next section, we present results to assess filter performance with model errors.

4.4.2. Filter Performance with Exciter Model Mismatch

We consider the case when there is a mismatch between the model assumed for estimation and the actual model used in simulation. This can be representative for example, for a case when (i) one or more critical parameters within the subsystem are approximately known or (ii) there is a failure in the subsystem which can be captured parametrically. Here, we consider the circumstance corresponding to a partial loss of excitation (pLOE). In such scenarios, the proposed model is very advantageous as demonstrated by the following results. Note that IEEE type I excitation and control system is used in the test, the block diagram of the it can be found in [74]. Although the simulations are shown with this exciter model, the impact of model mismatch on filter performance will be similar for other types of exciter models.

First, we consider a case when the true value of the exciter gain (K_E) is 1.0 while the model used in a standard PF considers this to be 1.2. The state tracking results by the standard PF and the proposed method for generator #9 (denoted by G_9) for a line trip (26-29) at $t = 6s$ are shown in Fig. 4.6. It is clear from Fig. 4.6 that with a standard PF, such a parametric error leads to a steady drift between the theoretical and estimated state. Note that the illustrated case can either reflect a modeling inaccuracy or a glitch in one component of the equipment. As expected, the proposed dual filter tracks the states properly until the pole slipping starts (at $t = 17s$) despite this parametric discrepancy.

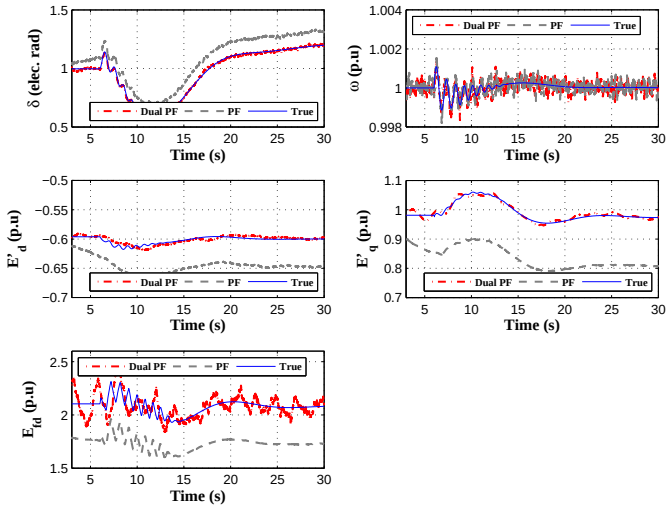

Figure 4.6. Discrepancy in estimation with approximate parameters for a standard PF with a line outage incident.

Next, we consider a more drastic case to mimic a pLOE condition by reducing the gain of voltage regulator (K_A) to 50 % of its nominal value. The state tracking results for generator #4 (denoted by G_4) is shown in Fig. 4.7. It can be seen that although estimations of two electromechanical states (angle, speed) by a standard PF roughly follow the theoretical trace, the post-disturbance estimates for field voltage and E'_q diverge. In contrast, estimations by the proposed method correctly track the variations despite the partial loss in regulator gain.

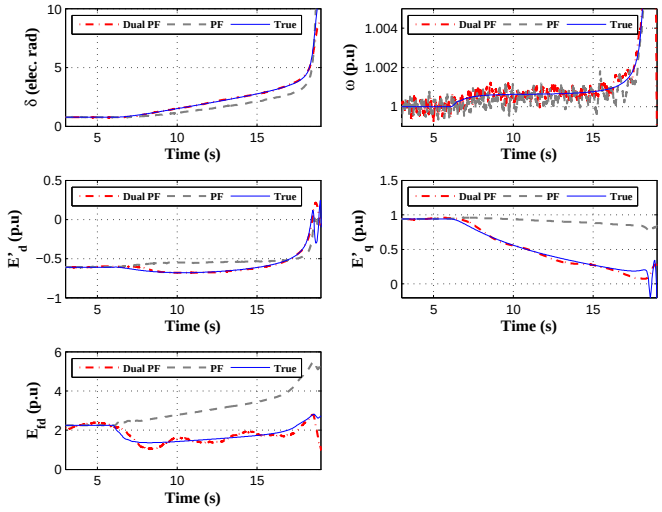

Figure 4.7. Tracking performance for a malfunctioning voltage regulator (pLOE), the generator loses its synchronism at $t = 17s$.

Next, we illustrate filter performance for partial and complete loss of excitation events.

4.4.3. Loss of Excitation Events

The loss of excitation events are analyzed for two different operating conditions as annotated in the figures. A pLOE for these initial loading conditions is achieved by reducing the voltage input of the field winding by 67% and 48% respectively for generator #1 (denoted by G_1), which is initiated at $t = 6s$. The complete loss of excitation is achieved by setting the terminal voltage of the field winding to zero (short circuit fault, $E_{fd} = 0$) for G_1, which would lead to a loss-of synchronism ultimately for two loading conditions. Fig. 4.8 shows the field voltage estimation mean values and the standard deviations based on 100 successful trials for both partial and complete LOE incidents. In the complete LOE cases, the generator loses synchronism (corresponding to a pole-slipping condition) shortly after $t = 12s$ $t = 10.5s$ respectively. The proposed filter tracks the field voltage faithfully up to the pole-slipping instant.

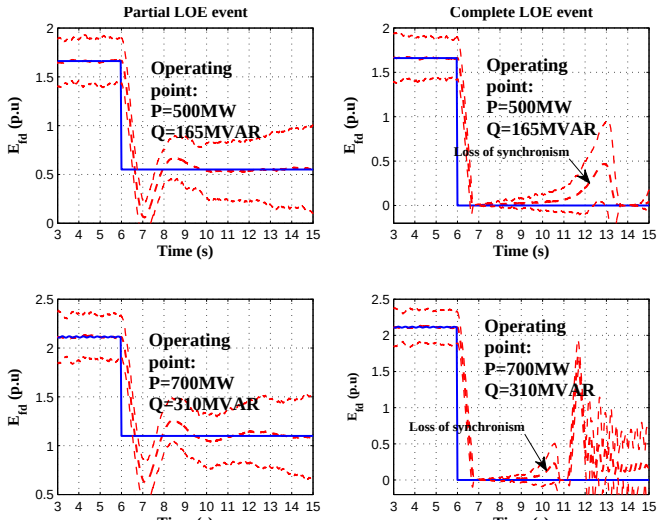

Figure 4.8. Field voltage tracking results by proposed dual-estimator with partial and complete LOE incidents.

4.5. Discussion

One of the potential applications for dynamic state estimation is the possibility of detecting an internal failure in a component such as the excitation system considered here. For such applications, selectivity is an important attribute. For the class of disturbances analyzed here, the simulation results indicate reliable tracking of E_{fd}, which suggests the possibility that the proposed method could be used to detect a failure/malfunction within the excitation system status. It should also be noted that the other dynamic states $\{\delta\ \omega\ E'_d\ E'_q\}$ for all these cases are reasonably estimated as well.

In contrast, we observe that the onset of pole slipping (loss of synchronism) considerably influences the estimates in Fig. 4.5 and 4.8. This is because the estimation of field voltage (Eqn. (4.14)) depends on the internal voltage and its derivative (E'_q and $\dot{E}'_q$) (see Eqn. (4.9)), existing model is not sufficient enough to describe the fast dynamics cause by loss of synchronism and degradation continues sequentially in between the state and parameter estimators. Generally, the tracking accuracy can be improved with a higher estimation sampling rate at the expense of increased computational burden. For dynamic tracking applications, there always exists a time delay between the points of collecting measurements and the instant when estimates are available. It is challenging to achieve the near-real-time requirement with a PF-based estimator where there is a natural trade-off between the number of particles (computational burden) and accuracy. In this study, the pseudo-measurements between two filter iterations are assumed to be unchanged. Alternatively, a multi-step interpolation method [75, 76] and the prediction approach [61] can be used, where the balance between the estimation accuracy and computational time could be adjusted. PF-based approaches are computationally more expensive compared to other Bayesian tracking techniques such as the EKF. The simulations in this paper are implemented on a desktop PC with *core i7* $3.4GHz$ processor, and $8GB$ memory. The average time consumption of a PF-based dual-estimator on a 30-second simulation is $28.10s$. If parallel computations, as suggested in [77] can be further exploited, the computational burden of PF-based methods could be reduced accordingly.

4.6. Conclusion

A particle filtering based method is proposed to estimate the dynamic states for synchronous generators considering the field voltage as an unknown input. The method is particularly useful

in modeling scenarios when the actual model of the excitation is either unknown, or when there is an internal failure in the excitation system resulting in partial or complete loss in excitation, or when the parameters within the system are not known precisely. The particle filter is modified to estimate the states and the unknown parameter in a sequential manner. The proposed method is evaluated via dynamic simulations on a 10-machine, 39-bus system with case studies under routine disturbances and under loss of excitation conditions along with comparisons with Kalman filter-based methods. The results indicate while the tracking accuracy of the proposed filter is comparable to that of EKFUI method for the internal states, there is a drastic reduction in the field voltage estimation error for noise levels up to 5%. The robustness of the filter to noise and performance under these modeling assumptions suggest that the such a filter may serve as a *computational surveillance* unit to supervise the functioning of excitation systems.

5. A NEW APPROACH FOR EVENT DETECTION BASED ON ENERGY FUNCTIONS

This chapter is based on the work "A New Approach for Event Detection Based on Energy Functions," *2014 IEEE PES General Meeting — Conference & Exposition*, National Harbor, MD, 2014, pp. 1-5 (doi: 10.1109/PESGM.2014.6939804). The authors of the paper are Rajesh G. Kavasseri, Yinan Cui[1] and Sukumar M. Brahma.

5.1. Introduction

Power blackouts over the world have shown that power systems, though carefully planned and protected, suffer from unforeseen events triggering instability. Such events often include misoperations of relays that result in unintended line trips, load shedding and generation trips. Sometimes, these misoperations go unchecked because global knowledge about actual system conditions is lacking. In the form of global knowledge related to tripping, control centers simply acquire relay trip flags, circuit breaker (CB) status flags, and sometimes line currents and voltages for more reliable interpretation of these flags. These signals in most cases do not convey whether the trip was as per design (correct) or it was a misoperation. Disturbance data from phasor measurement units (PMUs) have been used for identifying different disturbance events. The crucial step in this process is *feature extraction*, and the method used by many researchers [78–82] for this step is the Minimum Volume Enclosing Ellipsoid (MVEE) algorithm. In this method, a multidimensional ellipsoid is used to enclose a given set of PMU measurements. The geometrical properties of the MVEE such as volume, change in volume, center, length of semi-axis are used as features.

However, the biggest disadvantage of this method is that it is *purely data-driven* [83]; there is no physical basis to understand or correlate which feature is most affected by which disturbance event, or whether such one-to-one mapping even exists. Therefore, this approach requires the user to select a set of features simply by trial and error. Due to this uninformed implementation, the resulting feature vector is huge. For example, the feature vector used in our clustering work [82] had 102 features. In contrast, this paper explores an alternative method based on energy functions.

[1]Yinan Cui was the co-author and responsible applying simulation tests and writing the simulation section. Dr. Rajesh G. Kavasseri was responsible for writing the manuscript and Dr. Sukumar M. Brahma served as the proofreader and gave recommendations on drafting the paper.

5.2. Key Ideas

Any *event* or a disturbance in the system will leave a signature (like a *fingerprint*) in Wide Area Measurement Systems (WAMS) datasets as evidenced by our previous research [82]. While there is no dearth of such data, extracting this fingerprint from concurrent data traces still remains an open problem. While all prior research has been based on empirical methods - (purely from a data standpoint) that are impervious to the dynamics of the physical systems, we contend (and demonstrate) that such a signature is actually buried in the components that constitute the energy function for the system. The trick is in determining which (among the numerous) components of the energy function is sensitive, or reflective of the corresponding disturbance. In other words, *our aim is to establish a mapping between the energy traces and events in the power system, and in future use this mapping to detect and distinguish disturbance events.*

By construction, the components of an energy function depend on bus voltages that can be measured directly, as well as several internal state variables of generators that can neither be measurable directly nor estimated easily with conventional (i.e. non-phasor) measurements [84,85]. Thus, energy function (and its time derivative) evaluations on a numerically simulated trajectory are not useful enough for a real or even near-real time applications, because a high-fidelity simulation that includes full state representation of all dynamic components takes significantly more time compared to the real-time response, despite the availability of hardware acceleration and GPU based integrators. In contrast with all prior work that use energy functions for stability assessment, our aim is to show how, the individual terms can be used to detect and distinguish events that occur in the system. The main steps in our approach are:

- step 1: estimate the internal states of generators using a particle filter;
- step 2: use the estimated states (from step 1) and bus voltage phasor information from PMUs to construct energy function components;
- step 3: monitor the sensitivity of specific energy function components to detect and classify events.

These key steps for this method are described next.

5.2.1. The Particle Filter

Assuming that $\{w_k\}$ and $\{v_k\}$ are independent white noise processes with known pdf ($\sim N(0, R)$), consider the following models for the system dynamics and measurements:

$$x_{k+1} = f_k(x_k, w_k) \tag{5.1}$$

$$y_k = h_k(x_k, v_k) \tag{5.2}$$

Based on the pdf of the initial state $p(x_0)$, N particles, denoted by $x^+_{0,i}$ are generated ($i = 1 \dots N$). The higher the number of particles, the better the accuracy. Hence N parameterizes the computational effort-accuracy tradeoff.

For each time step k:

- The *a priori* particles $x^-_{k,i}$ are computed from the system dynamics ($f()$) and the known pdf of the process noise.

$$x^-_{k,i} = f_{k-1}(x^+_{k-1,i}, w^i_{k-1}),\ i = 1 \dots N. \tag{5.3}$$

- For m measurements, the probability q_i of $x^-_{k,i}$ conditioned on the measurement ($y = y_0$) is given by:

$$q_i \sim \frac{1}{(2\pi)^{m/2}|R|^{1/2}} exp(\frac{-Q^t_k R^{-1} Q_k}{2}),$$
$$Q_k = y_0 - h(x^-_{k,i}) \tag{5.4}$$

- The probabilities are normalized: ($q_i = \frac{q_i}{\sum q_i}$) and the *a posteriori* particles $x^+_{0,i}$ are re-sampled, i.e., $x^+_{k,i} = x^-_{k,j}$ with probability q_j. This re-sampling step requires two additional steps:

- First, generate a random number r uniformly distributed in $[0, 1]$.

- Form a partial sum of q_i - up to an index j until it exceeds r (i.e. find j such that $\sum_{m=1}^{j-1} q_m < r$ and $\sum_{m=1}^{j} q_m \geq r$) in which case, the new particle $x_{k,i}^{+}$ is set to the old particle $x_{k,j}^{-}$. Since the particles $x_{k,i}^{+}$ are now distributed with pdf $p(x_k|y_k)$, any statistical measure of this pdf can be calculated. Typically, the algebraic mean of the particles (providing the estimate we seek) is calculated from:

$$E(x_k|y_k) = \frac{1}{N}\sum_{i=1}^{N} x_{k,i}^{+} \tag{5.5}$$

We consider dynamic models for the generator based on the 1.1 model [85] with the IEEE type one excitation system and a general steam turbine model for the prime mover control system. The internal state variables for each generator are: $\mathbf{x}_g = (\delta, \bar{\omega}, E'_q, E'_d, E_{fd})$. The dynamic model defines the process equations - Eqn.(5.1). The measurement set includes the real and reactive powers at each generator as functions of $\mathbf{x}_g$. This defines the measurement equations - Eqn.(5.2). The states estimated via particle filtering are used to construct the components of the energy function, which is described in the following section.

5.2.2. Construction of Energy Function Components with Particle Filter Estimates

The application of energy or Lyapunov-like functions has been extensively studied: [86–94], mainly for transient stability assessment. A comprehensive collection can be found in [85, 95, 96]. It is also been applied for voltage stability assessment [97] and dominant power transfering paths monitoring and analysis in large power systems [98].

However, the critical difference between *all* prior work in energy functions and our work is that we construct each of the components of the energy function explicitly. Doing this requires full knowledge of the dynamic state - acquired through the particle filter and phasor information - available from PMU measurements.

Here, we assume that the system is completely observable through PMUs, i.e. phasor information of bus voltages and line currents are known. The assumption is required for the particle filter based dynamic state estimation. Considering the proliferation of PMUs and given the evolution of future power systems, this is a very reasonable assumption. Thus, all bus voltage measurements are available, including the phase angles of bus voltages and line currents at generator buses.

We consider an energy function of the form, [85]:

$$W(\mathbf{x}, \mathbf{y}, t) = W_{KE} + W_{PE}$$
$$W_1 = W_{KE} = \frac{1}{2}\sum_{i=1}^{M} M_i \bar{\omega_i}^2, \;\; W_{PE} = \sum_{i=1}^{11} W_{2i} \tag{5.6}$$

The energy function has contributions from different entities in the system as explained below.

Loads:

Consistent with the assumptions made in transient stability analysis, the load at bus i is represented as follows:

$$P_L^i = f_{pi}(V_i) = a_{0i} + a_{1i}V_i + a_{2i}V_i^2$$
$$Q_L^i = f_{qi}(V_i) = b_{0i} + b_{1i}V_i + b_{2i}V_i^2 \tag{5.7}$$

where V_i is the voltage magnitude at bus i. The contribution of the load components (active, reactive) to the energy function is then given by:

$$W_{22}(t) = \sum_{i=1}^{N} \int_{t_0}^{t} f_{pi}(V_i) \frac{d\phi_i}{dt} dt$$
$$W_{23}(\mathbf{V}) = \sum_{i=1}^{N} \int_{V_{i0}}^{V_i} \frac{f_{qi}(\sigma_i)}{\sigma_i} d\sigma_i \tag{5.8}$$

Here, W_{22} and W_{23} are the relative (i.e., with respect to a steady state operating condition) changes in the potential energy terms due to active and reactive components of a load. Here, ϕ_i denotes the angle of the terminal voltage at a generator bus, with respect to the center-of-inertia (COI), i.e. $(V_{qi} + jV_{di})e^{j\theta_i} = V_i e^{j\phi_i}$ and θ_i denotes the rotor angle with respect to the COI, [85]. The subscript "0" refers to the values prior to a fault. Note that these functions can be calculated for all non-generator buses simply through PMU measurements (no particle filter required), with the assumption that the system is observable through PMUs.

Transmission lines:

The relative change in magnetic energies stored in the transmission lines is captured by the component W_{25} given by:

$$W_{25} = -\frac{1}{2}\sum_{i=1}^{N}\sum_{j=1}^{N} B_{ij}(V_i V_j \cos(\phi_{ij}) - V_{i0}V_{j0}\cos(\phi_{ij0})) \tag{5.9}$$

Here, $\phi_{ij} = \phi_i - \phi_j, B_{ij} = Imag(Y_{ij})$ (Y_{ij} is the system bus admittance matrix), the subscript "0" denoting the prefault value. The term W_{25} is made of ℓ (= number of buses + lines) components. Each of the ℓ components can be individually determined because the system is assumed observable in a wide-area sense, as mentioned above. Again, note that a particle filter is not required to calculate this term of the energy function. System wide observability from PMUs provides sufficient information.

Generator:

The energy contributions from a generator arise from the magnetic energies stored in the machine reactances, damper windings on the d, q axes and the field circuit (with the AVR). The specific functional form of these terms are given as follows. It is important to note that to compute these terms individually, it is necessary to know the state variables $\mathbf{x}$ associated with the machine. With the 1.1 model, the internal state variables for each machine are: $\mathbf{x} = (\delta, \bar{\omega}, E'_q, E'_d, E_{fd})$. Except the speed $\bar{\omega}$ which is measurable, the other state variables cannot be directly measured and hence need to be estimated. The particle filter based estimator (section 5.2.1) provides estimates of these variables which are used to construct each of these terms individually.

$$\begin{aligned}
W_{21}(\mathbf{y}) &= -\sum_{i=1}^{M}\int_{t0}^{t} P_{mi}(t)\frac{d\theta_i}{dt}dt \\
W_{24}(\mathbf{x},\mathbf{y}) &= \sum_{i=1}^{M}[f_{24}^i - f_{24,0}^i], \\
f_{24}^i &= {E'_{qi}}^2 + V_i^2 - 2E'_{qi}V_i\cos(\theta_i - \phi_i) \\
W_{26}(\mathbf{y}) &= \sum_{i=1}^{M}[f_{26}^i - f_{26,0}^i], \\
f_{26}^i &= [V_i^2(\cos 2(\theta_i - \phi_i) - 1)]\frac{x'_{di} - x'_{qi}}{4x'_{qi}x'_{di}}
\end{aligned}$$

$$
\begin{aligned}
W_{27}(\mathbf{x},\mathbf{y}) &= \sum_{i=1}^{M}[f_{27}^{i} - f_{27,0}^{i}], \\
f_{27}^{i} &= [{E'_{di}}^{2} + V_i^2 + 2E'_{di}V_i\sin(\theta_i - \phi_i)]\frac{1}{x'_{qi}} \\
W_{28}(\mathbf{y}) &= -\sum_{i=1}^{M}\frac{V_i^2 - V_{i0}^2}{2x'_{qi}} \\
W_{29}(\mathbf{x}) &= -\sum_{i=1}^{M}\int_{t0}^{t}[\frac{E_{fdi}}{x_{di} - x'_{di}}]\frac{dE'_{qi}}{dt}dt \\
W_{210}(\mathbf{x}) &= \sum_{i=1}^{M}\frac{{E'_{qi}}^{2} - {E'_{qi0}}^{2}}{2(x_{di} - x'_{di})} \\
W_{211}(\mathbf{x}) &= \sum_{i=1}^{M}\frac{{E'_{di}}^{2} - {E'_{di0}}^{2}}{2(x_{qi} - x'_{qi})}
\end{aligned}
\tag{5.10}
$$

- The component W_{29} is the contribution from the field circuit (on the d axis). The term W_{210} is the contribution from the d axis. Note that if the AVR is considered, then the integral in this component is path dependent because the field voltage E_{fd} is time varying;
- The components W_{27}, W_{28}, W_{211} are contributions from the q axis and the damper windings;
- The component W_{26} is zero if transient saliency is neglected (i.e. when $x'_q = x'_d$);
- The component W_{24} is the change in magnetic energy stored in the machine reactances;
- The component W_{21} is the change in potential energy due to the mechanical input to the machine relative to the center of inertia.

These components provide a signature that can be exploited for event detection as explained next.

5.2.3. Sensitivity of Energy Function Components

- The component W_{25} captures the total magnetic energy stored in the transmission lines. Therefore, it is natural to expect that this component will be strongly sensitive to any event that directly involves a transmission line: such as fault, line trip, reclosing etc.
- Similarly, the components W_{22} and W_{23} capture the potential energy contributions from the active and reactive power components of the loads respectively. Hence, these components will be strongly sensitive to events that involve a significant loss or addition of load.

- Likewise, the component W_{21} captures potential energy changes due to changes in prime-mover inputs to the machine. Hence, this component will be strongly sensitive to significant addition/loss in generation.

Hence, continuously monitoring the sensitivity of these traces over a moving window gives a method to pick up and classify disturbances. Preliminary results with this approach on a small multi-machine system are shown next.

5.3. Results and Discussion

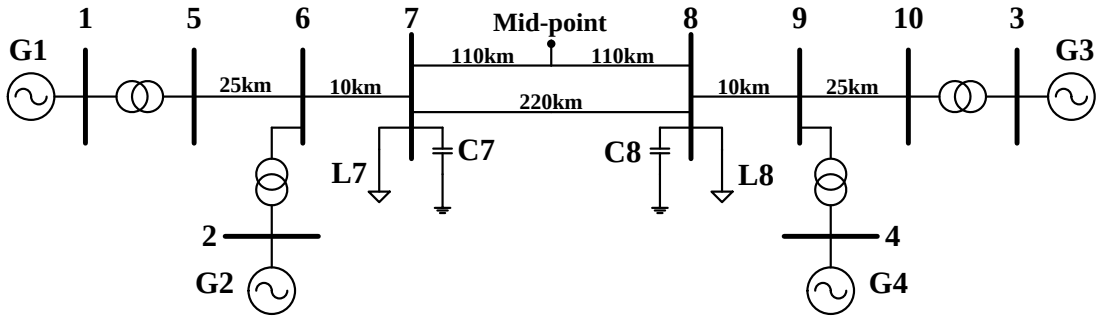

Figure 5.1. Four-machine, two-area system.

We consider the 2 area, 4 machine system [99] as shown in Fig. 5.1. We consider four events:

- Event 1: Temporary (6 cycles) 3 phase to ground fault on line;
- Event 2: 3 phase to ground fault on line section: 7-8 followed by permanent loss of line
- Event 3: Sudden addition of load at bus 8
- Event 4: Step change in reference power for generator

Preliminary results obtained with particle filtering for dynamic state estimation and construction of the energy function components are shown in Fig. 5.2.

For brevity, particle filter estimates are only shown for event 1. For all events, the particle filter with $N = 80$ particles provided reasonably accurate tracking results. The estimated states are used to compute the energy function components, which are shown next for all events.

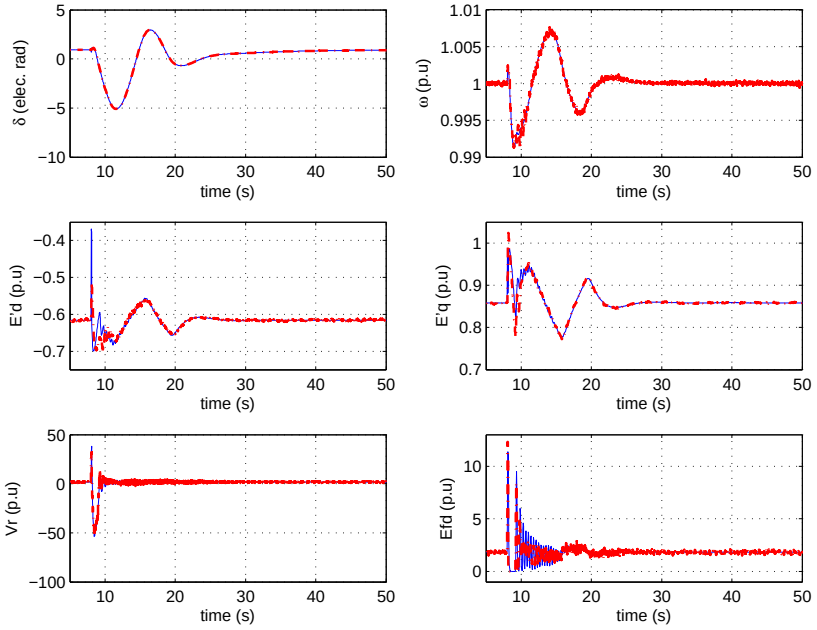

Figure 5.2. Dynamic states $(\delta, \bar{\omega}, E'_q, E'_d, E_{fd})$ estimated from the particle filter for Generator 1 in Event-1. The dashed/red lines denote estimated values. The solid/blue lines denote actual values from a numerical dynamic simulation.

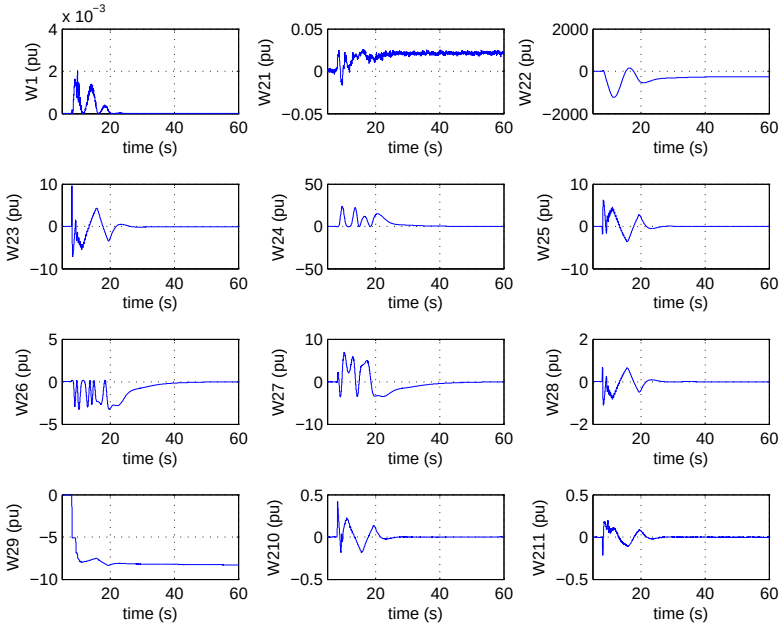

Figure 5.3. Energy function components constructed with particle filtering estimated states for Event 1

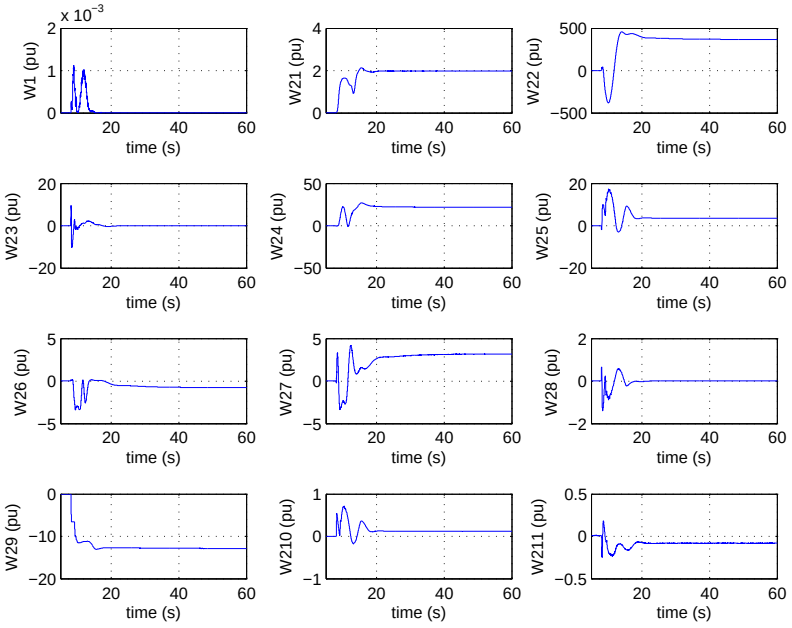

Figure 5.4. Energy function components constructed with particle filtering estimated states for Event 2

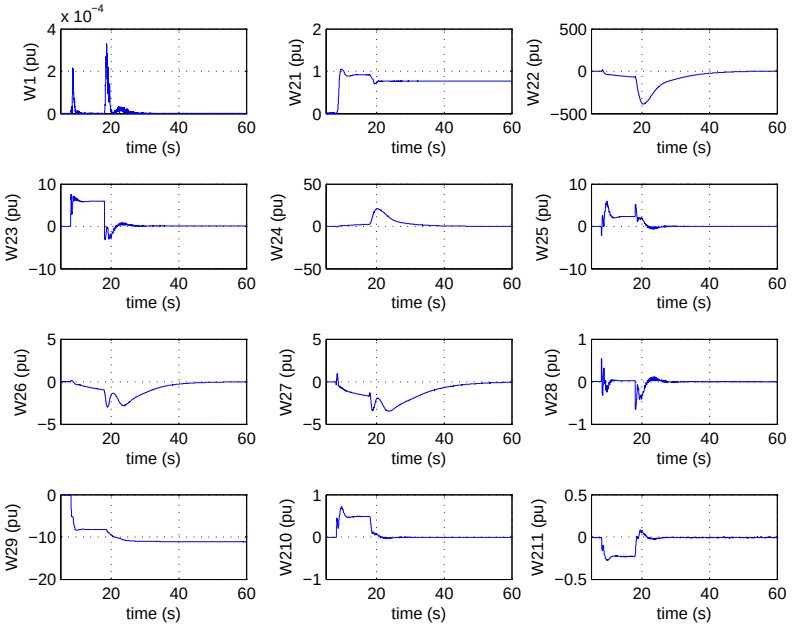

Figure 5.5. Energy function components constructed with particle filtering estimated states for Event 3

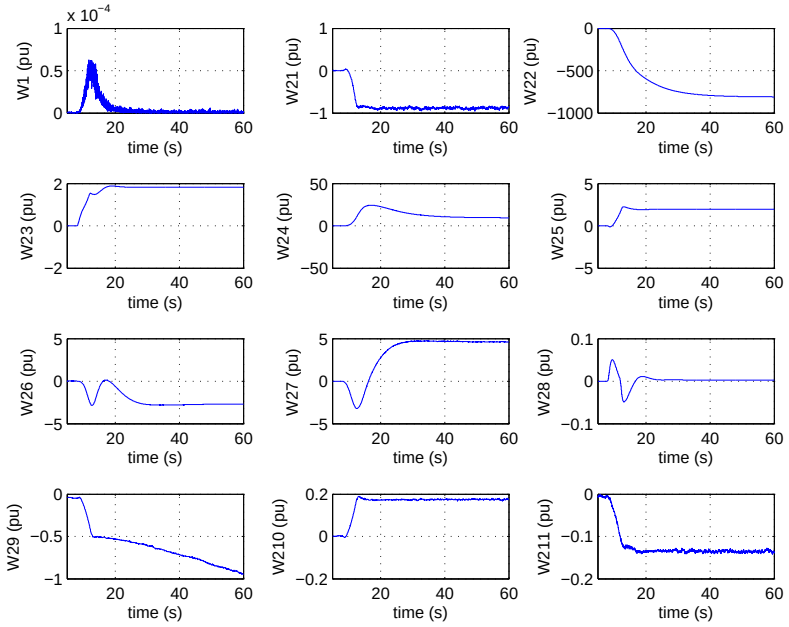

Figure 5.6. Energy function components constructed with particle filtering estimated states for Event 4

Events 1-4 represent four distinct classes of system events or disturbances. While Event-2 involves a line, Event-4 involves a generator. These two events result in two distinct signatures that are apparent from the energy function traces. It could been seen from the presented figures, the component W_{25} is strongly influenced by the line event (Event-2) in Fig. 5.4 compared to the generator event (Event-4) in Fig. 5.6. On the other hand, the potential energy term W_{21} in Fig. 5.6 for the generator event (Event-4) regarding a mechanical power reference change increases negatively while it grows positively for the other events. Comparing Event-3 (the load event) with Event-4 (the generator event), it is evident that the components W_{22} and W_{23} for the generator event (Event-4) in Fig. 5.6 are less sensitive than for the load event in Fig. 5.5. Steady-state values of a specific component could also indicate the manifest signature between two events. Consider the first two events (both relate to a three-phase ground fault), Event-2 involves a line trip while the network structure stays unchanged for Event-1. Differences in steady-state values are apparent by comparing the component W_{25} Fig. 5.4 for Event-2 versus Fig. 5.3 for Event-1. Since the energy function terms $W()$ are examined as a whole, this is a "coarse grained" approach to tag an event

under a suitable category. Each constituent in an energy function term has contributions, in turn from the specific individual components. For example, the term W_1 has M contributions, from each of the generators in the system. Likewise, the term W_{25} has contributions from each individual line in the system. Monitoring the statistical properties of each of these terms can hence give a "fine-grained" approach to pinpoint a disturbance, after it is tagged within a category. While these results provide a proof of concept on a small system, our future work will include this application on larger test systems.

5.4. Conclusions

This paper presents a novel framework for event detection in power systems based on energy functions. The key idea is the contention that the components of the energy function (rich in event information) provide a basis to "mine" events by establishing a direct correlation, or one-to-one mapping between an event and one or more distinct components of the energy function. Wide area data assumed available from PMUs is used to estimate the dynamic (internal) states of all the generators in the system via a nonlinear particle filtering approach. The estimated states and PMU data are used to construct individual components of the energy function. Preliminary simulations show that for four classes of events, there is a direct correlation between the event and the sensitivity of one of the energy function components. The proposed method thus opens up a potentially new way for feature extraction and event identification from wide area data sets that is grounded in the underlying system dynamics.

6. MODELING AND SIMULATION OF DYNAMIC COMMUNICATION LATENCY AND DATA AGGREGATION FOR WIDE-AREA APPLICATIONS

This chapter is based on the work "Modeling and simulation of dynamic communication latency and data aggregation for wide-area applications," *2016 Workshop on Modeling and Simulation of Cyber-Physical Energy Systems (MSCPES)*, Vienna, 2016, pp. 1-6. (doi: 10.1109/MSCPES.2016.7480225). The authors of the paper are Yinan Cui[1], Rajesh G. Kavasseri, and Nilanjan Ray Chaudhuri.

6.1. Introduction

Phasor Measurement Units (PMUs) and the integration of communication technologies are rapidly enabling several Wide-Area monitoring and control (WAMC) applications for bulk power systems. Increased deployment of PMUs however, result in increases in the volume of the data which has to be accommodated by communication networks while honoring the timing requirements for WAMC applications. This requires careful analysis of two factors: the latencies introduced by (a) the communication network and (b) the Phasor Data Concentrator (PDC)- the entity responsible for time alignment of PMU data. Since latencies can significantly influence control performance, there has been considerable focus on the design of latency-aware wide-area controllers. In [100], latency present in the communication channels for WAMC system is formulated with stochastic model and its influence on the wide-area control system is studied. The impact of time delay for a closed-loop controller is investigated in [101] along with a design for a robust supervisory power system stabilizer. In [102–104], the contribution of signal transmission delay is taken into account (a priori) when designing the wide-area measurement-based stabilizing controllers. It is shown in [105] that variable latencies up to tens of milliseconds can be tolerated for several WAMC applications.

[1]Yinan Cui was the first author and responsible for writing the manuscript and applying simulation tests. Dr. Rajesh G. Kavasseri and Dr. Nilanjan Ray Chaudhuri served as the proofreader and gave recommendations on drafting the paper.

However, there are certain scenarios where the latencies can build up to hundreds of milliseconds [7] (e.g communication system error correction). If such latencies are experienced during transient power swings, it can have an adverse impact for WAMC applications. An adaptive phasor power oscillation damping controller is proposed in [105] to continuously compensate time-varying and possibly large latencies.

The importance of accurate modeling of communication latencies and PDC in the context of WAMC applications for transmission system operators is discussed in [106]. While it is pointed out that the background traffic on the communication network and bandwidth determines the end-to-end delay of the link [106], the analysis is limited to static delays. A brief summary of communication delays from current PMU standards [7] is shown in Table 6.1. After the data's departure from PMUs, the latencies can vary depending on whether the data transmission uses: (a) dedicated channels with fixed (static) routing, or (b) shared channels with adaptive routing protocols. With the former, latencies are fixed and small, whereas in the latter, there can be considerable variation in latencies and the possibility for large scale fluctuations. For instance, when the transmitted data is lost and a retrieval is requested and performed, the time consumption of arrival at phasor data concentrator (PDC) side can be significantly prolonged. Generally, the end-to-end latency is affected by the network, transport, data link and the physical layer. Therefore, variability of the latency is subject to several non-deterministic factors. Currently, data re-transmission process is not supported in standard *C37.118.2-2011* [7], which however is evolving with time. If the waiting time threshold of PDC is sufficiently large, it will undoubtedly increase the latency at the PDC output-end due to the need of time alignment. Given the diversity in communication channels, routing protocols, and the competition for increased data throughput subject to finite link capacities, we argue here that the latencies that actually occur in these systems can be dynamic, i.e. time varying and develop models for the same. Specifically, the contributions of this paper are:

Table 6.1. Summary of delay source and range

Delay source	Delay range
Communication system I/O	$0.05ms$ to $30ms$
Communication distance	3.4 to 6 $\mu s/km$
Communication system buffering and error correction	$0.05ms$ to $8s$
PDC processing and time-alignment	$2ms$ to $2{+}s$

- We propose a transport delay model to account for continuously varying latencies in communication systems including large scale variations;
- We propose a PDC model for time synchronization subject to time varying latencies, and
- We illustrate the impact of these models for a typical WAMC application - namely power oscillation monitoring with standard modal analysis tools

The rest of the paper is organized as follows. A model for time-varying delays is presented in Sec. 6.2 presents and a model for PDC behavior in the wake of time varying delays is presented in Sec. 6.3. Dynamic simulation results on the IEEE 39 bus, 10 machine system illustrating the impact of these models for the WAMC application are discussed in Sec. 6.4 and conclusions are noted in Sec. 6.5.

6.2. Modeling Time-varying Delay

In general, a delayed data transmission process can be represented as an input signal $u(t)$ is "written" into the moving medium and afterwards "read" as the output $y(t)$ at a remote end [107]. This mechanism is displayed in Fig. 6.1, input signal $u(t)$ is written with speed $v_w(t)$, the moving

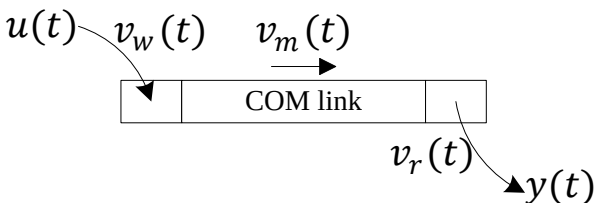

Figure 6.1. Representation of data transmission with time-delay

medium is traveling with speed $v_m(t)$ and output signal $y(t)$ is "read" with speed $v_r(t)$. The relationship between input and output with a time-varying delay τ is given by:

$$y(t) = u(t - \tau) \tag{6.1}$$

The time-varying delay is then can be obtained with respect to the time varying speed [107]:

$$v_r(t) - v_m(t) = [v_w(t - \tau) - v_m(t - \tau)](1 - \frac{d\tau}{dt})] \tag{6.2}$$

Between the data's departure at a local PMU (sending end) and arrival at the PDC, the time delay in the communication channel can be represented by the algebraic summation of different types of delays [100, 108]. The data propagation delay is only one component of the total latency and can be deterministically defined given a certain communication medium (e.g fiber-optic cable). If we treat the one-way communication process as the delivery of a datum via a specified route, the only contribution to the uncertainty of total end-to-end latency will depend on the velocity of transmission. The instantaneous delay (or total end-to-end latency) at time instant t is defined as:

$$\tau_{in}(t) = \frac{\ell}{v_m(t)} \tag{6.3}$$

where ℓ is the length of the communication route. The speed $v_m(t)$ is a time-varying variable reflecting the congestion and traffic in the channel. Therefore, we can obtain:

$$\ell = \int_{t-\tau}^{t} v_m(\eta) d\eta \tag{6.4}$$

We can reform the above equation into:

$$\int_{t-\tau}^{t} \frac{1}{\ell / v_m(\eta)} d\eta = \int_{t-\tau}^{t} \frac{1}{\tau_{in}(\eta)} d\eta = 1 \tag{6.5}$$

Where τ defines the actual time consumption of delivering the datum. And with respect to a reference time instant t_0, we have:

$$\int_{t_0}^{t} \frac{1}{\tau_{in}(\eta)} d\eta - \int_{t_0}^{t-\tau} \frac{1}{\tau_{in}(\eta)} d\eta = 1 \tag{6.6}$$

A direct method to solve for τ is introduced in [109] and it can be easily implemented in the programming environment (e.g "transport delay" in *Matlab/Simulink*). Differentiating (6.6) using *Leibniz*'s rule yields:

$$\frac{1}{\tau_{in}(t)} - \frac{1}{\tau_{in}(t-\tau)}\left(1 - \frac{d\tau}{dt}\right) = 0 \tag{6.7}$$

This relationship can be also obtained with (6.2) and (6.3) if we assume that processing speed at both ends of the communication link is high enough. The time-varying delay τ then can be calculated based on the instantaneous delay as:

$$\tau(t) = \int_{t-\Delta t}^{t} (1 - \frac{\tau_{in}(\eta - \tau(t - \Delta t))}{\tau_{in}(\eta)}) d\eta + \tau_0 \tag{6.8}$$

where τ_0 is the initial latency. Here, the instantaneous delay τ_{in} or transmission speed $v_m(t)$ is modulated to simulate the varying latency $\tau(t)$. The model can also be applied to the scenario where the datum is sent from PDC to control units in the system. In the next section, we present a model to process the received data at the PDC.

6.3. Data Aggregation at PDC

The primary function of the PDC is to receive data from multiple PMUs in the system and produce a time-aligned output data stream. A typical network structure for synchrophasor data collection is shown in Fig. 6.2. The phasor information collected by local PMUs are transmitted in real-time to a PDC at the central location of the utility. The data is aggregated with coordinated universal time (UTC) at the utility PDC and the synchrophasor information after time-alignment is then utilized for a WAMC application. While the PDC may serve other functions including error-correction, or data logging for offline analysis, we restrict our PDC model to that of time-synchronization. PDC standards are still evolving and their algorithms are vendor specific. For example, in case of congestion in one or more channels, a commercial PDC PCU400 waits till it

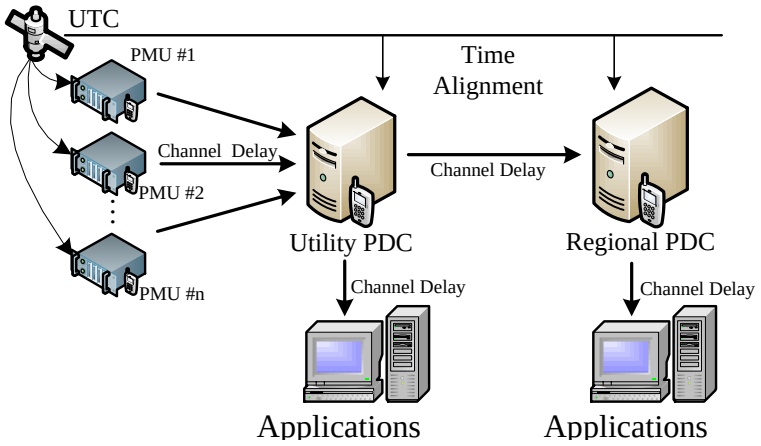

Figure 6.2. A typical structure for synchrophasor data collection

receives data from all the PMUs. Therefore, the total latency is the sum of latency in the most congested channel and the time required for synchronization [**?**]. Once the PDC receives data from all the channels it starts sending data to control center at a much faster rate (1 kHz max) until it clears the back-log. Since the time-alignment algorithms used in PDCs are vendor specific and proprietary, we consider the general model prescribed by [110] calling for a relative or absolute wait-time. The length of the waiting duration depends on the latency requirement for the subsequent applications (e.g real-time visualization or data storage). The latency processing model we consider here is illustrated in Fig. 6.3.

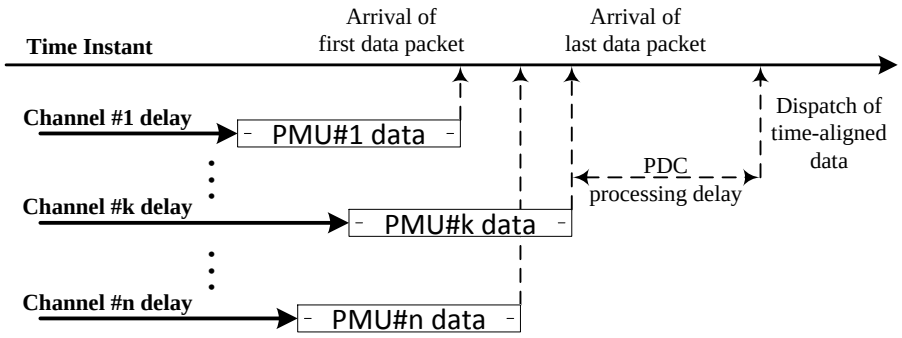

Figure 6.3. Latency of data aggregation in PDC

The time-delay τ_{PDC} between the data's departure at a local PMU and the PDC is equal to the latency τ_{last} of the last arrived PMU stream plus the PDC processing delay τ_p [105]:

$$\tau_{PDC} = \tau_{last} + \tau_p \tag{6.9}$$

While the processing delay τ_p due to the PDC depends on the algorithm implemented, it can be treated as a constant, given a specific PMU and hence we attribute *negligible variations* for τ_p. As is shown in Table 6.1, the size of the latency varies within a wide range. However, the processing delay can be anticipated according to the specified PDC functional requirements. The addition of this processing delay τ_p will only introduce a simple offset in the overall delay and does not contribute to dynamic latency variations. Therefore, the most congested channel determines the time-varying delay at the output end at the PDC. In the next section, simulation results with these models are described along with a WAMC application.

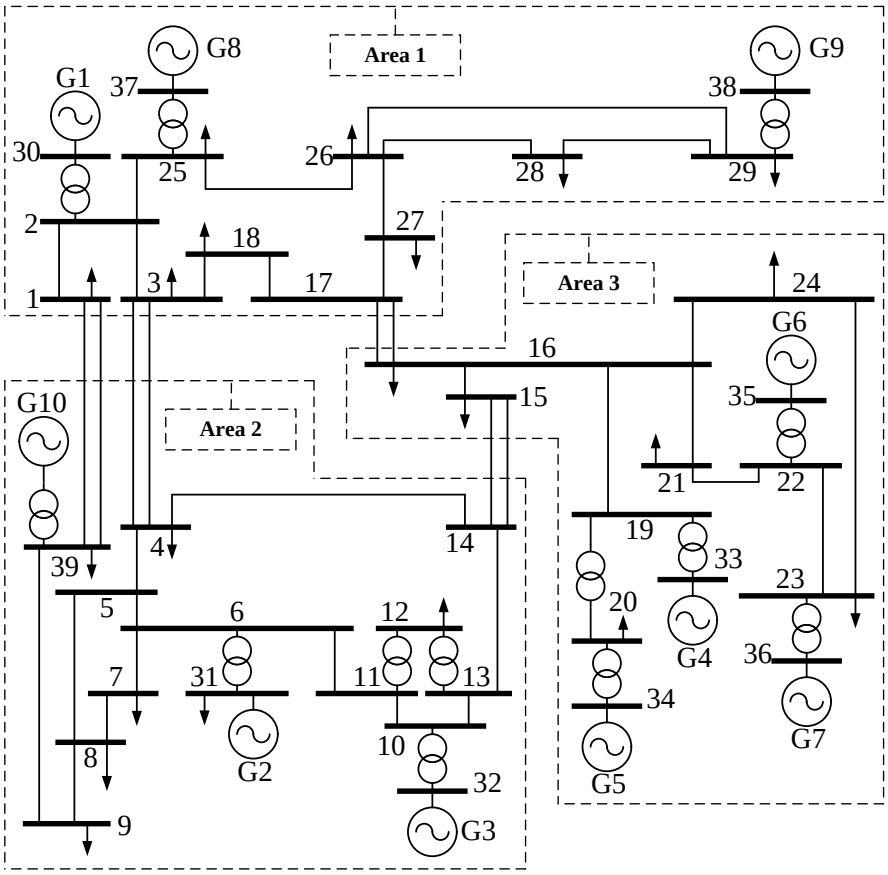

Figure 6.4. New England 10-generator 39-bus system

6.4. Results

The simulation results are presented on the New England 10-generator system [57] whose one-line diagram is shown in Fig. 6.4. The simulation is performed on *Matlab/Simulink*, where the generators are represented as a sixth-order (accounting for sub-transient dynamics) model. All generators host the steam turbine and governor except for generator 1, where the prime-mover is a hydraulic turbine. The IEEE DC1A excitation system is considered for generator 1 - 9 and power system stabilizer is also modeled and enabled at all locations. Generator 10 is assumed to have a constant field voltage input. PMUs are assumed available at the each generation site. The measurement reporting rate of the PMU is set at 60 frames per second [111]. First, in Sec. 6.4.1, we illustrate the effect of time-varying latencies by simulating a dynamic response and noting the corresponding response at the PDC end. It is important to note that the effect of dynamic latencies are most pronounced and hence more important, compared to steady state conditions. Following

this, we describe the modal analysis results with latency models, in Sec. 6.4.2. For this, note that the system is partitioned into three areas and PMU data from tie-lines between these areas (for example, line 1-39, between area 1 and area 2) is considered for the analysis.

6.4.1. Latency Variation During Transients

The power swing is initiated with a three-phase-to-ground fault. The fault is placed on one of the tie-lines (connecting *Area* 1 and 3) between bus 16 and bus 17 at $t = 6s$. The fault is then cleared by permanently tripping the line at $t = 6.08s$ (5 cycles later). All measurements are noise-free simulation results to highlight the impact of delay variations. The terminal voltage magnitude during the transients of generator 2 (denoted as G_2) is shown in Fig. 6.5. We can clearly observe the distorted signal due to the latency variation in the communication channel between PMU at G_2 and PDC. The latency build-up occurs at $t = 7s$ as the next new sample is received at PDC input-end 8 cycles later. Due to absence of new sample for the previous 7 cycles, the received data can be represented by duplication of last received sample (data holding). Note that the time-varying delay τ cannot change instantaneously as $\tau_{in}(t)$ does. Instead, it will gradually increase depending on $\tau_{in}(t)$. In the example, we apply a step-up change (from $25ms$ to $500ms$) to T_{in} at $t = 7s$. The "data holding" duration is even prolonged starting after $t = 7.1s$. This phenomenon continues until the cumulated delay τ reaches to a steady state value (approximately equal to $500ms$). Similarly to a step-down change at $t = 10s$ (from $500ms$ to $30ms$) time delay τ shifted to a new value (approximately equal to $30ms$) after 3 cycles instead of and abrupt change. Fig. 6.6 illustrates the zoomed-in version of the results shown in Fig. 6.5.

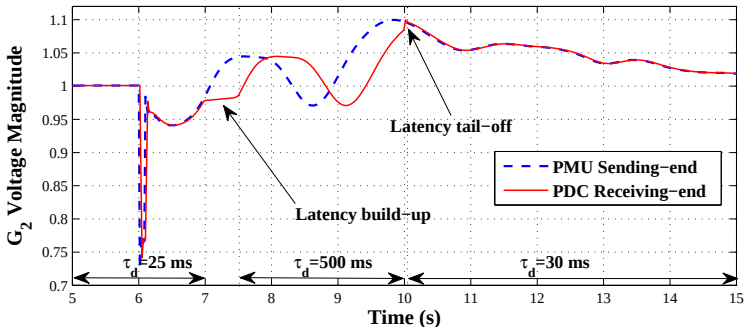

Figure 6.5. Distorted signal with time-varying latency received a PDC

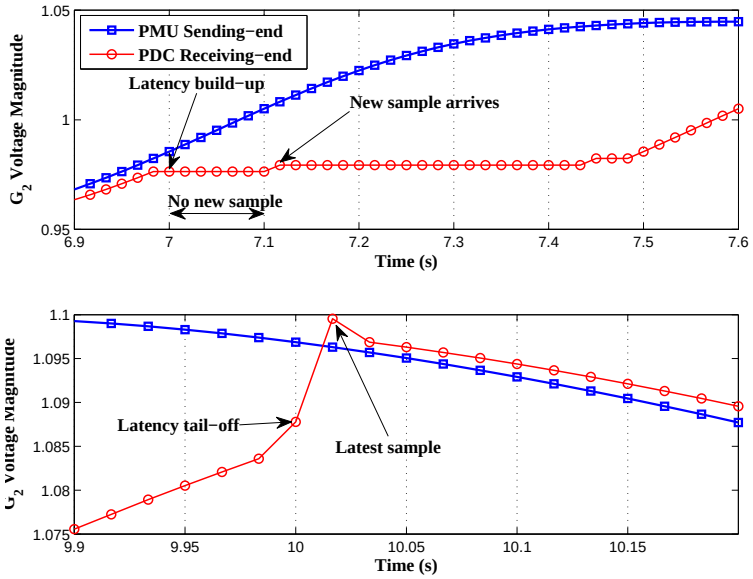

Figure 6.6. Latency change effect on PDC receiving-end

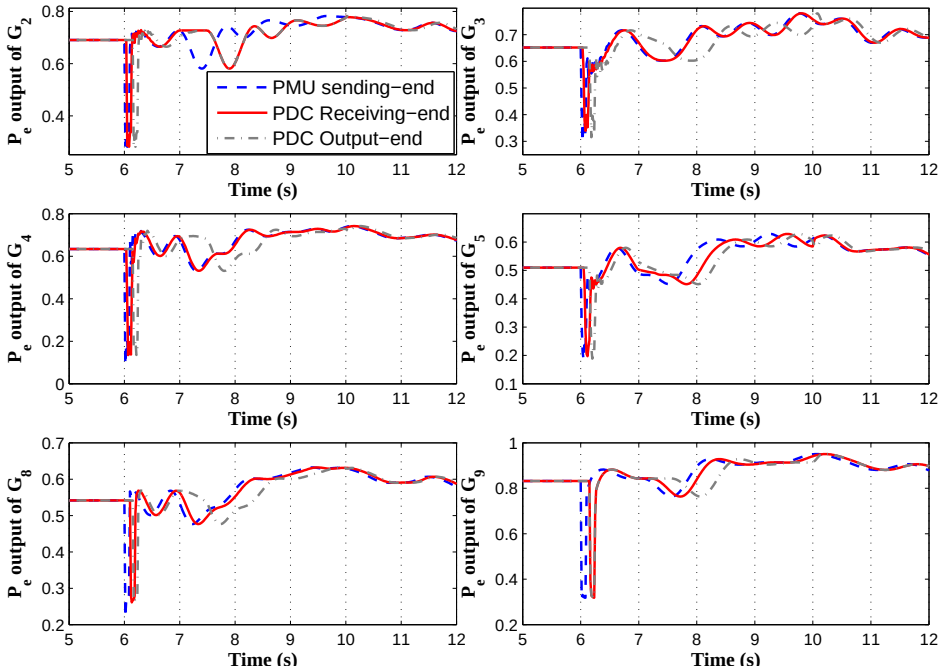

Figure 6.7. Comparison of P_e information at different locations due to delay variation

A brief summary of delay variation in communication channels for all 10 PMUs at all generation sites to PDC is given in Table 6.2. The latency build-up and tail-off in both channel "G_2 to PDC" and occur "G_5 to PDC" at $t = 7s$ and $t = 10s$ accordingly. The instantaneous latency is drawn from a Gaussian distribution whose mean and variance are shown in Table 6.2. The real power output of each generator (P_e) is collected by local PMU and then sent to PDC for

Table 6.2. Delay variation in the channels

Channel	Instantaneous Delay		
	$0 \sim 7s$	$7 \sim 10s$	$10 \sim 30s$
PMU at G_1 to PDC	$100ms$ mean $\pm$ $5ms$ std		
PMU at G_2 to PDC	$25ms$ mean $\pm$ $5ms$ std	$500ms$ mean $\pm$ $5ms$ std	$30ms$ mean $\pm$ $5ms$ std
PMU at G_3 to PDC	$40ms$ mean $\pm$ $5ms$ std		
PMU at G_4 to PDC	$40ms$ mean $\pm$ $5ms$ std		
PMU at G_5 to PDC	$60ms$ mean $\pm$ $5ms$ std	$300ms$ mean $\pm$ $5ms$ std	$25ms$ mean $\pm$ $5ms$ std
PMU at G_6 to PDC	$110ms$ mean $\pm$ $5ms$ std		
PMU at G_7 to PDC	$120ms$ mean $\pm$ $5ms$ std		
PMU at G_8 to PDC	$1000ms$ mean $\pm$ $5ms$ std		
PMU at G_9 to PDC	$150ms$ mean $\pm$ $5ms$ std		
PMU at G_10 to PDC	$80ms$ mean $\pm$ $5ms$ std		

data aggregation. A comparison of P_e at different locations (PMU sending-end, PDC receiving-end and output-end) in time-domain is shown in Fig. 6.7, 2 generator outputs are selected from each area. We can see that even though the delay variation of some channels is negligible (e.g PMUs at G_3 and G_4 to PDC), the output stream at the PDC end is clearly distorted because of the variable latencies and time-alignment at the PDC.

6.4.2. Estimation of Electromechanical Mode Using Ringdown Data

The PDC outstream can be used in several WAMC applications and transmission system operators may differ in priorities. For the Nordic region, the priorities from possible applications including: oscillation monitoring, voltage stability, frequency instability along with timing requirements and stream resolutions, is presented in [106]. The CIGRÉ working Group C4.34 on 'Application of PMUs for Monitoring Power System Dynamic Performance' is also looking into the present and future research directions for PMU applications which include model validation, load modeling and islanding detection.

Table 6.3. Latency variation in the channels

Instantaneous Delay		
$0 \sim 7s$	$7 \sim 9s$	$9 \sim 30s$
$40ms$ mean $\pm$ $5ms$ std	$300ms$ mean $\pm$ $5ms$ std	$30ms$ mean $\pm$ $5ms$ std

Here, we choose oscillation monitoring as an illustrative example, and show the impact of channel delay variations. Modal extraction from captured ringdown data for WAMC applications is discussed in [112]. The mode identification is implemented using Prony's method [55] with the sliding-window block-processing algorithm.

A power swing is initiated with a three-phase fault on line $5-6$ at $t = 6s$ and cleared at $t = 6.08s$ (5 cycles later) by tripping the line permanently. The ensuing swings are damped out within $20s$ after the disturbance. The sliding-window size is chosen to be $9s$. To create latency variations during transients, instantaneous delay at specific time instants is varied and the summary of latency variations is given in Table 6.3. This scenario is applied to all communication channels between PDC and local PMUs, which take tie-line power flow measurements. Note that there are 4 tie-lines connecting 3 areas in the system as illustrated in Fig. 6.4. The noise-free ringdown data of tie-line real power flow is shown in Fig. 6.8. To assess specific impact of the PDC, we show the modal analysis results for data at the (i) input end of the PDC and (ii) at the output end of the PDC.

6.4.2.1. Modal Analysis at the Input side of PDC

The modal characteristics for the first 9 seconds after the disturbance (from $t = 6.5s$ to $t = 15.5s$) are summarized in Table 6.4 where the raw measurements are assumed to have 1% additive Gaussian white noise.

For the first three dominant modes, the frequency and associated damping factor (DF) are noted. We observe that the presence of latency variation alters the estimated damping factors, which includes both underestimates and overestimates. There are substantial overestimates, for example, as in the damping factor for the 0.1 Hz mode on line $1-39$. Here, the consideration of latency results in an overestimate as the delayed samples are interpreted as a damped response. Similar observations are noted for the modes on line 4-3 and 16-17. Additionally, one of the

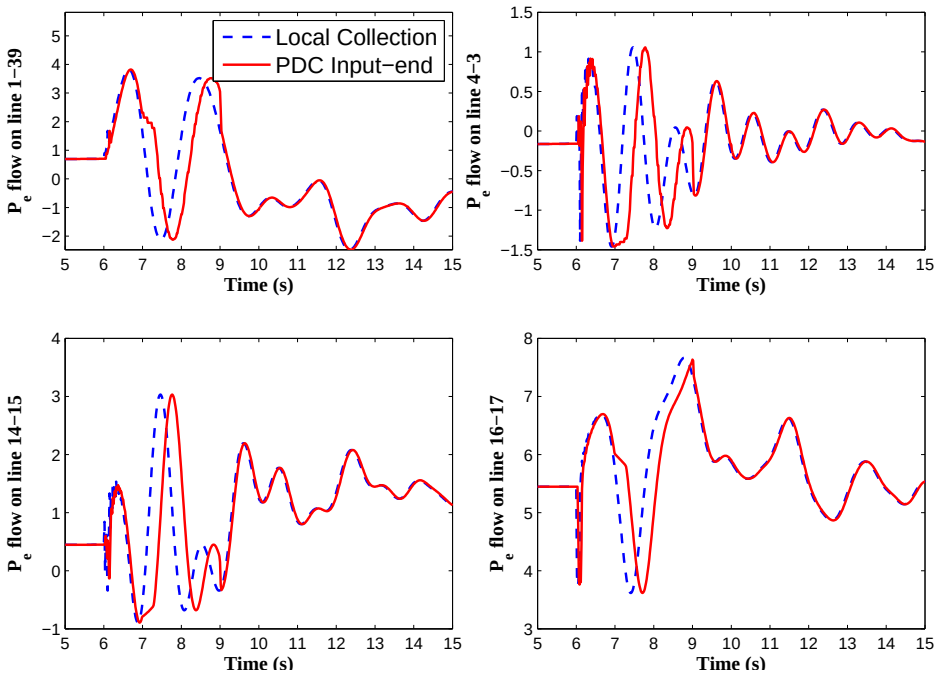

Figure 6.8. Comparison of P_e on tie-lines at different locations due to delay variation

dominant mode (0.87 Hz) for line $4-3$ is classified as 0.60 Hz. Note: The "x" denotes that the accurate damping factors are not reported when the observed mode has very weak content. Although most frequency components are not shifted significantly, the modal spectrum is mildly sensitive to the dynamic latency variations. Next, we show the results when the analysis is applied on the PDC output stream after time alignment.

6.4.2.2. Modal Analysis Results on time-aligned datastream at the PDC output end

Here, the latency variation described in Table 6.3 is applied to one of the four tie-lines. Because of the dependence on the PDC for time alignment, dynamic delays in one channel affect the output streams of all other channels. The modal results are shown in Table. 6.5. We observe both under and over-estimates of the damping factors. For the 1.03 Hz mode on line 4-3, the damping is now estimated at 11 % compared to 6 % in the absence of delays. For the same line, damping for the 0.45 Hz mode is estimated at 4 % compared to 9 % without delays, and 21 % accounting for delays. For line 1-39, both the 0.4 Hz and 0.6 Hz modes show mild sensitivity to latencies and PDC models.

Table 6.4. Modal analysis before time-alignment

Channel	Latency variation occurrence	Modes 1		Modes 2		Modes 3	
		Freq. (Hz)	DF (%)	Freq. (Hz)	DF (%)	Freq. (Hz)	DF (%)
Line flow	No	0.10	29	0.39	13	0.65	6
1-39	Yes	0.07	47	0.43	16	0.66	3
Line flow	No	0.50	9	0.87	19	1.03	6
4-3	Yes	0.46	21	0.60	45	1.11	5
Line flow	No	0.04	x	0.40	23	1.07	8
14-15	Yes	0.04	x	0.43	17	1.14	8
Line flow	No	0.19	26	0.39	15	0.61	x
16-17	Yes	0.22	29	0.4	11	0.64	x

Table 6.5. Modal analysis after time-alignment

Channel	Modes 1		Modes 2		Modes 3	
	Freq. (Hz)	DF (%)	Freq. (Hz)	DF (%)	Freq. (Hz)	DF (%)
Line flow 1-39	0.09	33	0.43	17	0.65	3
Line flow 4-3	0.46	4	0.76	7	1.07	11
Line flow 14-15	0.08	40	0.42	18	1.2	12
Line flow 16-17	0.13	50	0.45	9	1.13	7

Remarks

- We note that the modal distortion induced by latencies and/or the PDC properties depends on the swing modes, dynamic latencies in the channels and other factors: severity of the initial disturbance, time instant of the delay variation occurrence during the transients, magnitude of the latency deviation and duration of the congested conditions.
- A more severe case not reported here is when a dominant mode completely vanishes due to the extensively distorted dynamic swings.

Based on these results, we can see that the mode properties may accidentally convey optimistic system dynamics-overestimated damping factors, which can misrepresent field conditions when the mode of our interest is actually very poorly damped. Although most frequency components are not shifted significantly, the models influence modal damping factors substantially.

6.5. Conclusions

This paper proposed a transport delay model to simulate the effect of dynamic latencies in communication networks for synchrophasor-based applications. A data aggregation model for Phasor Data Concentrators is also considered to mimic the impact of dynamic latencies on time-aligned information. The resulting models are used in dynamic simulations on the IEEE 10 machine, 39 bus system for tie line oscillation monitoring using Prony analysis, a sample WAMC application. The results in general show that the proposed models significantly influence the modal spectrum, both in terms of the observed modes and their damping factors. The consideration of dynamic latencies alone was found to have a moderate impact on the modal spectrum with the modes being preserved and their damping factors mildly altered. However, the consideration of the PDC model induces strong distortions in the modal results with the modes being altered and both over- and underestimates of damping factors. The results suggest that dynamic communication latencies and PDC models must be given careful attention for designing wide-area control algorithms and remedial actions.

7. CONCLUSIONS AND RECOMMENDATIONS FOR FUTURE WORK

The integration of phasor measurement units have opened up opportunities to upgrade the existing electric grid monitoring and control system. The high sampling and reporting rate of the phasor measurements enable us to capture dynamic behavior of a power system. This is possible mainly through Dynamic State Estimation (DSE). This dissertation shows how particle filters can be tapped to robustly and accurately solve the DSE problem. The research work here is presented in five separate chapters based on previously published papers and the essential conclusions are as follows:

- Particle filters are pure probability-based Bayesian filters. Unlike existing methods based on variations of nonlinear Kalman filter. It is totally immune to the high nonlinearity of the dynamic model of the generator. A particle filter-based estimator is developed to dynamically estimate the internal states for a detailed synchronous generator model in a multi-machine setting. The method allows the inclusion of dynamic subcomponents—mainly the exciter and the prime mover control system. While the three IEEE standard exciters, a general steam turbine and a hydro-turbine model are considered. The filter utilizes the available measurements of the generator (real/reactive power outputs) and exploits phasor information (both stator voltage and current) from PMUs assumed available at the generator bus. The performance of the proposed filter is compared with the unscented Kalman filter (a prevalent and favorable choice among the existing methods for DSE) and assessed by determining the RMSD of the estimation. Time-domain simulations indicate that the proposed filter tracks the states with reasonable accuracy and reliability for different classes of disturbances on the IEEE 14-bus system. With improvements in computational power, the work suggests the potential of using particle filters for (near) real-time applications.

- We show how DSE is a powerful tool for system protection by developing a protection application. Due to the dearth of direct measurement of phasor angle difference, the classical and conventional OOS protection philosophy has been based on measuring the apparent

impedance trajectory. We introduce an OOS detection method based on direct estimation of angular difference to serve as a supervisory unit of conventional impedance type relays. The concept rests on two modules: the availability of PMU measurements at the generator bus and a PF-based dynamic state estimator. The two modules provide an estimate of the angular separation between the generator's rotor angle (treated as a dynamic state) and the external system. The separation is then analyzed using a modal analysis tool (matrix pencils) to determine the damping of the modal content(s) and the likelihood of potentially unstable swings. Simulation results on the 10-generator, 39-bus system show that the proposed approach matches the security and dependability of the most secure OOS scheme - single blinder scheme, while providing early detection of OOS for both monotonically unstable and marginally unstable swings.

- A dual-filter method is proposed to estimate the dynamic states for synchronous generators. The method is particularly useful for scenarios where the actual model of the excitation is either unknown, or when there is an internal failure in the excitation system resulting in partial or complete loss in excitation, or when the parameters within the system are not known precisely. The particle filter is modified to estimate the states and the unknown parameter in a sequential manner. Time-domain simulations on a 10-machine, 39-bus system with case studies under routine disturbances indicate while the tracking accuracy of the proposed filter is comparable to that of EKFUI method for the internal states, there is a drastic reduction in the field voltage estimation error for noise levels up to 5%. The robustness of the filter to noise and performance under these modeling assumptions suggest that the such a filter may serve as a *computational surveillance* unit to supervise the functioning of excitation systems.

- Event detection is an essential function in modern EMS as it helps improve situational awareness for securing the operation of the system.We propose a novel framework for event detection in power systems based on energy functions. The key idea is that the components of the energy function with rich dynamic information provide a basis to identify events by establishing a direct correlation, or one-to-one mapping between an event and one or more distinct components of the energy function. Wide area measurements assumed available from PMUs is used to estimate the dynamic (internal) states of all the generators in the system via the

proposed particle filtering approach. The estimated states and PMU data are then used to construct individual components of the energy function. Preliminary simulations show that for four classes of events, there is a direct correlation between the event and the sensitivity of one of the energy function components.

- Deployment of synchrophasor-based application creates challenge for big data transmission. The centralized functions in EMS are implemented in real time or near real time, it is necessary to consider the latency factors from the communication network and phasor data concentrator, which is in charge of time-alignment for PMU measurements collected at different locations. We propose a transport delay model to simulate the effect of dynamic latencies in communication networks. A data aggregation model for phasor data concentrators is considered to mimic the impact of dynamic latencies during time alignment process. The proposed models are used in dynamic simulations on the IEEE 10 machine, 39 bus system for tie line oscillation monitoring using Prony analysis. The results suggest that dynamic communication latencies and PDC models must be given careful attention for designing wide-area control algorithms and remedial actions.

Apart from the mentioned EKF and UKF method, other approach like ensemble Kalman filter and extensions of generic filtering techniques are proposed to solve the DSE problem. Some of the methods have been tested and proved to have a better performance than the generic PF method discussed in this dissertation. PF method should NOT be treated as the unique solution and only option for tracking the dynamic states. We shall consider the application accuracy requirement and computational resource we have in order to select the appropriate method. One problem that still remains open is the sensitivity analysis of the dynamic model when applying the filtering techniques. The dissertation has already attempted to analyze the performance of PF with dynamic model uncertainty, but how much impact each model constant will bring when the model is not accurate needs further investigation.

In this dissertation, only rotor angle estimation is used for a new local protection method. With a detailed generator dynamic model, plenty of internal states can be captured in the DSE process, other protection and control methods can be designed based on these rich dynamics. Currently only directly measured phasor information is transmitted to a PDC for applications in

WAMS. If the dynamic states of the inter-connected synchronous generators can be aggregated for centralized application, it would open up a new stage for wide area monitoring, protection and control system. Conventional relay and other controllers are designed based on local data, future analysis would consider the protection and control applications from a global standpoint and involve coordination between components from different regions. The corresponding tests and simulation should be implemented on larger scale systems to validate such ideas.

REFERENCES

[1] A. Abur and A. G. Expósito, *Power System State Estimation: Theory and Implementation*. New York: CRC Press, 2004.

[2] Z. Huang, K. Schneider, and J. Nieplocha, "Feasibility studies of applying kalman filter techniques to power system dynamic state estimation," in *Power Engineering Conference, 2007. IPEC 2007. International*, 2007, pp. 376–382.

[3] E. Ghahremani and I. Kamwa, "Dynamic state estimation in power system by applying the extended kalman filter with unknown inputs to phasor measurements," *Power Systems, IEEE Transactions on*, vol. 26, no. 4, pp. 2556–2566, 2011.

[4] S. Wang, W. Gao, and A. Meliopoulos, "An alternative method for power system dynamic state estimation based on unscented transform," *Power Systems, IEEE Transactions on*, vol. 27, no. 2, pp. 942–950, 2012.

[5] A. Singh and B. Pal, "Decentralized dynamic state estimation in power systems using unscented transformation," *IEEE Transactions on Power Systems*, vol. 29, no. 2, pp. 794–804, March 2014.

[6] D. Simon, *Optimal State Estimation: Kalman, H_∞, and Nonlinear Approaches*. Hoboken, NJ: Wiley-Interscience, 2006.

[7] "IEEE Standard for Synchrophasor Data Transfer for Power Systems," *IEEE Std C37.118.2-2011 (Revision of IEEE Std C37.118-2005)*, pp. 1–53, Dec 2011.

[8] C. Gharban and B. Cory, "Non-linear dynamic power system state estimation," *IEEE Transactions on Power Systems*, vol. 1, no. 3, pp. 276–283, Aug 1986.

[9] "Setting-less protection method (PSERC Project S-48G)," Electric Power Research Institute (EPRI), Grid Transformation Workshop Results, 2012.

[10] Z. Huang, K. Schneider, and J. Nieplocha, "Feasibility studies of applying kalman filter techniques to power system dynamic state estimation," in *Power Engineering Conference, 2007. IPEC 2007. International*, 2007, pp. 376–382.

[11] S. Wang, W. Gao, and A. Meliopoulos, "An alternative method for power system dynamic state estimation based on unscented transform," *IEEE Transactions on Power Systems*, vol. 27, no. 2, pp. 942–950, 2012.

[12] E. Ghahremani and I. Kamwa, "Dynamic state estimation in power system by applying the extended kalman filter with unknown inputs to phasor measurements," *IEEE Transactions on Power Systems*, vol. 26, no. 4, pp. 2556–2566, 2011.

[13] ——, "Online State Estimation of a Synchronous Generator Using Unscented Kalman Filter From Phasor Measurements Units," *IEEE Transactions on Energy Conversion*, vol. 26, no. 4, pp. 1099–1108, 2011.

[14] D. Meng, N. Zhou, S. Lu, and G. Lin, "Estimate the electromechanical states using particle filtering and smoothing," in *Power and Energy Society General Meeting, 2012 IEEE*, 2012, pp. 1–7.

[15] N. Zhou, D. Meng, and S. Lu, "Estimation of the Dynamic States of Synchronous Machines Using an Extended Particle Filter," *IEEE Transactions on Power Systems*, vol. 28, no. 4, pp. 4152–4161, 2013.

[16] M. Arulampalam, S. Maskell, N. Gordon, and T. Clapp, "A tutorial on particle filters for online nonlinear/non-gaussian bayesian tracking," *IEEE Transactions on Signal Processing*, vol. 50, no. 2, pp. 174–188, 2002.

[17] A. Kong, J. S. Liu, and W. H. Wong, "Sequential imputations and bayesian missing data problems," *Journal of the American Statistical Association*, vol. 89, no. 425, pp. pp. 278–288, 1994.

[18] S. G. Arnaud Doucet and C. Andrieu, "On sequential monte carlo sampling methods for bayesian filtering," *Statistics and Computing*, vol. 10, no. 3, pp. 197–208, 2000.

[19] R. Douc and O. Cappe, "Comparison of resampling schemes for particle filtering," in *Image and Signal Processing and Analysis, 2005. ISPA 2005. Proceedings of the 4th International Symposium on*, 2005, pp. 64–69.

[20] P. W. Sauer and M. A. Pai, *Power System Dynamics and Stability.* Upper Saddle River, NJ: Prentice Hall, 1998.

[21] P. Kundur, *Power System Stability and Control.* New York, NY: McGraw-Hill Professional, 1994.

[22] J. Arrillaga and N. R. Watson, *Computer Modelling of Electrical Power Systems.* Hoboken, NJ: Wiley, 2001.

[23] M. Eremia and M. Shahidehpour, *Handbook of Electrical Power System Dynamics: Modeling, Stability, and Control.* Hoboken, NJ: Wiley-IEEE Press, 2013.

[24] "IEEE Recommended Practice for Excitation System Models for Power System Stability Studies," *IEEE Std 421.5-2005 (Revision of IEEE Std 421.5-1992)*, pp. 1–85, 2006.

[25] "Dynamic models for steam and hydro turbines in power system studies," *IEEE Transactions on Power Apparatus and Systems*, vol. PAS-92, no. 6, pp. 1904–1915, 1973.

[26] K. R. Padiyar, *Power System Dynamics: Stability & Control.* Hyderabad, India: B. S. Publications, 2008.

[27] D. Ramey and J. Skooglund, "Detailed hydrogovernor representation for system stability studies," *IEEE Transactions on Power Apparatus and Systems*, vol. PAS-89, no. 1, pp. 106–112, Jan 1970.

[28] J. Burnett, R.O., M. Butts, and P. Sterlina, "Power system applications for phasor measurement units," *Computer Applications in Power, IEEE*, vol. 7, no. 1, pp. 8–13, 1994.

[29] L. Freris and A. Sasson, "Investigation of the load-flow problem," *Electrical Engineers, Proceedings of the Institution of*, vol. 115, no. 10, pp. 1459–1470, October 1968.

[30] "Real-time application of synchrophasors for improving reliability," North American Electric Reliability Corporation (NERC), NERC Report, 2010.

[31] "IEEE Standard for Synchrophasors for Power Systems," *IEEE Std C37.118-2005 (Revision of IEEE Std 1344-1995)*, pp. 1–57, 2006.

[32] J. H. Kotecha and P. Djuric, "Gaussian particle filtering," *IEEE Transactions on Signal Processing*, vol. 51, no. 10, pp. 2592–2601, 2003.

[33] "Power swing and out-of-step considerations on transmission lines," IEEE Power System Relaying Committee (PSRC) Working Group D6, Report, 2005.

[34] "IEEE tutorial on the protection of synchronous generators," Power System Relaying Committee Report by J Subcommittee, Tech. Rep., 2012.

[35] D. Reimert, *Protective Relaying for Power Generation Systems*. Boca Raton, FL: CRC Press.

[36] "Setting-less protection method," Electric Power Research Institute (EPRI), Grid Transformation Workshop Results, 2012.

[37] S. Paudyal, G. Ramakrishna, and M. Sachdev, "Application of equal area criterion conditions in the time domain for out-of-step protection," *IEEE Transactions on Power Delivery*, vol. 25, no. 2, pp. 600–609, April 2010.

[38] B. Shrestha, R. Gokaraju, and M. Sachdev, "Out-of-step protection using state-plane trajectories analysis," *IEEE Transactions on Power Delivery*, vol. 28, no. 2, pp. 1083–1093, April 2013.

[39] K. Malmedal, P. Sen, and J. Nelson, "Application of out-of-step relaying for small generators in distributed generation," *IEEE Transactions on Industry Applications*, vol. 41, no. 6, pp. 1506–1514, Nov 2005.

[40] P. Kundur, J. Paserba, V. Ajjarapu, G. Andersson, A. Bose, C. Canizares, N. Hatziargyriou, D. Hill, A. Stankovic, C. Taylor, T. Van Cutsem, and V. Vittal, "Definition and classification of power system stability IEEE/CIGRÉ joint task force on stability terms and definitions," *IEEE Transactions on Power Systems*, vol. 19, no. 3, pp. 1387–1401, Aug 2004.

[41] C.-W. Liu, M.-C. Su, S.-S. Tsay, and Y.-J. Wang, "Application of a novel fuzzy neural network to real-time transient stability swings prediction based on synchronized phasor measurements," *IEEE Transactions on Power Systems*, vol. 14, no. 2, pp. 685–692, May 1999.

[42] W. Rebizant and K. Feser, "Fuzzy logic application to out-of-step protection of generators," in *Power Engineering Society Summer Meeting, 2001*, vol. 2, 2001, pp. 927–932 vol.2.

[43] J. Yan, C.-C. Liu, and U. Vaidya, "PMU-Based Monitoring of Rotor Angle Dynamics," *IEEE Transactions on Power Systems*, vol. 26, no. 4, pp. 2125–2133, Nov 2011.

[44] K. Padiyar and S. Krishna, "Online detection of loss of synchronism using energy function criterion," *IEEE Transactions on Power Delivery*, vol. 21, no. 1, pp. 46–55, Jan 2006.

[45] Z. Huang, N. Zhou, R. Diao, S. Wang, S. Elbert, D. Meng, and S. Lu, "Capturing real-time power system dynamics: Opportunities and challenges," in *Power Energy Society General Meeting, 2015 IEEE*, July 2015, pp. 1–5.

[46] E. Ghahremani and I. Kamwa, "Local and Wide-Area PMU-Based Decentralized Dynamic State Estimation in Multi-Machine Power Systems," *IEEE Transactions on Power Systems*, vol. 31, no. 1, pp. 547–562, Jan 2016.

[47] A. Singh and B. Pal, "Decentralized Control of Oscillatory Dynamics in Power Systems Using an Extended LQR," *IEEE Transactions on Power Systems*, vol. 31, no. 3, pp. 1715–1728, May 2016.

[48] "IEEE Guide for AC Generator Protection," *IEEE Std C37.102-2006 (Revison of IEEE Std C37.102-1995)*, pp. 1–173, Aug 2013.

[49] E. Clarke, "Impedances seen by relays during power swings with and without faults," *Transactions of the American Institute of Electrical Engineers*, vol. 64, no. 6, pp. 372–384, June 1945.

[50] C. Taylor, J. Haner, L. Hill, W. Mittelstadt, and R. Cresap, "A new out-of-step relay with rate of change of apparent resistance augmentation," *IEEE Transactions on Power Apparatus and Systems*, vol. PAS-102, no. 3, pp. 631–639, March 1983.

[51] "IEEE Standard for Synchrophasor Measurements for Power Systems," *IEEE Std C37.118.1-2011 (Revision of IEEE Std C37.118-2005)*, pp. 1–61, Dec 2011.

[52] Y. Wang, C. Wang, F. Lin, W. Li, L. Y. Wang, and J. Zhao, "Incorporating generator equivalent model into voltage stability analysis," *IEEE Transactions on Power Systems*, vol. 28, no. 4, pp. 4857–4866, Nov 2013.

[53] Y. Cui and R. Kavasseri, "A particle filter for dynamic state estimation in multi-machine systems with detailed models," *IEEE Transactions on Power Systems*, vol. 30, no. 6, pp. 3377–3385, Nov 2015.

[54] M. Eremia and M. Shahidehpour, *Handbook of Electrical Power System Dynamics: Modeling, Stability, and Control*. Hoboken, NJ: Wiley-IEEE Press, 2013.

[55] J. Hauer, C. Demeure, and L. Scharf, "Initial results in prony analysis of power system response signals," *IEEE Transactions on Power Systems*, vol. 5, no. 1, pp. 80–89, Feb 1990.

[56] M. Crow and A. Singh, "The matrix pencil for power system modal extraction," *IEEE Transactions on Power Systems*, vol. 20, no. 1, pp. 501–502, Feb 2005.

[57] M. A. Pai, *Energy Function Analysis for Power System Stability*. Norwell, Massachusetts: Kluwer Academic Publishers, 1989.

[58] C. R. Mason, "A new loss-of-excitation relay for synchronous generators," *Transactions of the American Institute of Electrical Engineers*, vol. 68, no. 2, pp. 1240–1245, July 1949.

[59] J. Berdy, "Loss of excitation protection for modern synchronous generators," *IEEE Transactions on Power Apparatus and Systems*, vol. 94, no. 5, pp. 1457–1463, Sept 1975.

[60] L. L. Grigsby, *Power System Stability and Control (Electric Power Engineering Handbooks)*. Boca Raton, FL: CRC Press, 2012.

[61] Z. Huang, K. Schneider, J. Nieplocha, and N. Zhou, "Estimating power system dynamic states using extended kalman filter," in *2014 IEEE PES General Meeting — Conference Exposition*, July 2014, pp. 1–5.

[62] R. Kavasseri, Y. Cui, and S. Brahma, "A new approach for event detection based on energy functions," in *PES General Meeting — Conference Exposition, 2014 IEEE*, July 2014, pp. 1–5.

[63] Y. Cui, R. Kavasseri, and S. Brahma, "Dynamic state estimation assisted posturing for generator out-of-step protection," in *2016 IEEE Power and Energy Society General Meeting (PESGM)*, July 2016, pp. 1–5.

[64] Z. Huang, P. Du, D. Kosterev, and S. Yang, "Generator dynamic model validation and parameter calibration using phasor measurements at the point of connection," *IEEE Transactions on Power Systems*, vol. 28, no. 2, pp. 1939–1949, May 2013.

[65] D. Meng, N. Zhou, S. Lu, and G. Lin, "An expectation-maximization method for calibrating synchronous machine models," in *2013 IEEE Power Energy Society General Meeting*, July 2013, pp. 1–5.

[66] M. Ariff, B. Pal, and A. Singh, "Estimating dynamic model parameters for adaptive protection and control in power system," *IEEE Transactions on Power Systems*, vol. 30, no. 2, pp. 829–839, March 2015.

[67] B. Zaker, G. B. Gharehpetian, M. Karrari, and N. Moaddabi, "Simultaneous parameter identification of synchronous generator and excitation system using online measurements," *IEEE Transactions on Smart Grid*, vol. 7, no. 3, pp. 1230–1238, May 2016.

[68] A. Zia, T. Kirubarajan, J. Reilly, D. Yee, K. Punithakumar, and S. Shirani, "An em algorithm for nonlinear state estimation with model uncertainties," *IEEE Transactions on Signal Processing*, vol. 56, no. 3, pp. 921–936, March 2008.

[69] C. Nemeth, P. Fearnhead, and L. Mihaylova, "Sequential monte carlo methods for state and parameter estimation in abruptly changing environments," *IEEE Transactions on Signal Processing*, vol. 62, no. 5, pp. 1245–1255, March 2014.

[70] J. Liu and M. West, "Combined parameter and state estimation in simulation-based filtering," in *Sequential Monte Carlo Methods in Practice*, A. Doucet, N. de Freitas, and N. Gordon, Eds. Springer New York, 2001, pp. 197–223.

[71] I. Collings, V. Krishnamurthy, and J. Moore, "On-line identification of hidden markov models via recursive prediction error techniques," *IEEE Transactions on Signal Processing*, vol. 42, no. 12, pp. 3535–3539, Dec 1994.

[72] N. Daroogheh, N. Meskin, and K. Khorasani, "Particle filtering for state and parameter estimation in gas turbine engine fault diagnostics," in *American Control Conference (ACC), 2013*, June 2013, pp. 4343–4349.

[73] C. Andrieu, A. Doucet, S. S. Singh, and V. B. Tadic, "Particle methods for change detection, system identification, and control," *Proceedings of the IEEE*, vol. 92, no. 3, pp. 423–438, Mar 2004.

[74] "IEEE Recommended Practice for Excitation System Models for Power System Stability Studies," *IEEE Std 421.5-2005 (Revision of IEEE Std 421.5-1992)*, pp. 1–85, 2006.

[75] S. Akhlaghi, N. Zhou, and Z. Huang, "Exploring adaptive interpolation to mitigate non-linear impact on estimating dynamic states," in *2015 IEEE Power Energy Society General Meeting*, July 2015, pp. 1–5.

[76] ——, "A multi-step adaptive interpolation approach to mitigating the impact of nonlinearity on dynamic state estimation," *IEEE Transactions on Smart Grid*, vol. PP, no. 99, pp. 1–1, 2016.

[77] N. Zhou, D. Meng, Z. Huang, and G. Welch, "Dynamic State Estimation of a Synchronous Machine Using PMU Data: A Comparative Study," *IEEE Transactions on Smart Grid*, vol. 6, no. 1, pp. 450–460, Jan 2015.

[78] J. Ma, R. Diao, Y. V. Makarov, P. V. Etingov, N. Zhou, and J. E. Dagle, "Building decision trees for characteristic ellipsoid method to monitor power system transient behaviors," in *Power and Energy Society General Meeting, 2010 IEEE*, July 2010, pp. 1 –8.

[79] J. Ma, Y. V. Makarov, C. H. Miller, and T. B. Nguyen, "Use multi-dimensional ellipsoid to monitor dynamic behavior of power systems based on PMU measurement," in *Power and Energy Society General Meeting, 2008, IEEE*, July 2008, pp. 1 –8.

[80] F. Lingling, R. Kavasseri, M. Zhixin, D. Osborn, and T. Bilke, "Identification of system wide disturbances using synchronized phasor data and ellipsoid method," in *Power and Energy Society General Meeting, 2008, IEEE*, July 2008, pp. 1 –10.

[81] O. P. Dahal and S. M. Brahma, "Preliminary work to classify the disturbance events recorded by phasor measurement units," in *Power Energy Society General Meeting, 2012, IEEE*, July 2012, pp. 1 –8.

[82] Om Prasad Dahal, Sukumar Brahma, and Huiping Cao, "Comprehensive clustering of disturbance events recorded by phasor measurement units, *In Press, Power Delivery, IEEE Transactions on*," October 2013. [Online]. Available: https://www.dropbox.com/s/jr3ie5ydq7vi5bl/previouswork.pdf

[83] P. Kumar and E. A. Yildirim, "Minimum-volume enclosing ellipsoids and core sets," *J. Optim. Theory Appl.*, vol. 126, pp. 1–21, 2005.

[84] M. Pavella and P. G. Murthy, *Transient Stability of Power Systems: Theory and Practice*. John Wiley and Sons, Sussex, 1994.

[85] K. R. Padiyar, *Structure Preserving Energy Functions: Theory and Applications*. CRC Press, Boca Raton, FL, 2013.

[86] A. H. El-Abiad and K. Nagappan, "Transient stability regions of multimachine power systems," *Power Apparatus and Systems, IEEE Transactions on*, vol. PAS-85, no. 2, pp. 169–179, 1966.

[87] J. Willems and J. Willems, "The application of lyapunov methods to the computation of transient stability regions for multimachine power systems," *Power Apparatus and Systems, IEEE Transactions on*, vol. PAS-89, no. 5, pp. 795–801, 1970.

[88] N. Kakimoto, Y. Ohsawa, and M. Hayashi, "Transient stability analysis of multimachine power system with field flux decays via lyapunov's direct method," *Power Apparatus and Systems, IEEE Transactions on*, vol. PAS-99, no. 5, pp. 1819–1827, 1980.

[89] K. R. Padiyar and H. S. Y. Sastry, "Fast evaluation of transient stability of power systems using a structure preserving energy function," *Electric Machines &*

Power Systems, vol. 11, no. 5, pp. 421–441, 1986. [Online]. Available: http://www.tandfonline.com/doi/abs/10.1080/07313568608909198

[90] V. Vittal, S. Rajagopal, A. A. Fouad, M. A. El-Kady, E. Vaahedi, and V. F. Carvalho, "Transient stability analysis of stressed power systems using the energy function method," *Power Systems, IEEE Transactions on*, vol. 3, no. 1, pp. 239–244, 1988.

[91] V. Vittal, E.-Z. Zhou, C. Hwang, and A.-A. Fouad, "Derivation of stability limits using analytical sensitivity of the transient energy margin," *Power Systems, IEEE Transactions on*, vol. 4, no. 4, pp. 1363–1372, 1989.

[92] H.-D. Chiang, F. Wu, and P. Varaiya, "Foundations of the potential energy boundary surface method for power system transient stability analysis," *Circuits and Systems, IEEE Transactions on*, vol. 35, no. 6, pp. 712–728, 1988.

[93] ——, "A bcu method for direct analysis of power system transient stability," *Power Systems, IEEE Transactions on*, vol. 9, no. 3, pp. 1194–1208, 1994.

[94] R. Davy and I. Hiskens, "Lyapunov functions for multimachine power systems with dynamic loads," *Circuits and Systems I: Fundamental Theory and Applications, IEEE Transactions on*, vol. 44, no. 9, pp. 796–812, 1997.

[95] A.-A. Fouad and V. Vittal, *Power system transient stability analysis using the transient energy function method.* Prentice Hall , Englewood Cliffs, NJ, 1992.

[96] M. Pai, *Energy function analysis for power system stability.* Kluwer Academic, 1989.

[97] T. Overbye and C. DeMarco, "Improved techniques for power system voltage stability assessment using energy methods," *Power Systems, IEEE Transactions on*, vol. 6, no. 4, pp. 1446–1452, 1991.

[98] J. Chow, A. Chakrabortty, M. Arcak, B. Bhargava, and A. Salazar, "Synchronized phasor data based energy function analysis of dominant power transfer paths in large power systems," *Power Systems, IEEE Transactions on*, vol. 22, no. 2, pp. 727–734, 2007.

[99] P. Kundur, *Power System Stability and Control.* McGraw-Hill, 1993.

[100] J. Stahlhut, T. Browne, G. Heydt, and V. Vittal, "Latency viewed as a stochastic process and its impact on wide area power system control signals," *IEEE Transactions on Power Systems*, vol. 23, no. 1, pp. 84–91, Feb 2008.

[101] H. Wu, K. Tsakalis, and G. Heydt, "Evaluation of time delay effects to wide-area power system stabilizer design," *IEEE Transactions on Power Systems*, vol. 19, no. 4, pp. 1935–1941, Nov 2004.

[102] B. Chaudhuri, R. Majumder, and B. Pal, "Wide-area measurement-based stabilizing control of power system considering signal transmission delay," *IEEE Transactions on Power Systems*, vol. 19, no. 4, pp. 1971–1979, Nov 2004.

[103] D. Dotta, A. e Silva, and I. Decker, "Wide-area measurements-based two-level control design considering signal transmission delay," *IEEE Transactions on Power Systems*, vol. 24, no. 1, pp. 208–216, Feb 2009.

[104] W. Yao, L. Jiang, J. Wen, Q. Wu, and S. Cheng, "Wide-area damping controller of facts devices for inter-area oscillations considering communication time delays," *IEEE Transactions on Power Systems*, vol. 29, no. 1, pp. 318–329, Jan 2014.

[105] N. Chaudhuri, S. Ray, R. Majumder, and B. Chaudhuri, "A new approach to continuous latency compensation with adaptive phasor power oscillation damping controller (pod)," *IEEE Transactions on Power Systems*, vol. 25, no. 2, pp. 939–946, May 2010.

[106] M. Chenine and L. Nordstrom, "Modeling and simulation of wide-area communication for centralized pmu-based applications," *IEEE Transactions on Power Delivery*, vol. 26, no. 3, pp. 1372–1380, July 2011.

[107] R. Johnson, "General analysis of time-variable delay devices," *Electronics Letters*, vol. 4, no. 13, pp. 263–264, June 1968.

[108] B. Naduvathuparambil, M. Valenti, and A. Feliachi, "Communication delays in wide area measurement systems," in *System Theory, 2002. Proceedings of the Thirty-Fourth Southeastern Symposium on*, 2002, pp. 118–122.

[109] F. Zhang and M. Yeddanapudi, "Modeling and simulation of time-varying delays," in *Proceedings of the 2012 Symposium on Theory of Modeling and Simulation - DEVS Integrative M&S Symposium*, ser. TMS/DEVS '12, 2012, pp. 34:1–34:8.

[110] "IEEE Guide for Phasor Data Concentrator Requirements for Power System Protection, Control, and Monitoring," *IEEE Std C37.244-2013*, pp. 1–65, May 2013.

[111] "IEEE Standard for Synchrophasor Measurements for Power Systems," *IEEE Std C37.118.1-2011 (Revision of IEEE Std C37.118-2005)*, pp. 1–61, Dec 2011.

[112] J. Hauer, D. Trudnowski, and J. DeSteese, "A Perspective on WAMS Analysis Tools for Tracking of Oscillatory Dynamics," in *Power Engineering Society General Meeting, 2007. IEEE*, June 2007, pp. 1–10.

APPENDIX

A.1. Network Algebraic Constraints and DSE using global measurements from WAMS

The network algebraic constraints for the generator and load equivalent circuits at all the buses in the system can be represented by the following two equations:

$$\begin{aligned} & |V_i|e^{j\theta_i}(i_{d_i} - ji_{q_i})e^{-j\delta_i} + P_{L_i}(|V_i|) + jQ_{L_i}(|V_i|) \\ &= \sum_{k=1}^{n} |V_i||V_k|Y_{ik}e^{j(\theta_i-\theta_k)} \quad i = 1, \ldots, m \\ & P_{L_i}(V_i) + jQ_{L_i}(V_i) = \sum_{k=1}^{n} |V_i||V_k|Y_{ik}e^{j(\theta_i-\theta_k)} \\ & i = m+1, \ldots, n \end{aligned} \tag{A.1}$$

where P_{L_i} and Q_{L_i} are voltage dependent function (usually nonlinear) for real and reactive load at bus i for a m-machine, n-bus system; Y is the network admittance matrix.

If we consider only transient dynamics and neglect transient saliency and stator resistance, the armature current quantity in (A.1) can be represented by:

$$(i_{d_i} + ji_{q_i})e^{j\delta_i} = \frac{1}{jX'_i}[(E'_{q_i} + jE')_{d_i})e^{j\delta_i} - |V_i|e^{j\theta_i}] \tag{A.2}$$

where $X'_i = X'_{d_i} = X'_{q_i}$ when transient saliency is neglected.

Substituting the corresponding armature current in (A.1) using (A.2), the network algebraic constraints become functions of measurable voltage phasors and power consumptions with respect to dynamic state variables (δ, E'_d and E'_q). Instead of using local power outputs in (2.21), the measurement representation can be replaced with (A.1) if power consumption at each bus is known; this would form a real-time DSE using global measurement from WAMS.

A.2. Implementation of physical limit constraints in PF

As is mentioned in Section III, for a multi-machine dynamic model, physical constraints in (2.16) have to be included in the DSE process. It is found that in each case, the particle filter manages to track the dynamic states of the system considering the constraints. Since the PF is a

probability based filter, it is simple to alter the particle value based on the pre-defined condition for the state variables (V_R and P_{go}). Therefore, it is feasible to set the threshold value to any particle which exceeds the bound since the weight for having such a condition is 0%. Note that we don't consider gate opening rate limit since the true rate does not apply to the particle's propagation with random process noise which may lead to divergence.

A.3. Definitions for constants in synchronous machine modeling

Table A.1. Definitions for constants in synchronous machine modeling

Constants	**Definitions**
K_A, T_A	Voltage regulator gain and time constant
K_E, T_E	Exciter gain and time constant
K_f, T_f	ESS gain and time constant
R_p	Permanent droop for speed regulation
K_{sm}, T_{sm}	Gate servo-motor gain time constant
K_L	Integral control gain in LFC
T_{CH}	Steam chest and inlet piping time constant
K_a, K_i	Proportional and integral gains in PI controller

A.4. OOS relay settings

The blinder distance settings are given by :

$$d = \frac{1}{2}(X'_d + X_T)tan(90 - \frac{1}{2}\delta_c) \tag{A.3}$$

Table A.2. Generator Relay settings

Generator	**Mho Diameter (Center Position)**	**Blinder Distance**
G_8	1.488 (0,-0.396)	0.2315
G_2	1.769 (0,-0.509)	0.2734

whereX_T is the transformer impedance and δ_c is the critical value of the angular separation. In the paper we use the conservative 120° for this separation.

The circular mho unit is set to reach in the system direction at 1.5 times the transformer impedance, and in the generator direction the reach is chosen at twice generator's transient reactance [48].

In Sec. 3.4, two generators: G_8 and G_2 are involved in the simulation results; the dedicated OOS relay settings using the single blinder scheme is summarized in Table A.2. The Mho characteristics and the blinder separation (d) are given in per unit.